NTNU

Norwegian University of
Science and Technology

Experimental Studies of Cold Roll Bonded Aluminum Alloys

Steinar Lauvdal

Materials Science and Engineering
Submission date: August 2011
Supervisor: Bjørn Holmedal, IMTE

Norwegian University of Science and Technology
Department of Materials Science and Engineering

Declaration

I hereby declare that everything in this report is produced by the author himself. None of the work presented here has been published before and in those cases other work or theories has been touched or presented, this has been credited to the authorized source. Further on I give my word that everything, to the extent of my knowledge, is carried out accordingly to the laws of the Master of Science, Architecture and Engineering Exam at the Norwegian University of Science and Technology.

Trondheim, August 9th 2011

_____

Steinar Lauvdal

Abstract

This master's thesis is based on experimental studies of the parameters influencing cold roll bonding (CRB) of the aluminum alloys AA1200 and AA3103,in the work hardened and annealed condition. The effect on the bond strength from the preparations parameters as degreasing agent, scratch brushing and exposure time for oxide growth is investigated in comparison to former studies. Further the effect of rolling speed and effect from contributing factors from the different testing methods is discussed. Three different methods for testing the bond strength are used. One of them was established during this study and was named Tensile Bond Strength Test (TBST). A final investigation of the fracture surfaces and bond interface in a scanning electron microscope (SEM) was carried out to analyze the bond mechanism and distribution of fractured oxides.

The TBST is testing the direct bond strength with no peel or shear forces involved. It also only requires a fraction of the sample material for testing and any roll bonded sample is applicable for this test. These are the huge advantages with the test method. The test method is however still naive, and suffers from a series of challenges. The current test ranged is from 4MPa to 40MPa, but with potential for a large range expansion. Further are bond damaging effects, caused by the machining, reducing the accuracy of the measurements and compromising "grooving"; a measure taken for increasing the test range above 40MPa.

The strain rate at which the samples were tested, showed to have strong influence on the measured bond strength. Much higher than the effect of any work hardening on either of the alloys. The preparation prior to roll bonding including an only 90s exposure time to air, ensures a very thin oxide layer and bonding at reductions down at 22.3%. Ductile "stretch lips" was found on the fracture surface, and run in direction normal to the rolling direction. The fraction of bonded surface area did not seem to follow the percent of reduction during roll bonding, which indicates a thinning of the oxide layer.

Acknowledgement

This master thesis is connected to a larger project going under the name; *Development of lightweight structural materials by Accumulated Roll Bonding*. This project is fully funded by the Research Council of Norway.

In addition to the main topic of this thesis a small investigation into the preparations and circumstances around metal-to-metal gluing has been carried out and have to be presented in a separate report. The industrial grade glue utilized was delivered by Henkel Norway. All of the work in this study has been carried out at the Institute of Material Technology (IMT), NTNU, in the spring 2011.

Throughout work on this thesis several persons have been involved in the different stages. First I want to thank my main supervisor, Professor Bjørn Holmedal, for giving me the opportunity to work on this subject. I am grateful for all his support and help in all regarding matters.

PhD Candidate Nagaraj Vinayagam Govindaraj has been a severe asset in many parts of the practical work in this project. Along with his ideas and support throughout the work, I greatly appreciate his help.

Additionally I would like to direct thanks to the following people; Paal Skaret for all help at the MTS lab, the people at Finmekanisk Verksted in Realfagsbygget, especially Terje Rø and the workshop at Bergbygget for helping with my customized needs.

Table of Contents

Abbreviations

A(C)RB	Accumulated (Cold) Roll Bonding
TBS(T)	Tensile Bond Strength (Test)
SBS(T)	Shear Bond Strength (Test)
CDT	Critical Deformation Threshold
HAZ	Heat Affected Zone
CSRB	Cross Shear Roll Bonding
RB	Cold Roll Bonding
AT	After Tape
BT	Before Tape

1 Introduction

Traditionally joining methods for metals have in large consisted of fusion welding, where the two metals, with or without the use of filler material, are melted by electric arc, laser or electron beam. Bonding occurs in the mixed pool of liquid metals. A lot of the energy used in these processes goes to heating up the metal in and around the weld zone. This zone is commonly known as the heat affected zone (HAZ). In aluminum welding, the HAZ leads to huge concerns as it causes changes in the microstructure that inflict permanent degraded mechanical properties in the base material [19]. The grain size is increased resulting in a strongly affected strength and ductility properties. The HAZ is usually the most critical area for any loading-bearing constructions. Therefore alternative low temperature joining methods are desired. Methods like butt-welding (for wires), roll bonding and accumulated roll bonding (ARB), for plates, can be performed even at room temperature with high mechanical pressure.

Roll bonding was first applied in the production of compound plates in 1935. ARB [26] is the natural progression of roll bonding, where the process is simply repeated. The roll bonding process is described in more details throughout this report, but in general it is two metal plates pressed together between two rolls at very high pressure, resulting in permanent metallic bonding. When two plates are welded together, why not weld together several layers? The roll bonded plates can be folded and roll bonded again, now containing four layers welded together. In this manner, for each new pass, the number of layers doubles and the thickness of each individual layer is reduced, creating a very fine grained structure. This is the definition of accumulated roll bonding, or accumulated cold roll bonding (ACRB) if performed at low temperature. When this method is fully mastered it can offer plates with properties tailor made for a wide specter of uses. Different materials and alloys can be mixed to create the desired properties, or simply to make a material so hard that it is pushing the limit of the theoretical maximum strength.

As for today roll bonding is commonly used in a few well known every day products. Parts of the exhaust system on your car are most likely roll bonded layers of aluminum and steel; an inner layer of steel to strengthen the tube, and an outer aluminum layer to shield the steel from corrosion.

The aim of this project is to explore the bonding mechanisms between double layer

2 Theory

This chapter presents the most important theories, techniques and methods, upon which this thesis bases its interpretations of observations and assumptions.

2.1 Deformation

The deformation of a metallic material has large Impact on its properties, altering the strength, ductility, electrical conductivity and many more. Most of these effects can be explained by studying the changes in the microstructure. In this section, an introduction in what deformation of a material involves with regards to roll bonding is given.

2.1.1 Elastic Deformation

The definition of elastic deformation is this point where the external load applied to a solid material is no greater than the material will regain its original dimensions when the load is removed. A common example of elastic deformation is a rubber band. When the rubber band is stretched, it is deformed. If the shape is restored to original after stretching, the deformation has been elastic. On a much smaller scale this means that the atomic structure can be stretched or compressed, but the atoms relative position to each other is kept unchanged during loading, as illustrated in Figure 1. A plastic deformation of 0.2% after applied loading is considered the upper limit of elastic deformation. Comparing this to the analogy of the rubber bad, if the length of the band is less than 0.2% longer after the stretching cycle, the deformation is still considered fully elastic.

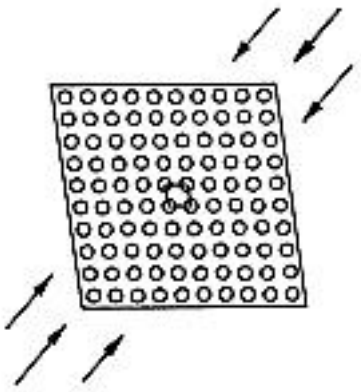

Figure 1: Elastic deformation with force applied. [2]

Below the elastic limit the behavior of a solid follows Hooks Law:

$$\sigma = \varepsilon E \qquad (1)$$

where σ is the stress, ε is the strain and E is the *modulus of elasticity* (*Young's modulus*). In reality most forces is not applied normal to any shape and no material has a 100% perfect structure. This fact introduce the shear stress, and it is defined as

$$\tau = G\gamma \qquad (2)$$

where G is the shear modulus and γ is the shear strain. [1]

2.1.2 Plastic Deformation

Plastic deformation is when an external load leaves a solid material in a permanent irreversible deformed state after the load is removed. Explained with the rubber band example, the deformation is plastic from the point where the band is more than 0.2% longer after a stretch cycle. An even better example, from everyday life, is to use something that is much less elastic, like a caramel. Just as the rubber band, this too can be stretched, but when the force is released, the caramel will remain in its stretched form. This deformation is fully plastic, meaning it is permanent. In Figure 2 below, one can see that the atomic structure is severely deformed under a plastic deformation in a metal.

The mechanics of the metal deformation relays upon movement of dislocations and the slip systems. Deformation of this type tends to occur stepwise, since metals are crystallographic, and always in the direction of least resistance. When moving through the material the dislocations can generate new defects, be stopped or annihilated when they interact with other defects throughout the material.

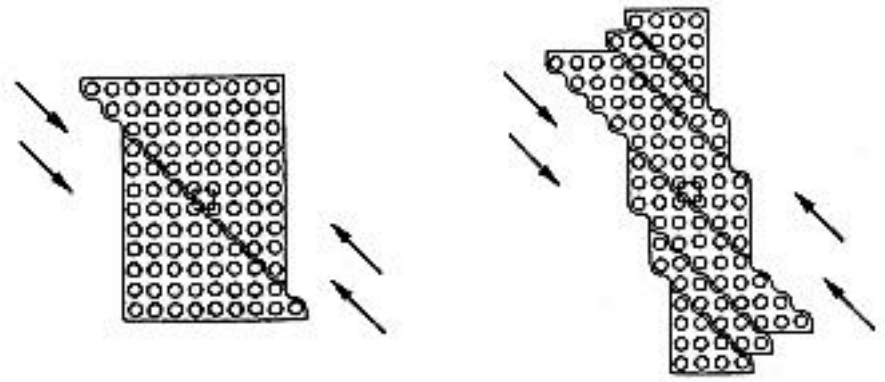

Figure 2: Progression of plastic deformation with load applied. [2]

Once plastic deformation starts, only a small increase in stress usually causes a relatively large additional deformation. This process is called *yielding*, and this behavior starts to be important at the stress value known as *yield strength*, σ_0 [1].The yield strength is a practical engineering limits that marks the transition between elastic and plastic deformation and is show in Figure 3 as the "Yield Strength Point".

2.1.4 The Stress-Strain Curve

A useful tool in the engineers' toolbox is the stress-strain curve. This curve, shown in Figure 3, describes the strength of a material as it is being strained until fracture. The first linear part of the curve shows the elastic deformation part which where explained in the previous section. The "yield strength point" marks the start of the plastic deformation, which last until fracture at the end of the curve. On the curves highest point, called the ultimate tensile strength (UTS), marks the highest stress for this material in regard to its initial dimensions. In reality the specific stress of the material (called the true stress) continues to increase until the point of fracture. When calculating the true stress, the measured stress is divided on the true area, which decreases as the material is stretched thinner. The reason the stress-strain curve decreases after stretching the UTS is because the stress still is divided on the initial cross-section area of the sample. This stress, which does not take in account the reduction in cross-section, is called the engineering stress.

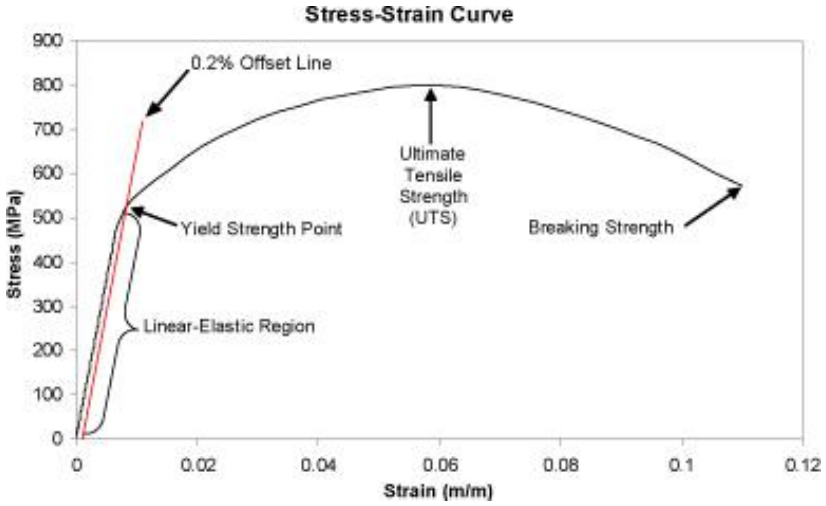

Figure 3: Stress-strain curve.

The engineering stress is defined as

$$S = P/A_0 \qquad (3)$$

where P is the load on the specimen and A_0 is the initial cross-sectional area near the center of the specimen. The engineering strain describes the elongation/compression of the sample, and is defined as

$$e = \Delta l/l = (l - l_0)/l_0 \qquad (4)$$

where l is the gauge length at a given load and l_0 is the original gauge length with no load. [1]

2.1.5 Strain Hardening (Work Hardening)

Strain hardening, more commonly known as work hardening or even cold working, is when the strength of a material increases during plastic deformation. This

phenomenon is directly related to the interactions between internal dislocations and boundaries within the material. In more technical terms, strain hardening describes the rise in the stress-strain curve after yielding, as the material is increasing its shear stress with increasing strain. A measurement of the degree of strain hardening due to Hollomon's equation is

$$\sigma = K\mathcal{E}_p^n \qquad (5)$$

where σ n is the stress, K is the strength index, ε_p is the plastic strain and n is the strain hardening exponent:

$$n = \sigma_u / \sigma_o \qquad (6)$$

where σ_u is the ultimate tensile strength and σ_o is the yield strength. This is illustrated in Figure 3.

The strain hardening of materials evolves in stages, where the first two stages describe the different hardening rates between single crystals and polycrystals as slip systems are activated.

Stage I and II is considered irrelevant for roll bonding, which occur at much higher deformation. These first two stages will not be explained in further detail, although more information on the subject can be found in "Mechanical Metallurgy" by Dieter, listed in the bibliography [1].

Going straight for stage III, the movement of screw dislocations is introduced, which allows piled up dislocations from stage II to escape and travel longer distances. There probability for these dislocations to meet another screw dislocation is high, and when sufficiently close to each other, they will start to annihilate or recover. Annihilation occur when dislocations with opposite direction to each other intercept and both dislocations "dissolves". The recovery phenomenon reduces the dislocation storage rate, and is explained closer in section 2.2.1. Both phenomena results in a reduction in dislocation density-increase, and the strain hardening rate is dampened. This stage is highly temperature-dependent., and both stage II and II is shown in Figure 4.

The fourth and most relevant stage for cold rolling is shown in Figure 4. The hardening rate at this stage is constant until saturation level is reached and has a dependency on the deformation temperature as well as the alloy composition. This is a very highly strained area where the dislocations have very little space to move, along with an indirectly increase in dislocation-density due to shrinking subgrain size. As some supplementary information on accumulated roll bonding (ARB), the thickness of each layer would decrease for every rolling pass, reducing the dislocations ability to move. In theory, with sufficient roll bonding passes, one could in the end have a structure

where all the dislocations were entirely immobilized, and the theoretical maximum strength is obtained.

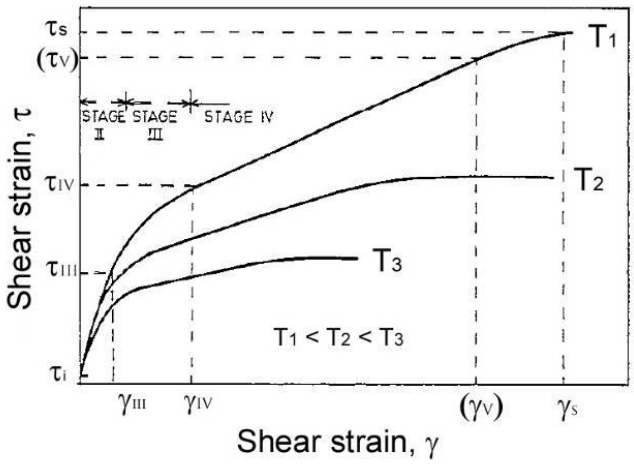

Figure 4: Graph showing the strain hardening though stage II, II and IV. [15]

2.1.5.1 von Mises Strain

In 1913 Richard Edler von Mises proposed that when the second deviatoric stress invariant J_2 reached a critical value k^2 yielding would occur. [1]

$$J_2 = k^2 \qquad (7)$$

In layman's terms the von Mises criterion describes the point where the material starts to "yield plastically" after a certain amount of elastic energy is reached.

When performing cold roll bonding it is more practical to calculate the von Mises strain directly from the reduction of the plate thickness-reduction

$$\acute{\varepsilon} = \frac{2}{\sqrt{3}} * \ln\left(\frac{t_2}{t_1}\right) \qquad (8)$$

Von Mises stain does not take in account if the material is anisotropic. Meaning, if such a material was strained from different directions, each direction would give a different von Mises value. The advantage by using von Mises is due to this exact same "flaw", as it can easily be used to compare strain applied form a wide number of various methods. In this case it is used to measure the strain by rolling.

By rearranging the nominal strain

$$\mathcal{E} = \frac{t_1 - t_2}{t_1} \Leftrightarrow \frac{t_2}{t_1} = (1 - \mathcal{E}) \qquad (9)$$

and when implemented it in equation (8), the von Mises Strain expressed by the nominal strain can be shown as

$$\acute{\varepsilon} = \frac{2}{\sqrt{3}} * \ln\left(\frac{t_2}{t_1}\right) = \frac{2}{\sqrt{3}} * \ln(1 - \mathcal{E}) \qquad (10)$$

In equation (8), (9) and (10) t_1 is the plate thickness before the deformation, and t_2 the thickness after the deformation has occurred. Below in Figure 5, the relations between von Mises criterion and Tresca Criterion are illustrated where σ is the yield stress.

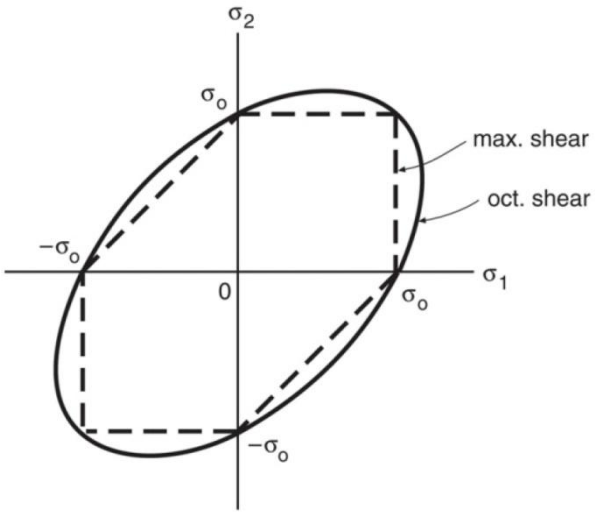

Figure 5: Failure criteria for plain stress. Elliptical line showing the von Mises Criterion and dashed line showing Tresca Criterion. [1]

2.2 Annealing

Cold rolling prior to roll bonding inflicts the material with high stresses that gives high strength, but may also decrease the ductility severely. To eliminate some or all of the effects of this work hardening, a heat treatment called annealing may be performed. However, the strength gained by cold rolling will decrease during this process as well. There are two main softening reactions occurring when a heavily deformed material is annealed, and these are called recovery and recrystallization. [9] Before explaining these two phenomena in more detail, let it be said that recovery and recrystallization is competing processes driven by the same stored energy, created by the deformation. Once the stored energy has been "consumed" by one or the other, no further recovery or recrystallization can occur. Hence they are strongly dependent on each other. [16]

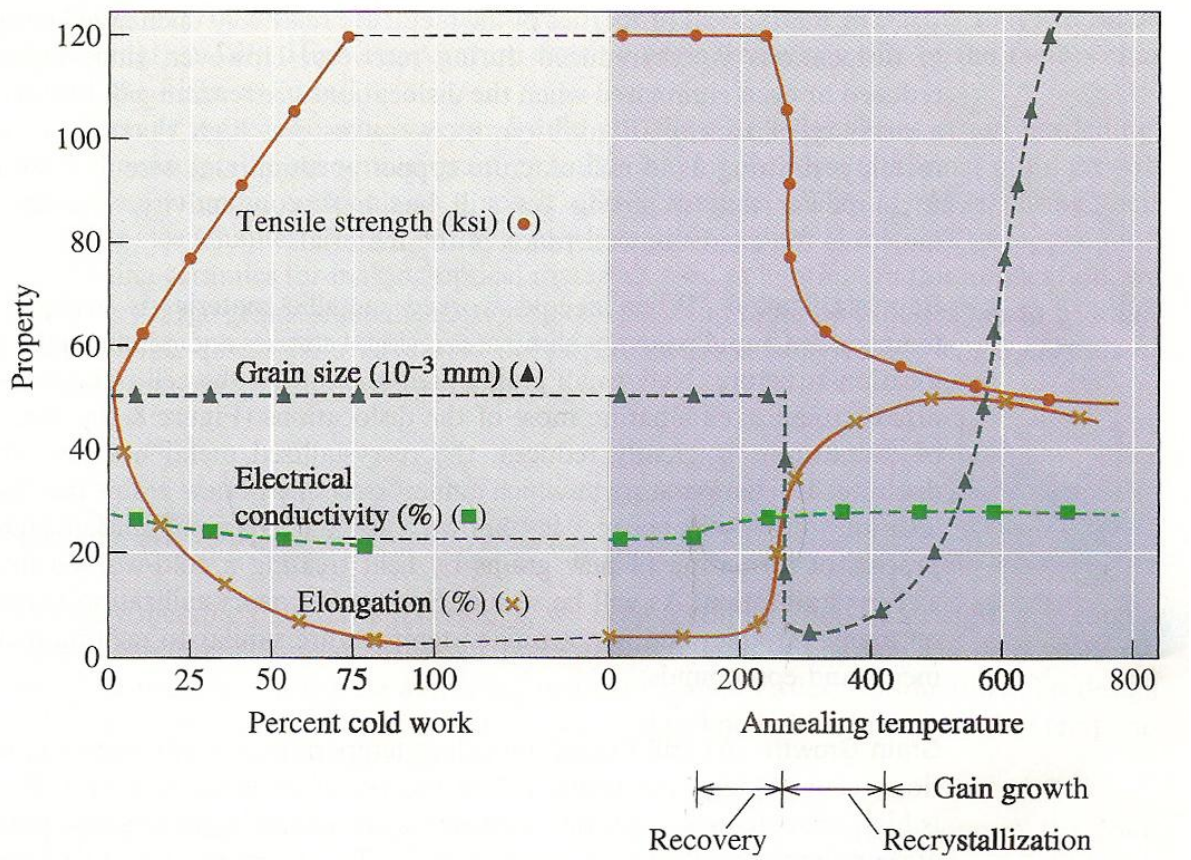

Figure 6: The effect of work-hardening and annealing temperatures on material properties. Here shown for a Cu-35% Zn-alloy with an end deformation of 75%. [9]

Note that the effects of work hardening and annealing temperatures in Figure 6 above does not represent the Aluminum-alloys in this report, but that of a Cu-Zn alloy. The graph is included here in the absence of a more relevant one. However, the general idea is the same and in fact almost identical, except for what happens with the elongation for a temperature of about 400 degrees and up, it continues to increase.

Figure 6 is showing, along with elongation, electrical conductivity and grain size, how the tensile strength is effected by in the different stages of an annealing process on work hardened (cold worked) materials.

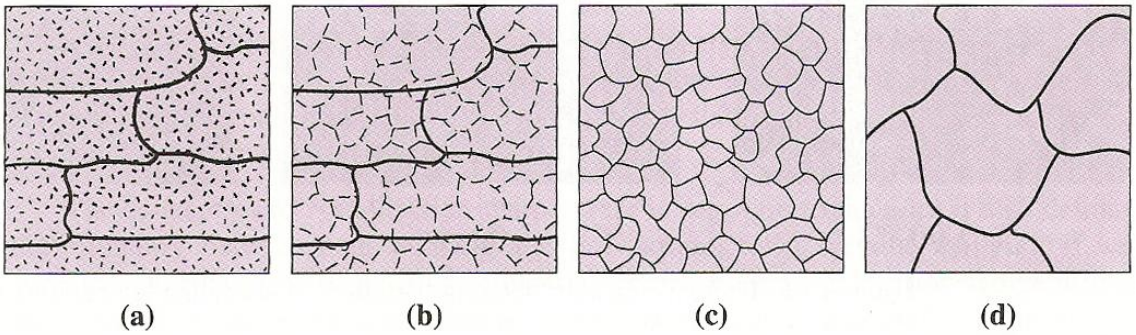

Figure 7: The effect of annealing temperature on the microstructure of cold work hardened metals. (a) work hardened, (b) after recovery, (c) after recrystallization, and (d) after grain growth. [9]

2.2.1 Recovery

After work hardening the microstructure is deformed containing a large number of tangled dislocations (Figure 7 (a)). If the material is given a low-temperature heat treatment, the additional energy allows the dislocations to move and form new boundaries. This new formation is called a polygonized subgrain structure, and is illustrated in Figure 7 (b). The term for this stage is recovery and refers to the changes in a deformed material which partially restore the properties to its pre-deformed state. Residual stresses due to work hardening are removed, although no change in dislocation density occurs. At this temperature the mechanical properties is relatively unchanged. [9][16]

2.2.2 Recrystallization

If the temperature is increased sufficiently, new fine grains will then nucleate on the cell boundaries of the polygonized subgrain structure formed in the recovery phase, and at the same time eliminating most of the dislocations. This large decrease in dislocations reduces the strength of the material, but also increases its ductility. The temperature at which the dislocation density is rapidly reduced is called the *recrystallization temperature*. This process of formation of new grains is called recrystallization, and is illustrated in Figure 7 (c).

As the amount of work hardening increases, the recrystallization temperature decreases. There is a minimum amount of work hardening for which recrystallization will not occur, which applies for deformations below 30 to 40%. This again has a direct relevance for roll bonding of aluminum, where bonding can occur well below these values. [9]

Increasing the temperature even further will initiate grain growth shown both in Figure 6 and Figure 7 (d). This stage of annealing is however of little interest in regards of most cold roll bonding situations, as annealing at these temperatures is not desired due to the rapid grain growth.

2.3 Bonding

2.3.1 Metallic Bonding Mechanics

The atoms in a metal are generally built up in a regular grid where nearby atoms share their valence electrons in what is commonly called an “electron sea”, as illustrated in Figure 8. This way of bonding gives the matrix a strong, but non-directional strength, a high ductility and Young’s modulus, among other characteristics. The way metals bond, is by an electromagnetic interaction between delocalized electrons, which is illustrated by the “electron sea”-parallel. For two metallic atoms to interact in such a bonding the distance between them needs to be less than one atomic radius. At this point they spontaneously bond by sharing their valence electrons. This is due to the attractive

forces decreases with the square of the distance. Put differently, two metallic plates need to be brought very close for metallic bonding to take place.[5]

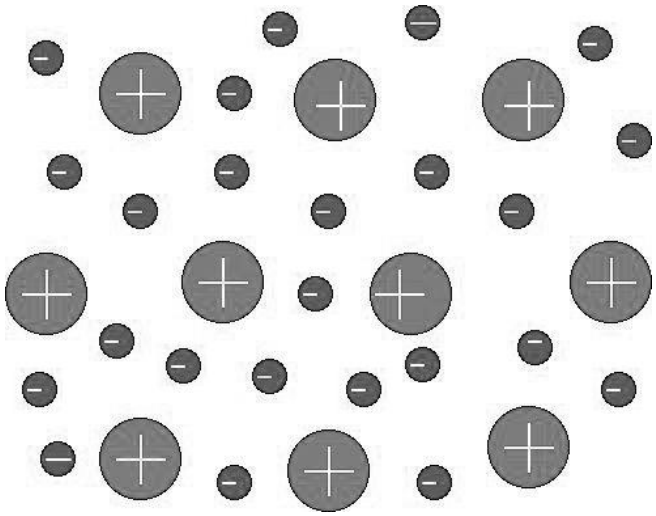

Figure 8: Metallic binding where protons are shearing their valence electrons in a so-called "electron sea".

2.3.2 Surface Interaction

The surface of even a fine rolled plate has a certain roughness and is far from being perfectly smooth. This roughness results in a major reduction in contact area when the two surfaces are brought together, as shown in Figure 9. When the normal load is increased the real contact surface is increasing proportional to the load applied.

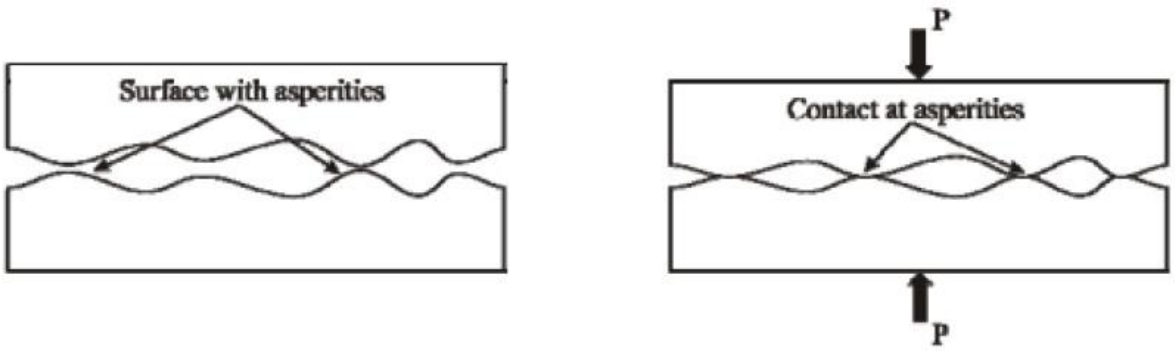

Figure 9: Contact area between two surfaces. [5]

Under this load the contact area is experiencing plastic deformation which hardens the material in contacting region and contributes to restraining further deformation and growth of contact area. In roll bonding of aluminum such rough surface texture can however be an advantage when it comes to bonding strength. The reason why will be explained and discussed later on.

2.3.3 Oxide Layer and bonding

Most metals, when they are exposed to oxygen in the atmosphere, over time develop an oxide layer on its surface. Such oxides, variously named, are hated as well as loved, depending on which material of where they are found. On iron based materials it is called corrosion, and is very porous, allowing for the oxidation to continue “eating” up

the metal. For other materials this layer helps protect in different ways depending on the material.

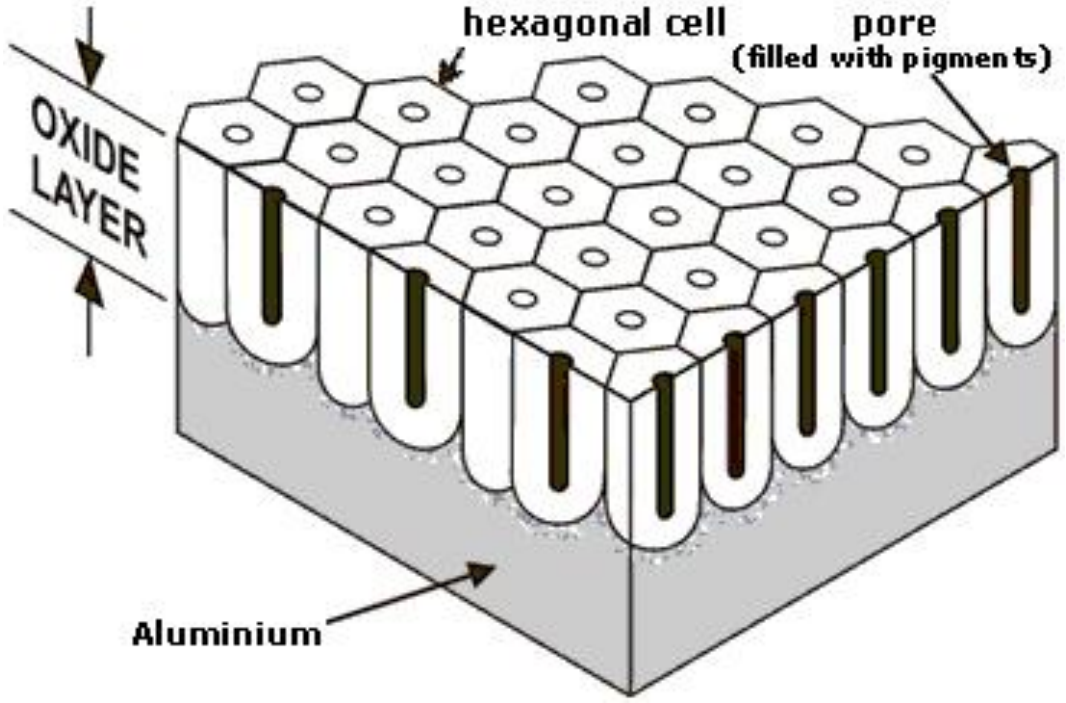

Figure 10: Oxide layer on a aluminum surface. [3]

On aluminum the natural oxide layer grows fast, thick and hard. In fact it is the second hardest substance known to man (sapphire), only second to the diamond. This hard surface shields the base material from any further oxidation (corrosion), but also acts like a barrier for when two surfaces are attempted joined. The oxide layers must be fractured to allow the two base materials beneath to interact. This mechanism elevates the energy required for cold welding of two surfaces. When a force is applied and the two surfaces are brought together, the asperities are the first to come in contact with each other, as seen in Figure 9 and Figure 11. Adhesion between the two oxide layers now makes them act as one. With increasing load the hard and brittle oxide layer starts to crack, and in between these cracks the base material is extruded and with sufficient force brought in contact with the base material from the other plate and metallic bonding is acquired. This exposed virgin material will not form any new oxide, as the compression forces are sufficient to create an airtight seal around these openings. Figure 11 illustrates this progression from (a) through (d) with increasing external load.

The obtained weld strength depends on the area of actual bonded base material which can be expressed as the exposed surface

$$Y=(A_1-A_0)/A_1 \qquad (11)$$

where A_0 is the initial surface area and A_1 is the final surface area after roll bonding. [5]

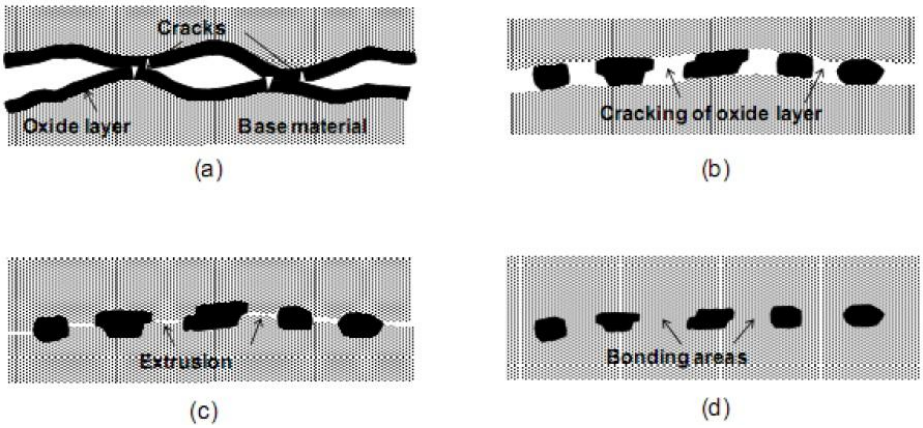

Figure 11: The progression of bonding between two aluminum layers under increasing load. [5]

2.4 Test Methods

Prior to this study, two methods for testing he bond strength was considered and also put to the test. This next part will present these two test methods.

2.4.1 Peel Test

The peel test was initially established for testing adhesive bonding, and there is made a standard for this peel method, which describes methods and procedures that in lag ear applicable for peel testing of roll bonded plates as well. [25]

The peel test, as the name reveals, tests the bond strength by peeling the two layerered sheet apart from one side to the other, as illustrated in Figure 12 b.

The preparations for a peel test are simple and require very simple tools, though the preparations start ahead of the roll bonding process. Once all the sheets are cut to desired size for roll bonding, one has to make a decision. To be able to peel test the sample after it has been bonded, a section of the sheet has to be fairly easy to peel open, so that the tensile machine have something to fasten its grip onto. To attain such a section, there are many choices, but the basic rule is that any bonding have to be prevented or severely reduced in this section. One method is to add some non-metallic material in between the sheets in this section to prevent bonding. This could be a piece of tape, some oil, or basically anything that prevents bonding.

When using such methods one should be wary on how this could influence the rest of the bond. As discovered in a study by Lauvdal [10], when using a piece of tape, a section stretching several centimeters into the bond was affected by the glue in the tape. The tape had been placed in the center of the sheets, so that the moisture in the tape (glue) has been squeezed ahead of the bond front moving the moisture far into the back side of the sheet. In Figure 32 a sample from this study, with the mentioned tape-issues can be found. Needless to say this reduced the bonding strength in the affected area. A secondary problem with using tape was that the material in that area fractured and cracked to such a degree that the material fractured when any load was

applied during testing. One simple solution to both these problems was found from these mistakes; simply avoid scratch brushing the area intended for grip, not using any tape, oils or any other material to prevent bonding. This method prevented strong bonding and the material was not left in a fractured state.

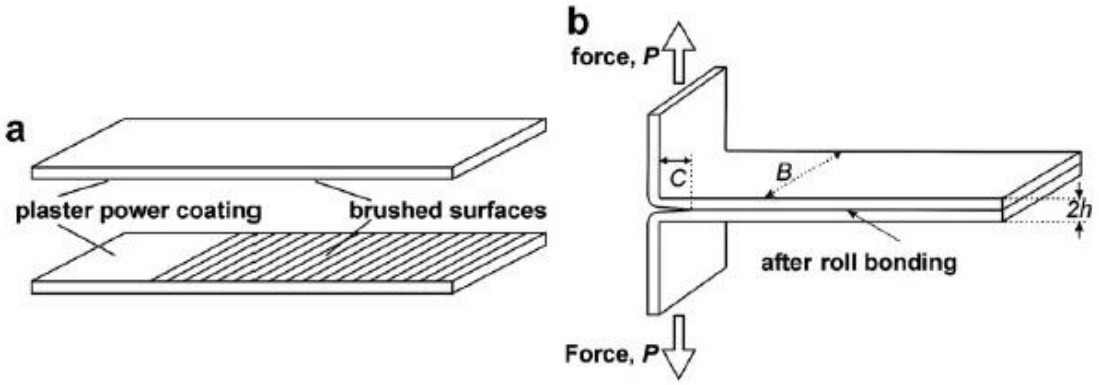

Figure 12: Illustration showing how the peel- test is performed. [6]

It is difficult to compare the results from a peel test carried out in different studies. As the results is usually measured in the load force applied to part a given area. The peel test is a continuous process and gives no real cross section to divide the load. The thickness and bond strength is also affecting the angle at which the sheets are parted, which directly influences the measured strength. Strong bonds will be peeled in a 90 degree angle apart from each other as in Figure 12 b, while weak bonds and/or thicker sheets will be peeled at a lower angle, giving more leverage on the crack front, resulting in a lower measured bond strength. These are some of the weaknesses in the peel test.

However, the advantage of such a test is that it only requires simple cutting tools and a tensile testing machine, which should be relatively easily accessed by people that have interest in performing such tests in the first place.

2.4.2 Shear Bond Strength Test (SBST)

The shear bond strength test, sometimes just called shear test, though it should not be confused with a traditionally shear test which is usually related to testing the shear force within a solid material, which has nothing to do with the testing of bond strength as in this case. The SBST can be referred to as the “state of the art” method for testing bond strength, as it is very adaptable for testing both weaker and stronger bonded samples, regardless of the thickness of the sheets.

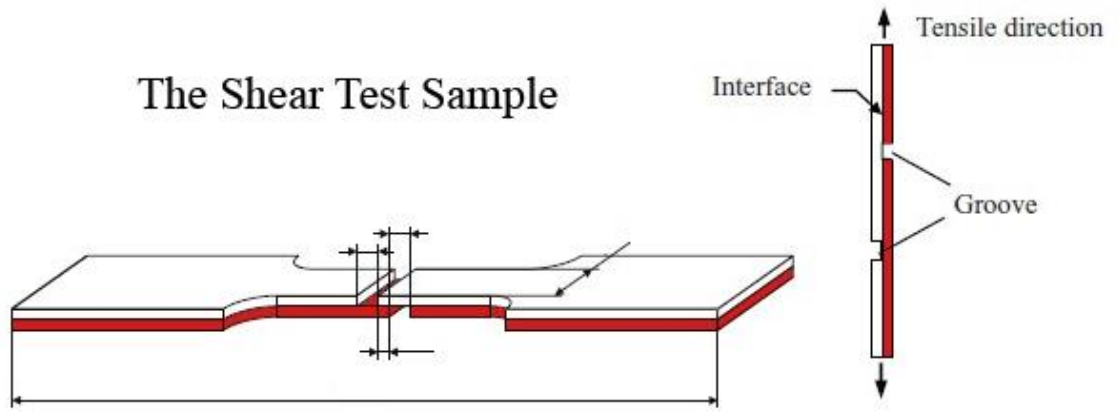

Figure 13: This image shows how the shear-test sample is cut and where the tensile force is applied. The actual dimensions will vary with the individual test and material properties.

Compared to the peel test a SBST requires no additionally preparation prior to roll bonding. After the bonding is complete however, some more high-tech equipment is needed. The first step is to cut the outer shape of the sample, like the item to the left in Figure 13. Further, each layer is dislocated on each side by cutting a groove across, so that only one section is overlapping in the center. This is illustrated in Figure 13 as well.

$$l = 1.2\tau_w \qquad (12)$$

where l is the overlap length, τ_w=τ- τ_1 is the final thickness of the weaker material.[17]

3 Experimental

This chapter contains a presentation of the materials and apparatus used in the experiments. The methods for preparing and testing the samples are explained in detail, along with limitary factors and special concerns connected to these. Also the full process of cold roll bonding is described.

3.1 The Apparatus

3.1.1 The Mill

For these experiments a custom built mill where used, therefore there are no datasheet or any other specified data to find on the mills specifications. For this reason, any desired specification had to be measured and calculated while operating the machinery. A separate hydraulic engine delivers the power, with a pressure fixed at 90 psi for both the pre rolling of the material and the cold roll bonding part of this experiment. The rolling speed is controlled by software that allows variation of the power to the engine. When measuring the speed on the roll surface, the velocity showed to be exponentially proportional with the speed-scale in the software, like the measured data can indicate in Figure 15. Figure 14 below, shows a picture of the operational part of the machinery with a close-up picture of the upper roll, which is 205 mm in diameter. To adjust the gap between the rolls, the wheel on top of the mill is rotated left or right. The solid steel goods helps the mill holding a steady gap-size during rolling, but still the goods yield slightly when very hard material is rolled.

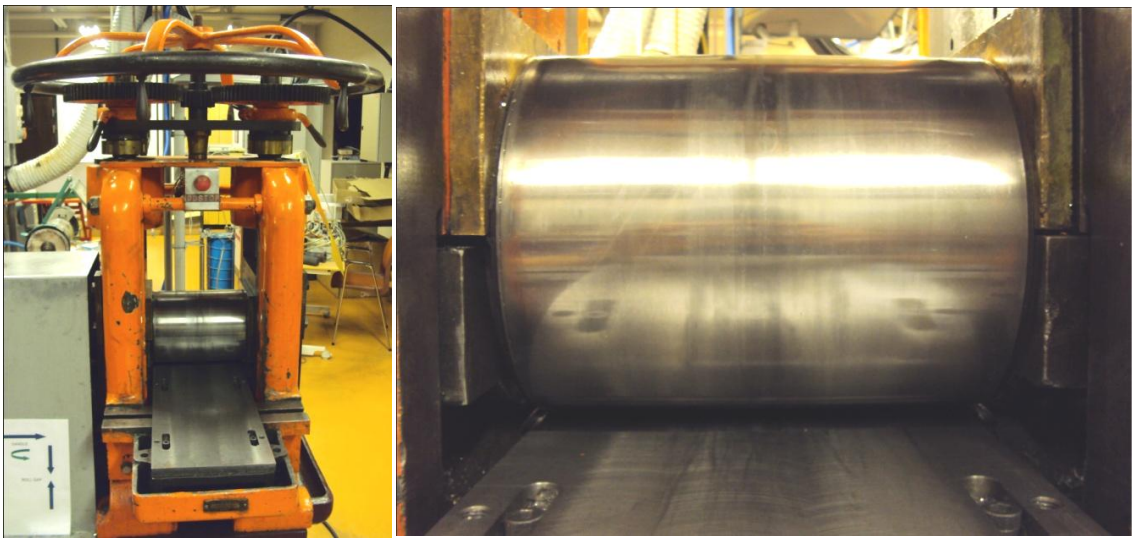

Figure 14: A picture of the mill with a close-up of the upper roller. The lower roll is below, not visible on this picture.

As the mill has no digital or even any usable analog scales for adjusting the roll gap, all rolling was performed on trial and error, mixed with an increasing amount of experience and a lot of calibration samples.

Table 1: Measured dimensions and velocities of roller.

Roll Circumference	645 mm
Roll Diameter	205 mm
Speed 2	9.11 mm/s
Speed 3	26.62 mm/s
Speed 4	67.32 mm/s

The speed on the surface of the roll was found by measuring the length around the roll and timing the rotation-time. Three different speeds where chosen for the measurement, speed 2, 3 and 4 in the software scale, going from 0 to 10. All the samples in this experiment was roll bonded with a speed of 3 (26.62 mm/sec). The additional two speeds were measured as a comparison to this one. When the tests were carried out, there was no resistance on the roll, which is likely to have an influence to some degree. The energy required to deform the samples will absorb some of the speed at which the sample passes through the mill. The closer this resistance is to the maximum capability of the mill, the slower it goes. When pushing and exceeding this limit, the mill struggles and finally stops with the sample half way through. This factor was not investigated any further than this. For calculating the diameter of the roll, the same mentioned measurements were used, and inn Table 1, all the measured specifications can be found.

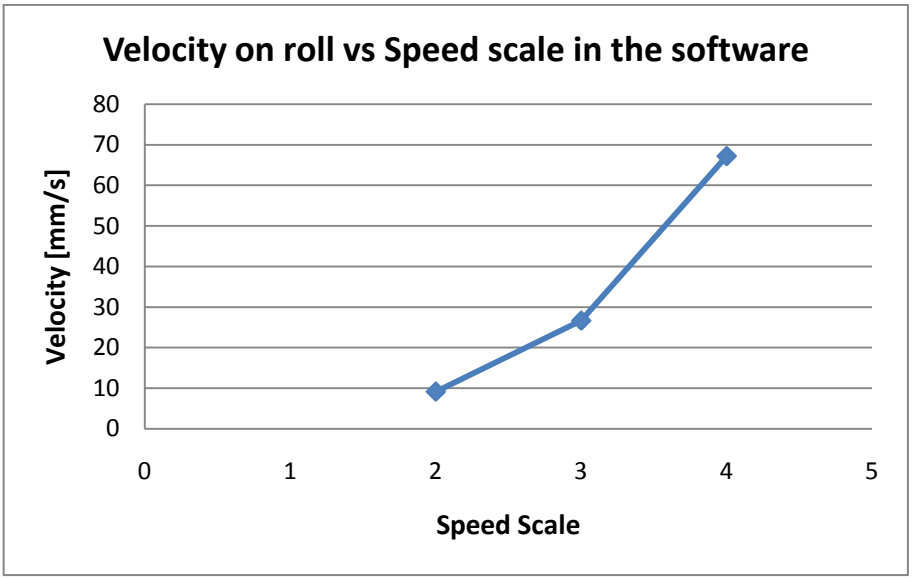

Figure 15: Graph showing the speed values in Table 1, indicating the start of an exponential increase.

3.1.2 The Scratch Brushing Tool

The surface of the connected layers where scratch brushed with a rotating steel brush with dimensions noted below, and shown in Figure 16. A INOX FLEX LE 14-7 125 IWOX was used for the scratch brushing, an electrical multi-speed angle grinder.

Table 2: Dimensions of the steel brush (left in Figure 16) and the rotation speed.

Brush diameter	100 mm
Wire Diameter	0.3 mm
Rotation Speed	3800 rpm

The choice of brushing parameters was based upon a previous study by Lauvdal [10], where a larger variety of both brush types and rotation-speeds were tested.

The reason this particular rotation speed was chosen, relayed upon 2 factors. The first being the desire for a high speed, as this increases the hardening of the surface material. A harder and less ductile surface cracks easier and allows for metallic bonding. All this is explained in further detail later in this report. The second factor is the one preventing the highest rotation speed to be chosen. It is established that with higher rotation speed the more sever is the deformation on the surface. On soft materials, like the annealed 1200 alloy, a high rotation speed removes a lot of material in a short instant. To make the grinding more controllable for the operator, a lower speed was therefore chosen.

Figure 16: The brush used in these experiments shown to the left, and the grinder to the right.

3.1.2 The Roughness Testing Apparatus

The surface roughness can play a significant role during roll bonding, as curvature on the surface focuses compression force on the asperities first, and creates shear stresses on the oxide layer so that it cracks. A Mitotoyo SJ-201 was used to measure the roughness of the samples, and is a rather simple testing method which gives one final roughness value for each test.

First the sample is placed in a track on the instruments table, while a thin needle is lowered in place on a selected area of the sample. Further the proper mode and

parameter is chosen on the instrument controller. For this test the *Ra* mode is chosen, as it measures the distance between the highest and lowest measured point in a given section length. Several such sections are measured and an average of all these is set as the roughness value. The parameter is chosen for each sample in consolidation with the NS-EN ISO 4288 standard, which specifies the suggested settings for any roughness. This means that it is advised to find a coarse measurement of the roughness so that the test parameters can be calibrated towards this particular roughness.

For the typical scratch brushed surface used in this experiment, the suggested settings where found to be Ra 2.5mm x 5 sections. Where Ra is the mode described above, 2.5mm is the length of one section, and 5 is the number of sections that is repeated in a straight line. Each section needs to be long enough to include enough peaks and valleys to ensure sufficient accuracy. Although, it has to be as short as possible, not to be majorly affected by any possible slope or large scale curvature on the surface. This would be the case if the sample is not perfectly flat. As an example; if the sample was higher in one end than the other, or just simply bent. This is also the reason the test is parted up in sections. The needle never stops, but the measured values are reset 4 times during the test. The difference between max and min for each section is calculated and an average of these 5 sections, is the output value on the instruments display.

For extra precaution this test is carried out two more times on the same sample and a final average of the three output values is chosen as the roughness value. The value is in the unit µm and is the average between the maximum distance between peak and valley from each of the sections measured.

As the test is using a needle which is in physical contact with the material, there is a chance that the needle will affect the surface of particular soft samples. This was not investigated further.

3.1.2 The Tensile Testing Apparatus

All three methods for testing bond strength were carried out on the same type of testing apparatus. A MTS (Modular Test System), which is a tensile testing apparatus pulling with a vertical load, while measuring the load and the elongation, and the option for attaching a gauge to measure elongations over a more specific area. For these experiments the apparatus was set to measure the load applied while maintaining a constant strain rate, until fracture.

For the tensile bond strength testing, a 100kN load element was used, while for the shear bond strength test and the prior peel test this was changed to a 5kN load element, which is more sensitive at the lower loads. The strain rate was subject to variation, and the sampling rate was adjusted after this.

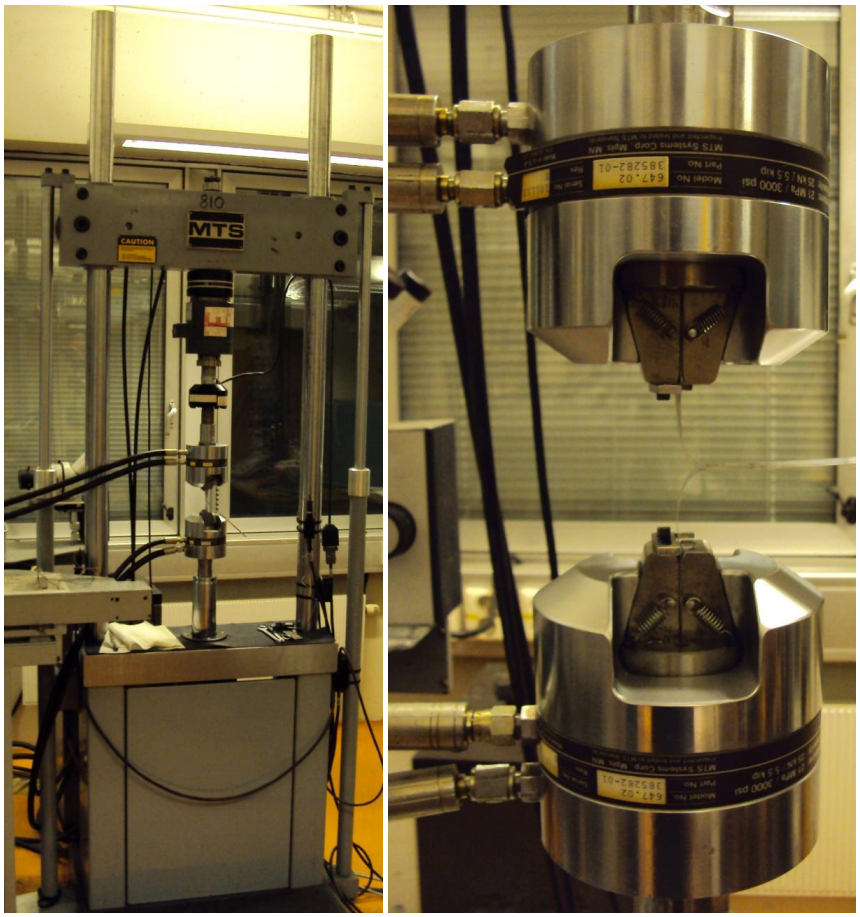

Figure 17: Two pictures showing the tensile testing apparatus, used for all three tests; peel-test, shear bond strength test and the tensile bond strength test. This picture was taken during a peel test.

3.1.2 The Scanning Electron Microscope (SEM)

Prior to investigating the fracture surface these samples were soaked in acetone or ethanol and went through ultrasonic cleaning for two minutes. The samples were thoroughly dried with a hair dryer before glued to a sample holder by carbon-tape and mounted in the SEM.

The samples for interface investigations went through the same cleaning before entering the SEM, but prior to this some additional preparation were performed. These samples were scratched on Si-carbide paper in steps from grit 80 to 2400, followed by polishing down to 1 µm. A final electro polish was performed on a Struers LectroPol-5 with parameters listed in Table 3. The samples were molded when electro polishing was executed.

Table 3: Showing the settings for electro polishing of samples.

Electrolyte	A2
Exposed Area	½ cm^2
Temp. Electrolyte	-36 C
Voltage	20V
Flow Rate	II
Time	10 sec

3.2 The Specimens

Figure 18: A piece of 3103 aluminum alloy prepared for rolling down to final sheet thickness.

The material selection is focused exclusively on aluminum alloys, specifically the 1200 and 3103 alloy. Here, the 1200 alloy is representing a very soft aluminum and the 3103 represents the middle of the tree. Both alloys where rolled stepwise, from blocks of aluminum (Figure 18), down to desirable plate thicknesses giving them a certain work hardening. This further work hardening and followed annealing created even more diversity in the material properties prior to roll bonding. Along the stepwise rolling, samples were picked out at the different thicknesses, so that even at different reduction the final thickness of the roll bonded sample should be approximately the same for all samples. In a later batch, a new approach was taken where the initial size of the sample sheets was the same and the final thickness was left to vary.

Table 4: This table lists the chemical composition of the aluminum alloys utilized in these experiments. Source: AluMatter.info [12].

1200		3103	
Si + Fe	<= 1.0	Mn	0.9 - 1.5
Total Other	<= 0.15	Fe	<= 0.7
Zn	<= 0.10	Si	<= 0.50
Other Elem	<= 0.05	Mg	<= 0.30
Ti	<= 0.05	Zn	<= 0.20
Mn	<= 0.05	Total Other	<= 0.15
Cu	<= 0.05	Zr+Ti	<= 0.10
Al	<= 99.00	Cr	<= 0.10
-	-	Cu	<= 0.10
-	-	Other Elem	<= 0.05
-	-	Al	Remainder

All compositions in wt%

The stepwise progression of cold rolling the samples to the desired thickness was logged and plotted, as shown in Figure 19. In Table A 1 in the appendix the data for this graph is listed.

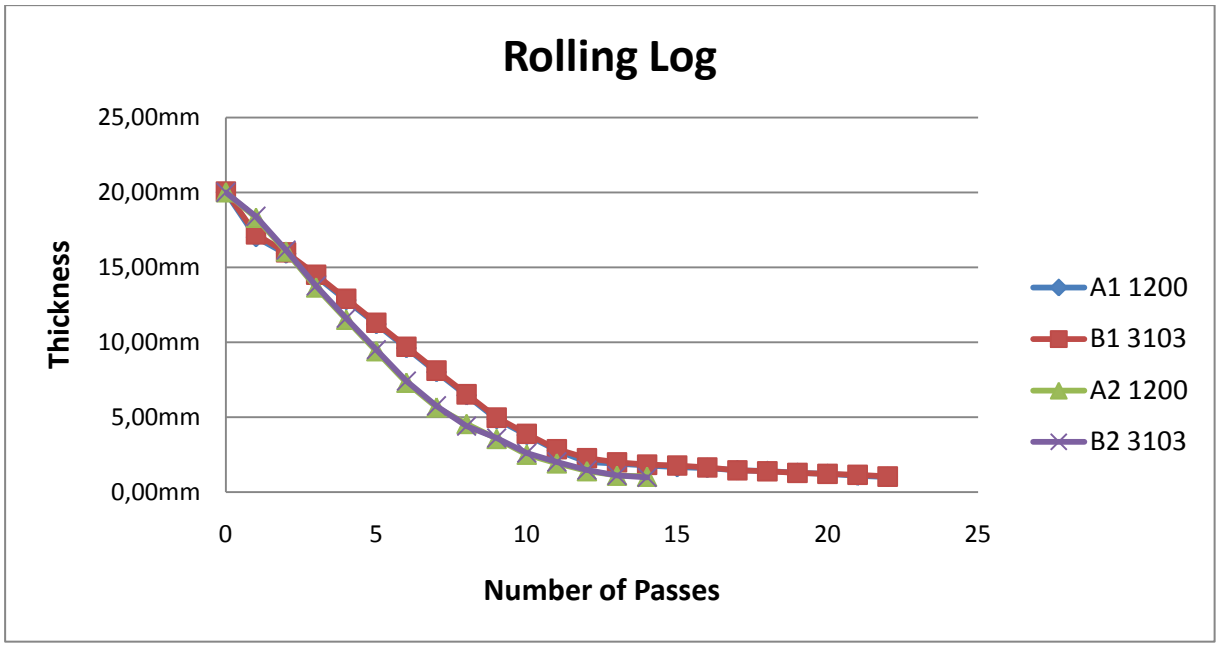

Figure 19: A graph showing the stepwise rolling of the four sample batches produced.

A1, A2, B1 and B2 in Figure 19 mark the different batch number and are used as a prefix in sample names in this study. A full explanation of how to read the sample names is given in the chapter presenting the results.

3.2.1 Annealing

Due to the high strains of the pre-rolling of the sample sheets, one half of each batch was put through an annealing process prior to roll bonding. The annealing temperature and time was set to reset all work hardening strain in the material, returning it to its pre-strained strength.

The sheets were stacked inside a furnace at room temperature and the temperature set to 450 degrees Celsius. Over a three hour time span the temperature steadily increased till it reached the set temperature, and were held there for 1.5 hours more. After being 4.5 hours in the furnace, the sheets were extracted from the furnace and cooled in air at room temperature. A graphical presentation of this annealing process is given in Figure 20. No fan or other air-circulation instrument were used, although the samples were stacked vertically on the side and slightly separated to increase cooling rate. All the plates from both the 1200 and 3103 batches had geometry similar to each other. The approximately geometry is given Table 5.

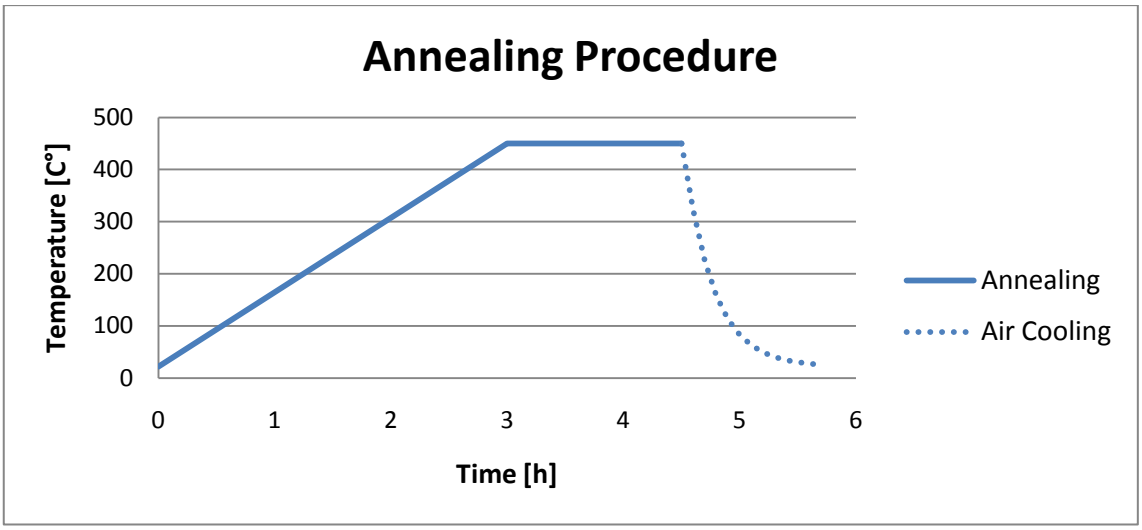

Figure 20: Graph showing the temperature-curve for the annealed samples used in this study. The dashed line shows the cooling in room temperature and is only an estimation.

In Figure 20 the cooling curve presented, is an estimation only, as the cooling rate was not measured.

Table 5: The average sample size when annealed.

Length	200 mm
Width	40 mm
Thickness	1-2 mm

3.2.2 Specimen Preparation

This following section is presenting the different sample preparation methods required for the two main testing methods utilized in this study. Both tests may use the same preparations until finished roll bonding. The roll bonded sheets can be seen in Figure 21, however from this point on, some more sophisticated cutting tools is required to produce the final test samples.

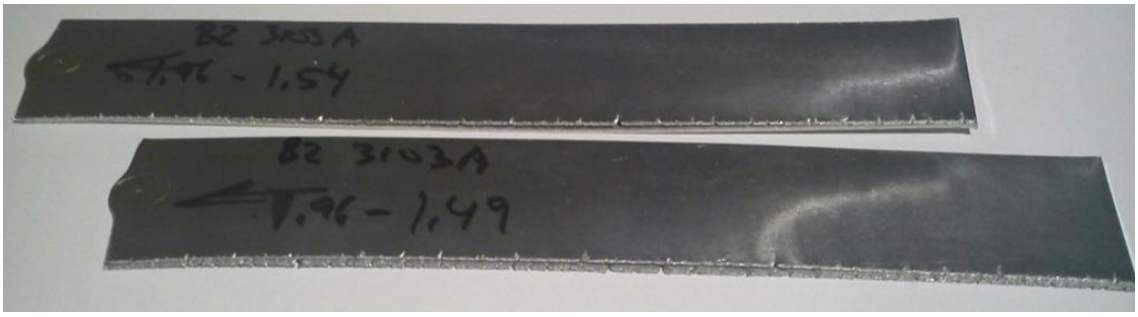

Figure 21: This figure is showing two ends of cold roll bonded strips as they look before they are cut into either a shear- or tensile- test sample.

3.2.2.1 Shear Bond Strength-test Samples

The cutting of shear-test samples was carried out in cooperation with people at the workshop. A template for the outer measurements of the shear bond strength (SBS) sample is the first required item. This template is a thick copper plate where the shape

has been drilled into the surface. It allows for a small plate roll bonded plate to be clamped as a drilling tool is machining the shape, seen in Figure 22.

Figure 22: A shear bond strength sample cut and prepared for testing.

The following step is to machine the grooves seen in both Figure 22 and Figure 23. Before cutting these samples, the thickness of each sheet was measured and as rule of thumb the cut was set at a depth of

$$\tau_1 = \frac{\tau}{2} + 0.1mm \qquad (12)$$

where τ_1 and τ is explained below with the rest of the dimensions seen in Figure 23.

This cut was made to disconnect one of the layers in the horizontal direction, better illustrated in Figure 13. When one side was cut through, the sample was released, flipped and fixed upside down in the exact same position, by hand. The drill was now programmed to cut through the opposite layer of the sample, again only dislocating this one layer in the horizontal direction. The two cuts were placed in a pre-calculated horizontal distance from each other, so that only a specific area of the two layers overlapped. This overlap, the distance l, was chosen by anticipation the strength of the bond to fit in between the upper and lower testing limitation of the shear-test. The lower being strong enough to prevent the sample from breaking during machining and the upper being the yield strength over the cross-section of the material.

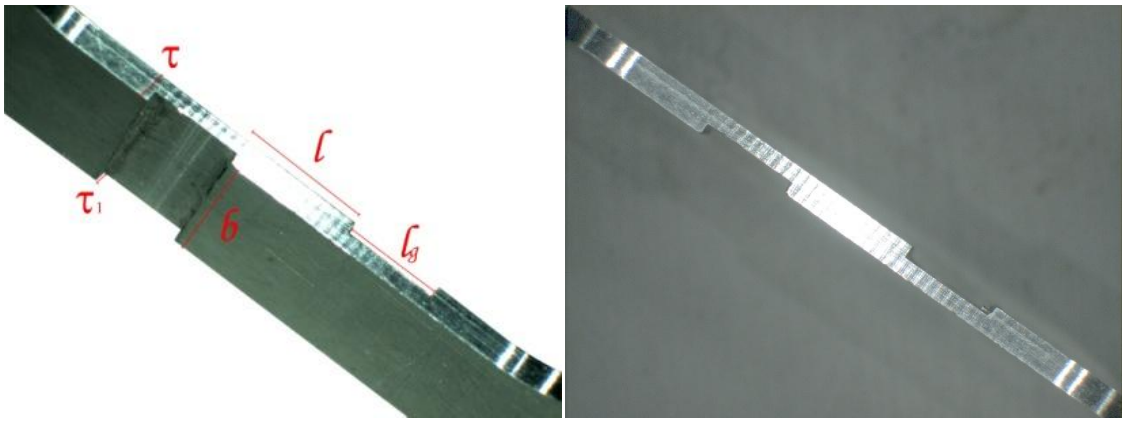

Figure 23: A machined shear-test sample ready for testing, seen from the side.

In Figure 23 τ is the thickness of the sample sheet, τ_1 is the depth of the groove, l is the length between the two cut grooves, l_g is the width of the groove and b is the width of the sample. The cross-section area is given by b*l.

3.2.2.2 Tensile Bond Strength-test Samples

This section describes how the sample for the new tensile bond strength test was performed. In general they were "coins" cut from the sample sheet with a diameter of 15mm, as seen in Figure 24.

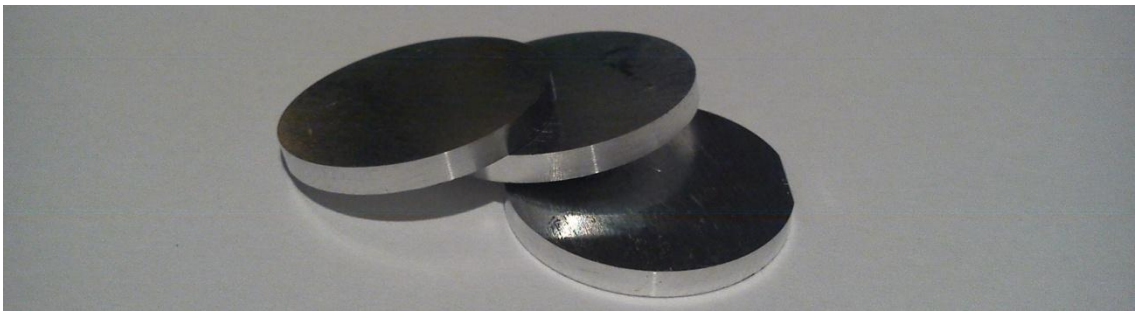

Figure 24: Disc samples like these are cut and machined from cold roll bonded sheets as the one in Figure 21.

A lathe was utilized for the cutting of these samples, after a few attempts on stamping them out showed to severely distort the sample. Other methods like water-jet cutting and even laser cutting was thought of, but disregarded due to high cost and heat concerns with the latter.

Some of the material tested in this study is extremely soft, and in the process of finding a satisfactory cutting method, many samples were strongly affected and some flat out ruined. Friction and adiabatic heating could potentially affect the properties and strength of the bond and for these reasons great care was taken when manufacturing these samples. The samples were first cut roughly to a circle-like shape. Then the last finish was machined with much care and plenty of cooling fluids, to the final diameter of 15mm. After the first set of samples was returned clearly too heavily deformed by the machining, the samples in the latter sets was machined one by one with a brass plate on each side to shield the sample. This brass plate prevented the soft aluminum samples from being welded together as the knife slide sideways over a full stack of them in the lathe. The new precautions ensured good samples quality from this point on.

As the samples with large reduction had bond strength overgrowing the upper limitation of this test-method, a groove was machined in the side of some samples in an attempt to raise the upper strength limit of the method. The idea behind this surgical intervention is to reduce the bonded area while leaving the full surface area of the coins to maintain optimal binding strength to the glue. In Figure 25 there is a sketch illustrating the position of the groove.

Figure 25: A sketch showing where the groove was cut to reduce the bond cross-section.

In cooperation with an employee in the workshop several tools where customized in an effort to achieve the desired result. This was a particular challenging work, as cutting a thin groove in the side of a disc that is no thicker then 1mm requires very small, precise and strong tools. The same type of lathe was used to machine the grooves. A thin knife with a thickness of 0.2 mm, fixed to a steady sliding part of the machine was used to cut the groove into the side of the discs.

3.3 The Roll Bonding Process

The procedure of roll bonding from the selection and preparation of the material through surface preparation and stacking to roll bonding is illustrated below in Figure 26. The surface preparations are explained in greater detail in the following section.

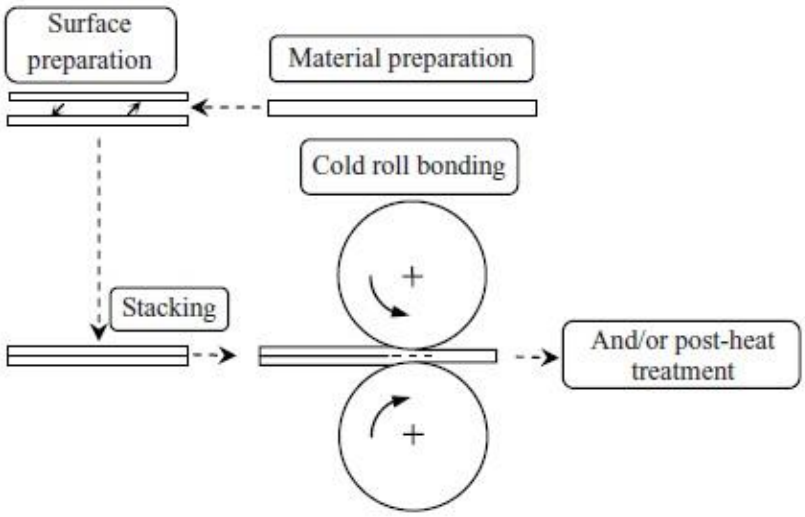

Figure 26: The procedure of roll bonding. [7]

3.3.1 Surface Preparation for Roll Bonding

The first step of the preparation is degreasing, this was carried out with acetone and a paper cloth. After a thorough surface cleaning, two holes were drilled in each end of the strips to enable a quick fixating of rivets in the stage just before roll bonding. Both sample sheets were clamped to the worktable and scratch brushed to remove the

oxide layer and create the desirable roughness in the surface. Scratch brushing on an aluminum surface creates a roughness and certain topography as seen in Figure 27 [4]. A surface such as this is considered well suited for roll bonding.

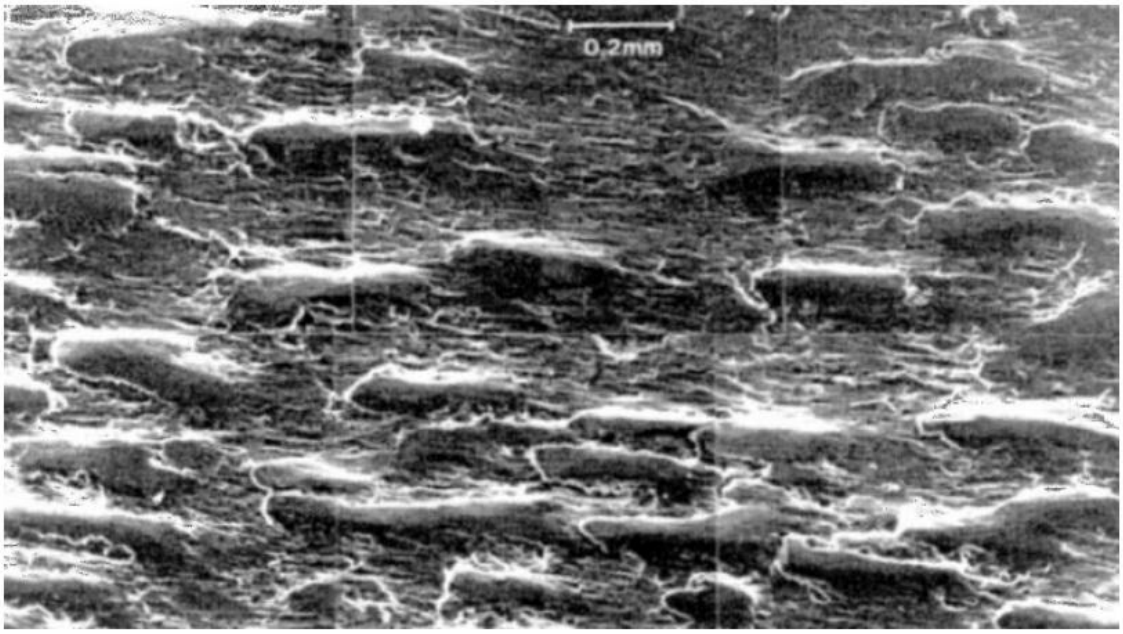

Figure 27: Scratch-brushed aluminum surface. [4]

The following procedure was to clamp the two plates together with rivets in both ends before proceeding to the final roll bonding. This was done to keep the two plates aligned through the mill. As the brushing was carried out by a hand-held machine and the force and intensity thus depend upon the operator, all surface preparation was carried out by the same person. This was done to ensure maximum consistency in this area. Also the time from scratch brushing was initiated to the sample entered the mill, was kept to an approximate constant. This time was for the majority of samples kept close to 90 seconds.

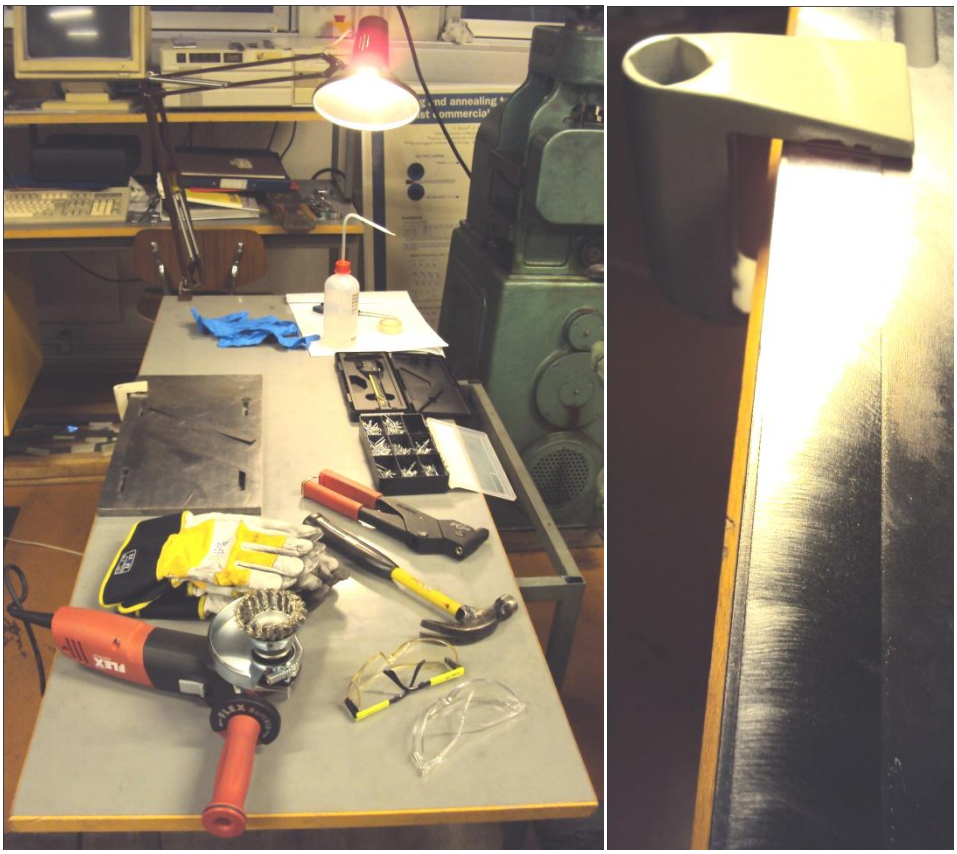

Figure 28: The preparation table and a close-up of a newly brushed sample. The picture is taken during preparation of a peel test sample [10].

3.4 Testing Methods

The two considered test methods; the peel test and the shear bond strength test, do not offer the ideal circumstances for a bond strength test. The peel test being very dependent on the thickness and strength of the bond, resulting in different tearing angle which influence the measured strength. It also cannot be compared to other test methods in a proper manner as the load applied is not distributed to a given area. When performing a SBS test it is the shear strength that is tested, and not the bond strength in a tensile direction.

For these reasons there was desire for a new testing method for evaluating the bond strength between two roll bonded plates. In the following section the preparations and procedures for this new test method, called the tensile bond strength test (TBST), is presented. The last part in this section includes the execution of the SBS test as well.

3.4.1 Tensile Bond Strength Test

The preparation and machining of the disc samples were explained in section 3.2.2.2, and this part will show the reason for these particular shapes. About 7 cm of each roll bonded strip was spent to cut four disc samples, and the rest was saved for comparison with another test.

Also from the workshop, a set of 120 mm long aluminum rods with a diameter of 15mm was ordered. Each of the sample discs was glued with industrial epoxy adhesives between two of these rods and left to cure, like shown in Figure 29. More details on the preparation and gluing is described in the following section.

Figure 29: To the left is a stack of the aluminum rods used to test the disc samples. On the right side is one of the samples fitted in-between two of the rods.

For the strongest bonds the glue alone was too weak and additional measures was taken in hope of raising the limit of the test. Some of the disc samples had a up to 0.3 mm deep groove machined in from the side. Reducing the boned area but leaving the full outer surface for gluing, as explained in section 3.2.2.2 and further discussed in section 5.3.2.

The final TBS testing was performed at different strain rates. While mounting the samples in the MTS, it was discovered that the upper and lower grip was not perfectly aligned, putting a small shear stress on the samples. This shear force was however small, and besides risking fracture while clamping the weakest sample, the small shear stresses was neglected in regards of the measured bonding strength.

3.4.1.1 Gluing Procedure

Some sense of skepticism was hanging in the air, when the idea of an adhesive that should be stronger than a metallic bonding. The first few attempts were made with commercial superglue, bought at a local store. This glue, by the mane Bostik epoxy Rapid, withheld a load of 20MPa before yielding, and can be found in Table C 1 in the appendix. While this glue was by no chance strong enough to overgrow the bond strength of the heavier deformed samples, the hunt for a much stronger adhesive had started. The search ended with a product from Henkel Technologies Norway; LOCTITE 9466 A&B [18]. This is the 2-component epoxy adhesive in the LOCTITE-repertory that reports the highest tensile strength between two metals cured at room temperature.

As for the preparation, slightly different advances were tried out. The general approach was to first pre-clean the surfaces of both rods and the sample with acetone, removing grease and pen marks. This was followed by gentle scratching of the surface on Si-carbide paper. The paper was placed on a flat surface and the sample/rod was scratched onto this, to avoid as much rounding of the edges as possible. Scratching of the surface is a common method in adhesive bonding to increase the grip surface of

the adhesive. After all four surfaces had been scratched the sample and rods were again cleaned in acetone then sprayed with LOCTITE 7063 cleaning spay and dried with a hair-dryer for the last time. Below, four types of slightly different preparation progression are described. Every sample tested, shown in Table C 1, is marked with one of these types.

Type 1: Scratched on Si-carbide paper – cleaned with acetone – dried with a hair dryer.

Type 2: Same as Type 1 + more thorough cleaning and scratching.

Type 3: Cleaned in acetone – scratched on Si-carbide paper in water – cleaned in acetone – cleaned with spray** – dried with a hair dryer.

Type 4: Cleaned in acetone – scratched on Si-carbide paper in water – cleaned in acetone – dried with a hair dryer.

Out of these four types, type 3 seemed to give a more steady results, with fewer samples failing in the glue much bellow the 40MPa region. While time is of the essence, no further investigation was put into this part once a stable method was found.

Figure 30: To the left is a picture of the gluing kit shown and to the right a sample clamped between two rods and a close-up of the glue used.

Due to the small quantities of glue needed per session the mixing tips that followed the glue was not used. Instead the glue was mixed manually on a piece of paper. A thin layer of glue was smeared onto each of the four surfaces, ensuring each surface is well covered and small air bubbles in the glue is minimized. To make sure the disc sample is aligned dead center between the two rods, a plate with a machined v-shaped groove was used when assembling. Figure 31 is showing how the sample is placed between the rods. Once the sample and rods are aligned, a clap, as seen in Figure 30, is gently used to put a compression load on the glued sample. Any excess glue is wiped off, and

for the samples with a machined groove on the side, the groove has to be cleaned thoroughly as it is easily filled with the adhesive during the process. The glued samples are now left for curing in compression for a minimum of 24 hours. Most samples are cured for 3 days or more before the TBS test is performed.

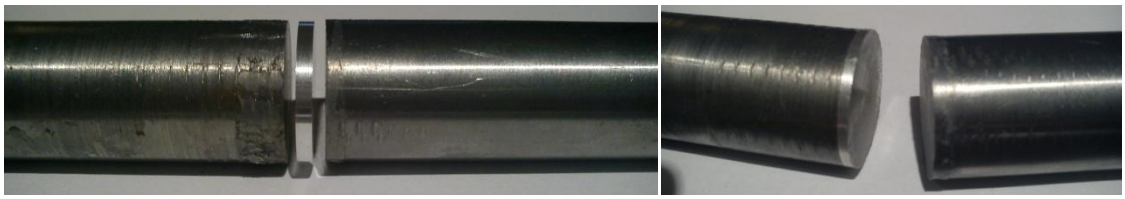

Figure 31: This figure shows how the disc samples are placed between the rods.

3.4.2 Shear Bond Strength Test

As earlier mentioned, a part of the roll bonded strips was saved; this part was used to compare the TBS test to the well established SBS test and machined as described in section 3.2.2.1.

The samples were mounted in the same tensile testing apparatus as the TBST samples, only now with flat clamps and the 5kN load element installed. Great care was taken when mounting the samples to a vertical position with as little angular deviation as possible. The small offset was again observed when the samples were mounted in the tensile machine, but still neglected as a huge concern. A strain rate of 0.2 mm/min with the sampling rate set at 10Hz was used for these tests.

Some angel deflection was observed as the tests were carried out; these observations are discussed further in 4.3.1 and 5.4.1.

4 Results

In this chapter the results of the mechanical testing are presented along with the observations made during a surface analysis in a scanning electron microscope (SEM). Also some results gathered during a previous study by Lauvdal [10] have been included for the sake of compensation.

Out of a total 60 pairs of roll bonded aluminum sheets, only samples from 17 of these sheets gave substantial results during testing. 31 of them where too well bonded for the TBS test and 12 sheets were ruined in the various machining and testing steps.

The samples cut for the TBS test, but outside the test limits of the test, were too small to be tested by both the SBS test and the peel test. The amount of excess material that was left from the roll bonded sheets was too little to create any more shear-test samples.

In this study the samples are named by a system that contains some information about the sample. It is build up of 5 elements; the alloy, batch number, whether it is annealed or not, the number in the batch and finally a test number for cases where several samples from the same sheet is tested. A breakdown of an example is shown below.

Example: A2NA07-T2

A2: The “A” sais that this is an 1200 alloy, while “2” means it is from the second 1200 batch rolled.

NA: ”NA” stands for non-annealed, and the notification for annealed is an “A” in this position. The term non-annealed have the same meaning as work hardened in this context.

07: This number divides the samples with different reduction within one batch.

T2: “T2” indicates that this is the second TBS test carried out on the set of samples that has all the prior notification in common.

4.1 Peel Test

This section holds some of the results achieved in a prior study by Lauvdal [10], which served as a precursor to the current study. The data is presented here for its relevance and direct influence on choices made for this project.

Figure 32: This figure shows how to intrepid the appellations of the peel-test samples. [10]

Figure 32 above, shows a picture of a cold roll bonded strip of aluminum and the different sections for which the samples in that report was named is illustrated.

Table 6: This table show the results from a peel-test carried out on a Al 1200 alloy, which where work hardened by cold rolling to a similar strength as the Al 1200 NA material used for both the tensile and shear test in this thesis. [10]

	Initial Properties								End Properties	
	Layer 1		Layer 2						PT	
#	Alloy	vonMises	Alloy	vonMises	Brush	Brush Speed	Reduction	Speed	Load	Bonding
23BT	Al (1200)	2,08	Al (1200)	2,08	SB 1	3800 rpm	**49,0 %**	3	16,8 N	KB
23AT	Al (1200)	2,08	Al (1200)	2,08	SB 1	3800 rpm	**49,0 %**	3	27,7 N	KB
24BT	Al (1200)	2,08	Al (1200)	2,08	SB 1	3800 rpm	**51,5 %**	5	24,6 N	KB+
24AT	Al (1200)	2,08	Al (1200)	2,08	SB 1	3800 rpm	**51,5 %**	5	19,9 N	
25BT	Al (1200)	2,08	Al (1200)	2,08	SB 1	3800 rpm	**55,1 %**	3	70,2 N	Bonded
25AT	Al (1200)	2,08	Al (1200)	2,08	SB 1	3800 rpm	**55,1 %**	3	55,3 N	Bonded
26BT	Al (1200)	2,08	Al (1200)	2,08	SB 1	3800 rpm	**71,9 %**	3	**254,3 N**	failed
27BT	Al (1200)	1,25	Al (1200)	1,25	SB 1	3800 rpm	**49,8 %**	3	15,1 N	weak KB
27AT	Al (1200)	1,25	Al (1200)	1,25	SB 1	3800 rpm	**49,8 %**	3	18,4 N	weak KB
28BT	Al (1200)	1,25	Al (1200)	1,25	SB 1	3800 rpm	**49,5 %**	3	13,3 N	weak KB
28AT	Al (1200)	1,25	Al (1200)	1,25	SB 1	3800 rpm	**49,0 %**	3	17,3 N	weak KB

In Table 6 the results from a peel-test carried out on a Al 1200 alloy, which where work hardened by cold rolling to a similar strength as the Al 1200 NA material used for both the TBS and SBS test in this thesis. The brush type SB 1, is the same steel-brush as used for scratch brushing the entire sample collection in this current study as well.

In Figure 33 the peak load during peel test from Table 6 is plotted against the reduction. Sample 26BT is removed as it fractured during peeling and is most likely to show the strength of the material itself rather than the bonding strength. The plots are also separated in two rolling speeds, where the velocity for speed 5 is estimated to a value of 150 mm/s, from the measured valued described in section 3.1.1.

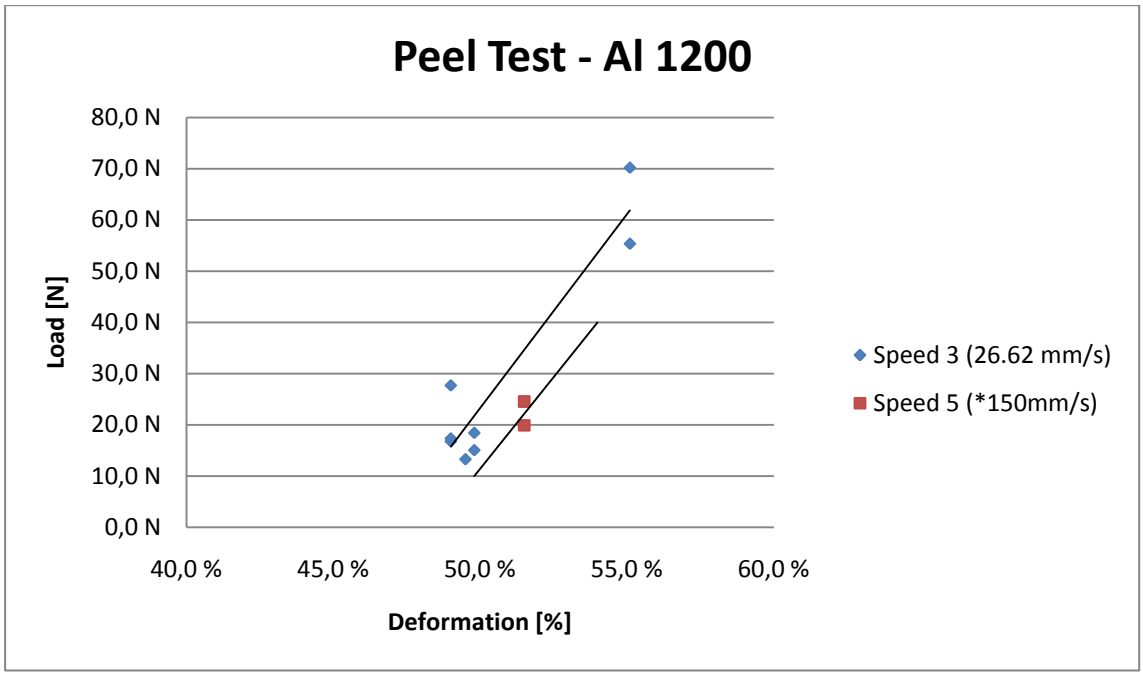

Figure 33: Peel test plots of pre work hardened Al 1200 strips; roll bonded at two different rolling speeds.

Despite a shortage on tested samples at speed 5, there is reasonable indication on lower bond strength at higher rolling speeds.

4.2 Tensile Bond Strength Test (TBST)

Due to a maximum strength limit on this test, samples with a bond strength above 40MPa was not possible to measure as all these samples failed in the glued part before reaching the strength of the bond between the sheets.

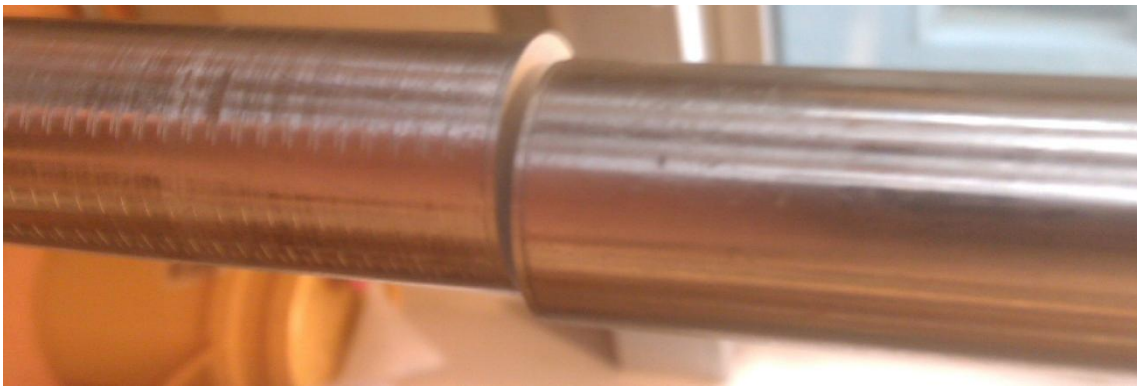

Figure 34: This picture is taken while the sample is in the tensile machine. The bonds have just successfully parted, and the misalignment is clearly visible.

A slight misalignment in a horizontal direction, as shown in Figure 34, caused the weakest samples to break when being clamped into the machine. To reduce this shear force, the upper grip was loosened so that it was able to automatically align itself with the lower grip once tensile force was applied. Any shear forces due to this misalignment, after testing was initiated, was neglected. However the weakest

samples were, as mentioned, ruined due to a short sudden shear force in the moment when the second clamp was fastened.

As a precaution to the misalignment, the rods which the samples was glued to, was clamped on the outer edge with as little grip as necessary. This was to increase the distance between the grips and reduce the influence of any possible misalignment during testing. A risk related to this was that the rod would not be fixed in a perfect vertical position. Any such deviations were kept an eye out for and corrected if necessary.

Some of the earliest TBST samples were ruined during machining. These samples are the non-annealed 1200 alloy samples found in Table B 2 in appendix B, sample A1NA01 trough A1NA07.

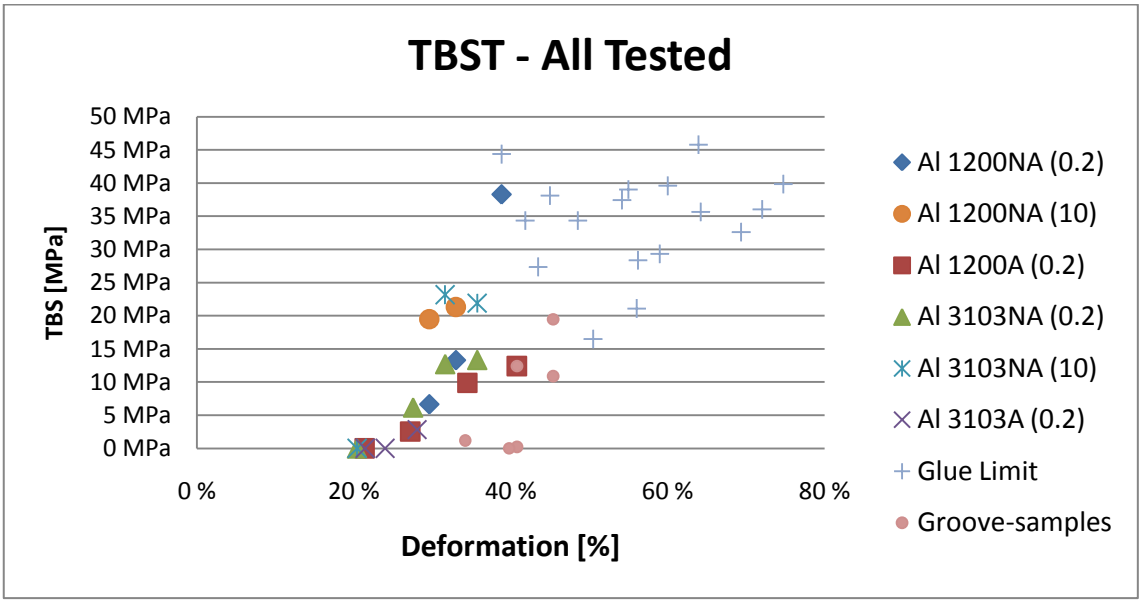

Figure 35: Overview of all samples tested using the TBST.

Figure 35 show the gathered data plots for all alloys, annealed and non-annealed, to give the general trend in increasing bond strength. When plotted together like this the deviations between the different alloys and strain rates are put in perspective. This is discussed further in section 5.3.

The samples marked as kissing bond do not show actual measured bond strengths, but a strength estimated by the operator that executed the test. The samples in question fractured while being mounted, indicating they were only barely bonded. These values are considered accurate within reasonable margins by the operator/author.

The term kissing bond is a trivial name on the initial phase of bonding between two roll bonded plates. It describes a barely bonded state where the sheets is easily separated and consists of more mechanical binding mechanisms then of metallic bonds.

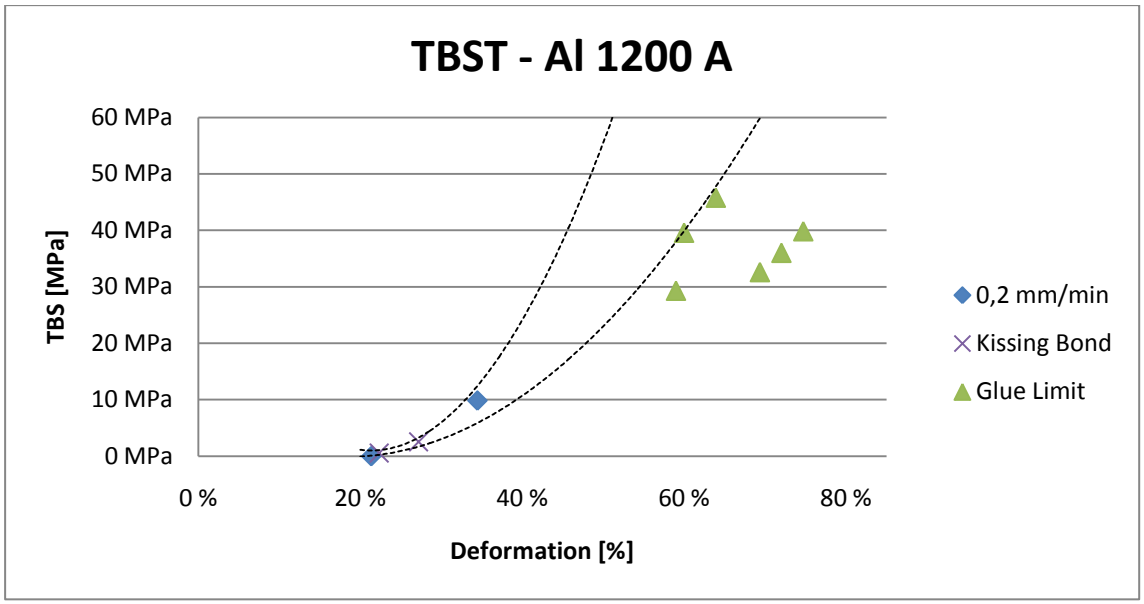

Figure 36: TBST of the annealed AA1200 samples. The lines in this graph are indicating the approximate path where the strength curve is expected to go with increased reduction.

Both the annealed sample collections were subject to a lot of ruined samples during the initial steps of sample preparations. A large portion of the low reduction samples were ruined in both machining of the shear samples and tensile samples. Hence the few data plots for this alloy, shown in Figure 36 and Figure 37.

In Figure 36 an estimated trajectory for the bond strength at increasing reduction, marked by the area between the two dashed lines. The base for this assumption is the measured data at low reductions and the minimum strength at higher reductions, made possible by the glue limit.

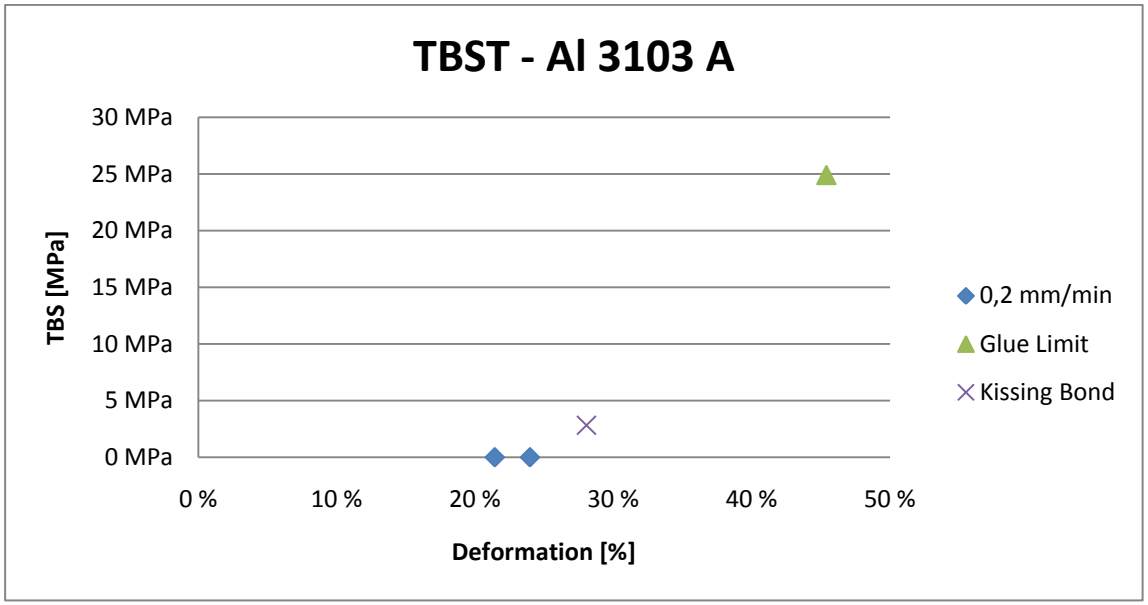

Figure 37: TBST of the annealed AA3103 samples suffered big losses in the machining phase and resulted in very limited results.

Some samples were made with a thin groove machined in depth of 1-3 mm in from the side, reducing the bonding area between the two sheets. The tested strength on these samples showed a negative deviation to the expected strength. Of all the samples with a groove machined in the side only three survived long enough to be tested. These samples can be seen in Figure 35 where they are clearly below the trend of all other samples.

4.2.1 Strain Rate

A few sample pairs were tested at different strain rates and the result from these experiments can be seen in Figure 38 and Figure 39. In first figure a trajectory is made for the combined path of assumed bond strength at increasing reduction. Yet again the glue limit is guiding the path.

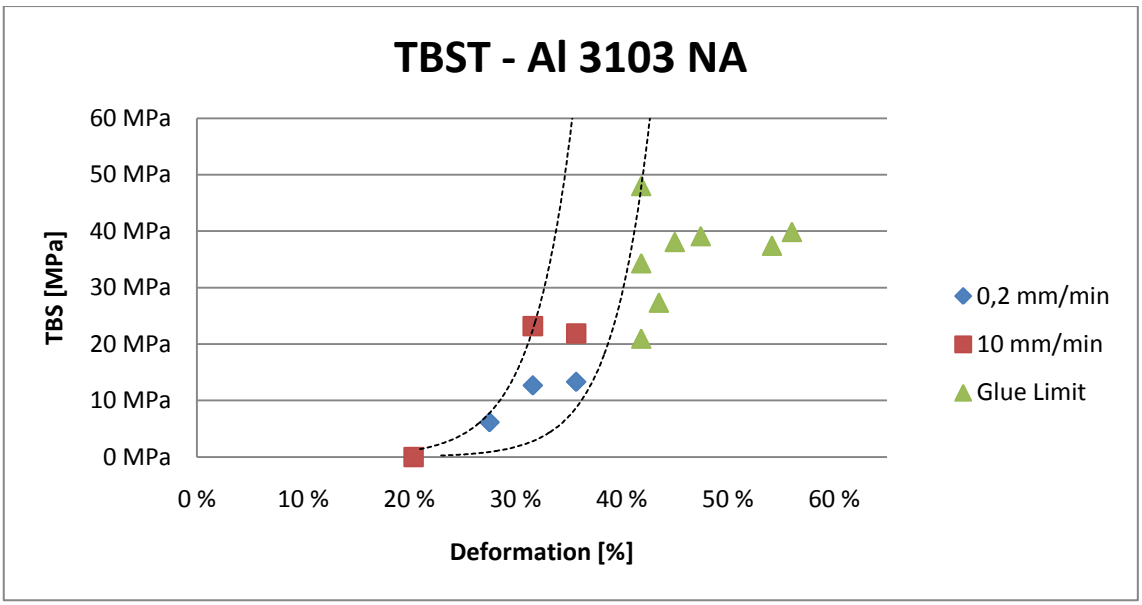

Figure 38: In this figure the gathered path of the assumed strength curve for both strain rates is sketched in for the 3103 samples in the TBST.

Similar results was found in the non-annealed 1200 alloy, shown in Figure 39, but here an individual trend line is added to illustrate the shift in bonding strength between a stain rate of 10 mm/s and 0.2 mm/s. The few plots, do not allow for a high accuracy on the trend lines, but the elevated strength found at 10 mm/s in both the 1200 and 3103 alloy seems clear.

Some sample, for instance the sample marked in Figure 39, under Glue limit at 40% reduction, is tested at a stain rate of 10 mm/min. All samples that failed in the glue are marked by one mutual symbol, regardless of the strain rate of which it was tested. The strain rate does however seem to have an influence on the measured value in both the adhesive bond and the metallic bind, and is discussed more in section 5.5.3.

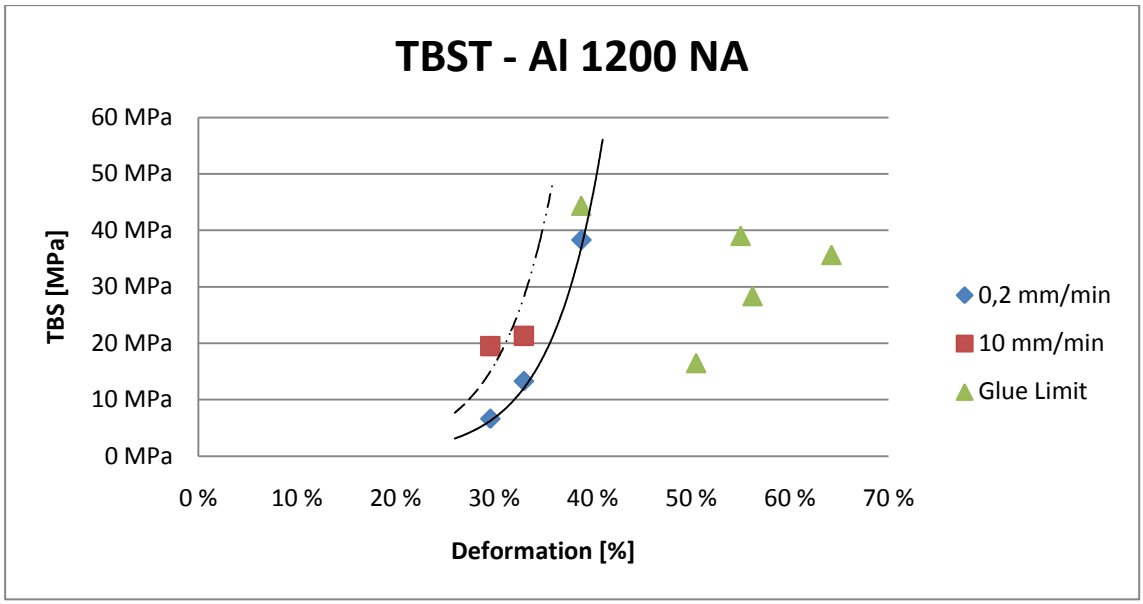

Figure 39: The graph is showing the plots of the Al 1200 samples in the TBST, with a plotted trend line for the samples tested at the two different strain rates.

4.2.2 Gluing Results

The fracture point for the samples that yielded in the glue, reaching from bellow 20MPa up to 40MPa. When a better preparation methods for gluing was established the deviation from what seemed to be the maximum achievable strength was reduced to barely fall below 35MPa. This is based on the waste majority of samples that where tested at a stain rate of 0.2 mm/min. For the samples tested at 10 mm/min the maximum bond strength of the glue was measured up to 48.02MPa.

All glue results can be found in Table C 1 and plotted in Figure 35 through Figure 39.

Except for in a few occasions, all the samples was glued to aluminum rods. The aluminum rods were chosen to ensure that the bonding between the glue and the rod did not have any disadvantage in bond strength when compared to the sample-glue bond strength. Later in the study however, as the datasheet for the new glue was inspected; stronger bonding properties was reported on steel surfaces. As a result to these findings some samples were tested glued to a steel rod. These samples did not distinguish themselves from the aluminum samples in any remarkable way. A further discussion on this topic is found in section 5.3.5.

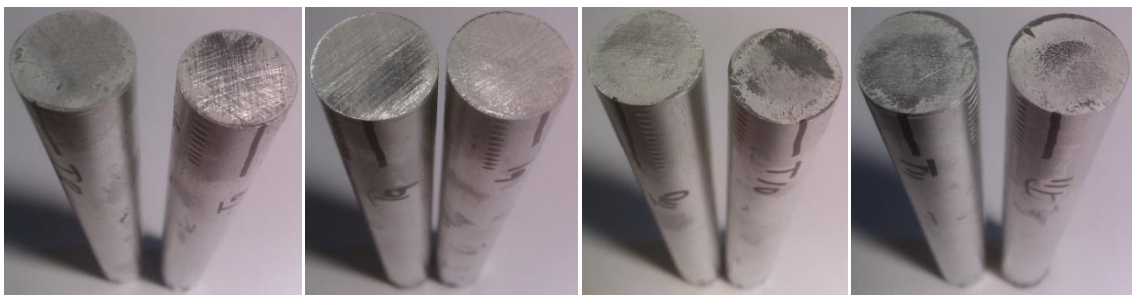

Figure 40: The fracture surface of samples which yielded in the glue. From the left: A1A01-T1, A1A02-T1, A1A04-T1 and A1A06-T1.

In Figure 40 is four pictures taken of the fracture surface of four samples where the glued bond was the first to yield. The surfaces of these samples and rods show a variation cover of epoxy residue. Some seem uneven, and some have a clean outer rim that could indicate no bonding in the area. This would reduce the strength directly by the fraction of the non-covered area. Attempts were made to improve and correct this as the experiments progressed by higher and lower compression during curing and by scratching with different grit size. The amount of other necessary variable made it impossible to confirm any improvement with the changes made and any further experimentation were not pursued. The grit size and preparation type for these samples can be found in Table C 1 in appendix C.

4.3 Shear Bond Strength Test (SBST)

As the "state of the art" method of testing bonding strength, this method was included as a comparison to the new TBST.

In the initial phase of machining the SBST samples, a few was ruined. Adjustments were made as a result of the losses, which lead to a much safer production. The method was now able to produce samples for testing that was just barely bonded.

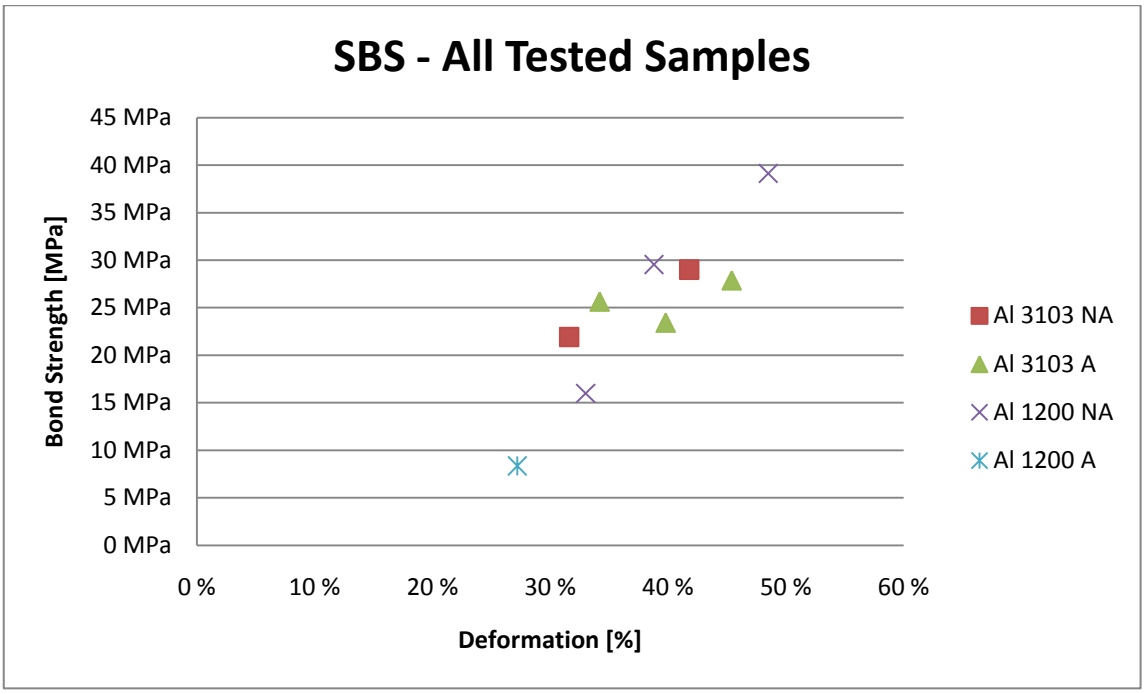

Figure 41: The graph shows the plot of all successful SBST samples.

Figure 41 show the full plot of all the successful SBS tests performed. Unfortunately in the majority of cases, either the SBST sample or the TBST sample from each pair was in some way ruined in an almost perfect overlapping pattern. Only a handful of the paired up comparison tests made it through all machining and testing phases. These

results are compared in Figure 42. The TBST samples are scattered on both side of the SBST strength curve. This is discussed further in section 5.5.

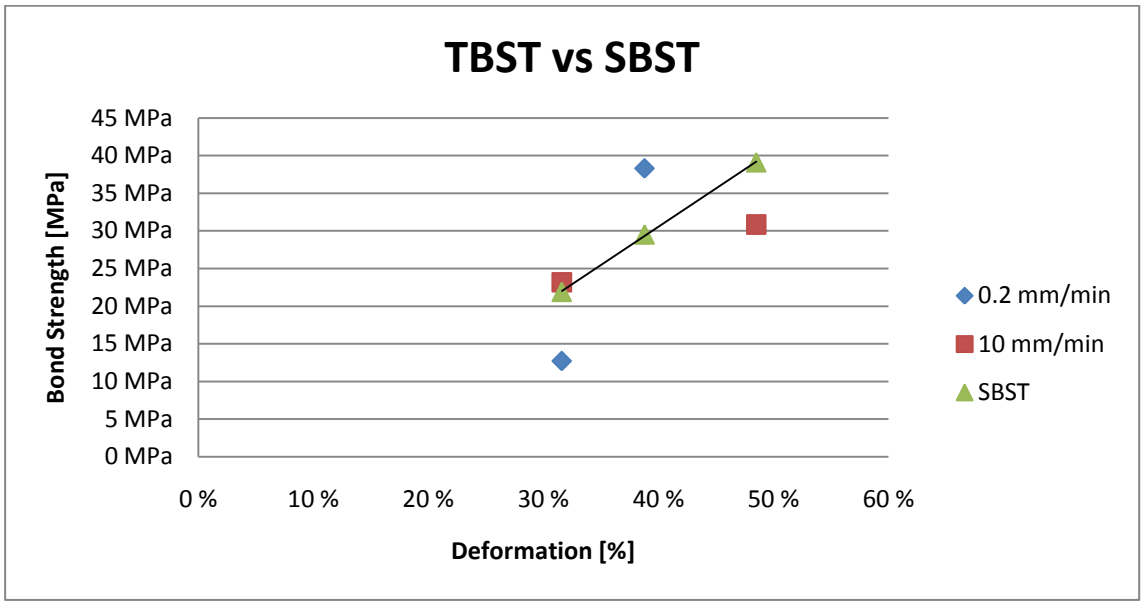

Figure 42: The graph is showing the compared results from an SBS test and a TBS test, where identical sample pairs have been tested against each other.

Table 7: This table is containing the data which Figure 42 is plotted from.

	TBST		SBST
Reduction	0.2 mm/min	10 mm/min	
38,80 %	38,29 MPa		29,54 MPa
48,50 %		30,85 MPa	39,12 MPa
31,60 %	12,70 MPa	23,17 MPa	21,92 MPa

4.3.1 Angular Deflection

While testing the SBST samples an observation was made. The angle at which the sample was split changed during the tensile loading. When mounted and before any load was applied all the samples were of course standing horizontally, and while the initial load was applied the stresses was 100% shear. As the load increased the angle increased as well, as seen in Figure 43 of a sample after fracture.

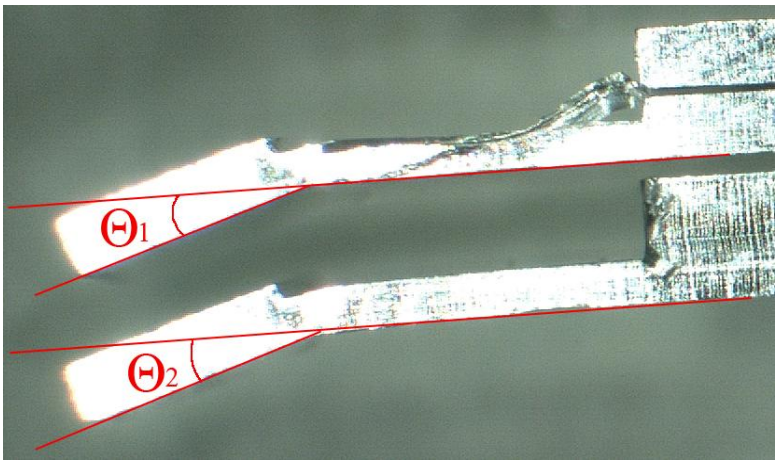

Figure 43: Illustrating how the angle was measured on SBST samples.

A set of macro pictures was taken of all the SBST samples and the angle was measured for both parts, as shown in Figure 43. The average value of the two measured angles was used as the angle for that sample, and everything is discussed in more detail in section 5.4.1.

Table 8: This table lists the correlations between the angle Θ, the overlap length l, the reduction % and the bond SBS.

Sample	Θ(snitt)	l	%	SBS
B2NA05	**3,1°**	2,50mm	41,8 %	29,00 MPa
B2NA03	**1,3°**	2,50mm	31,6 %	21,92 MPa
B2A06	**14,0°**	2,50mm	45,4 %	27,88 MPa
B2A05	**4,0°**	2,50mm	39,8 %	23,42 MPa
B2A04	**18,4°**	2,50mm	34,2 %	25,64 MPa
A2NA04	**19,2°**	2,50mm	48,5 %	39,12 MPa
A2NA03	**6,5°**	2,50mm	38,8 %	29,54 MPa
A2NA02	**3,9°**	5,00mm	33,0 %	15,98 MPa
A2A03	**4,5°**	10,00mm	27,2 %	8,36 MPa

To filter out static two of the samples which had a different overlap-length was discarded, when an attempt on connecting the angle deflection to the bond strength. These two samples are marked grey in Table 8 and the comparison to the degree of reduction is plotted in Figure 44.

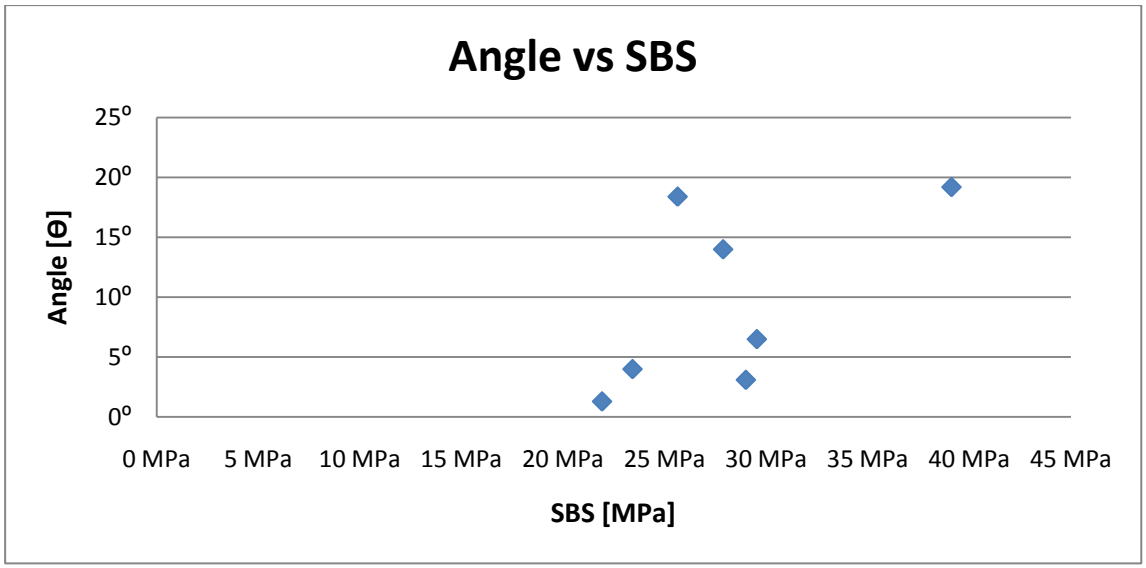

Figure 44: Shows a plot of samples in Table 8 comparing the angle with the SBS.

As the bond strength is directly influenced by the reduction, the angle can be compared to the reduction as well, seen in Figure 45.

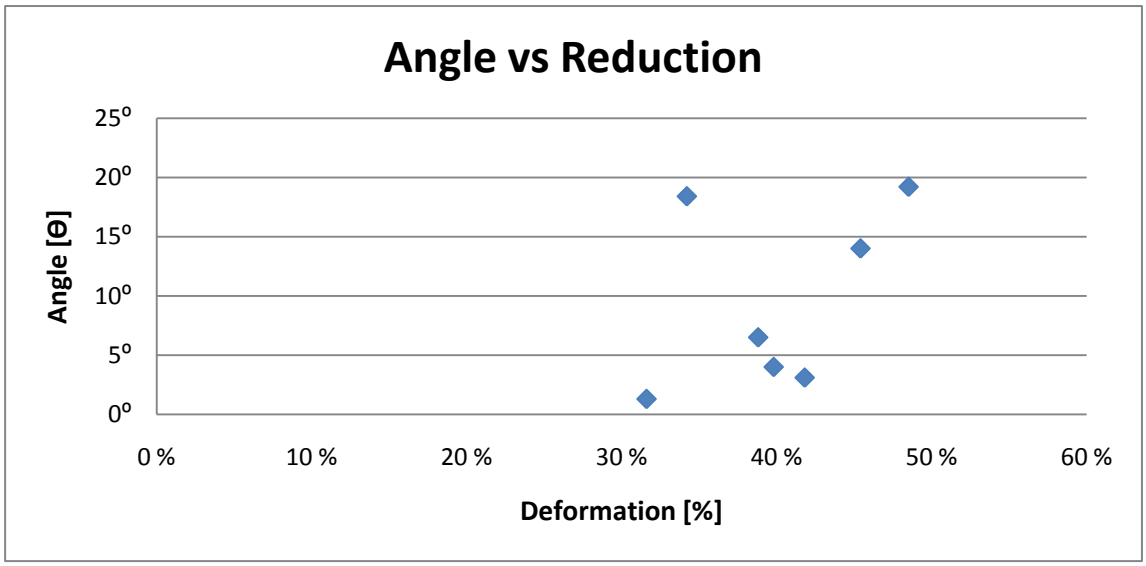

Figure 45: Shows a plot of samples in Table 8, comparing the angle directly to the reduction.

4.4 Fracture Surface Investigation

The fracture surface was investigated in a scanning electron microscope (SEM). The investigation focused on finding abnormalities, crack initiations, bonding patterns etc.

In addition to the pictures presented in this section, a larger selection of SEM-pictures of the fracture surfaces is listed in the appendix under section E.

4.4.1 Bond Types

The primary thing to look for is signs of bonding. Figure 46 shows the characteristics signs of a ductile fracture. Further details are also seen in Figure 55 in section 5.6.1 where the topic is discussed.

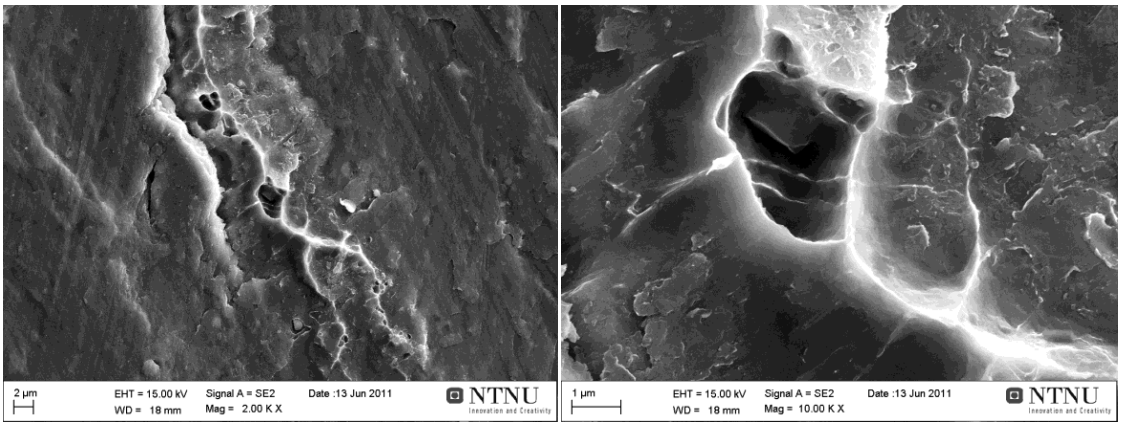

Figure 46: Typical sign of a ductile fracture seen on the fracture surface of sample B2A04-T1 A.

4.4.2 Crack Direction

At higher reduction it is clear, from observations in SEM images, that bonding mainly occurs in lines stretching normal to the rolling direction. Figure 47 shows the surface of a shear test sample with these categorist lines. Due to the shape of the sample the rolling direction, is known. The rolling direction is indicated by arrows in Figure 47. These characteristic lines were first observed on the fracture surface of a TBST sample, but with the information on rolling direction lost due to the circular shape of the samples, the mentioned hypothesis could not be confirmed at that point. More pictures showing these bonding lines can be seen in the additional pictures found in the appendix section D and E.

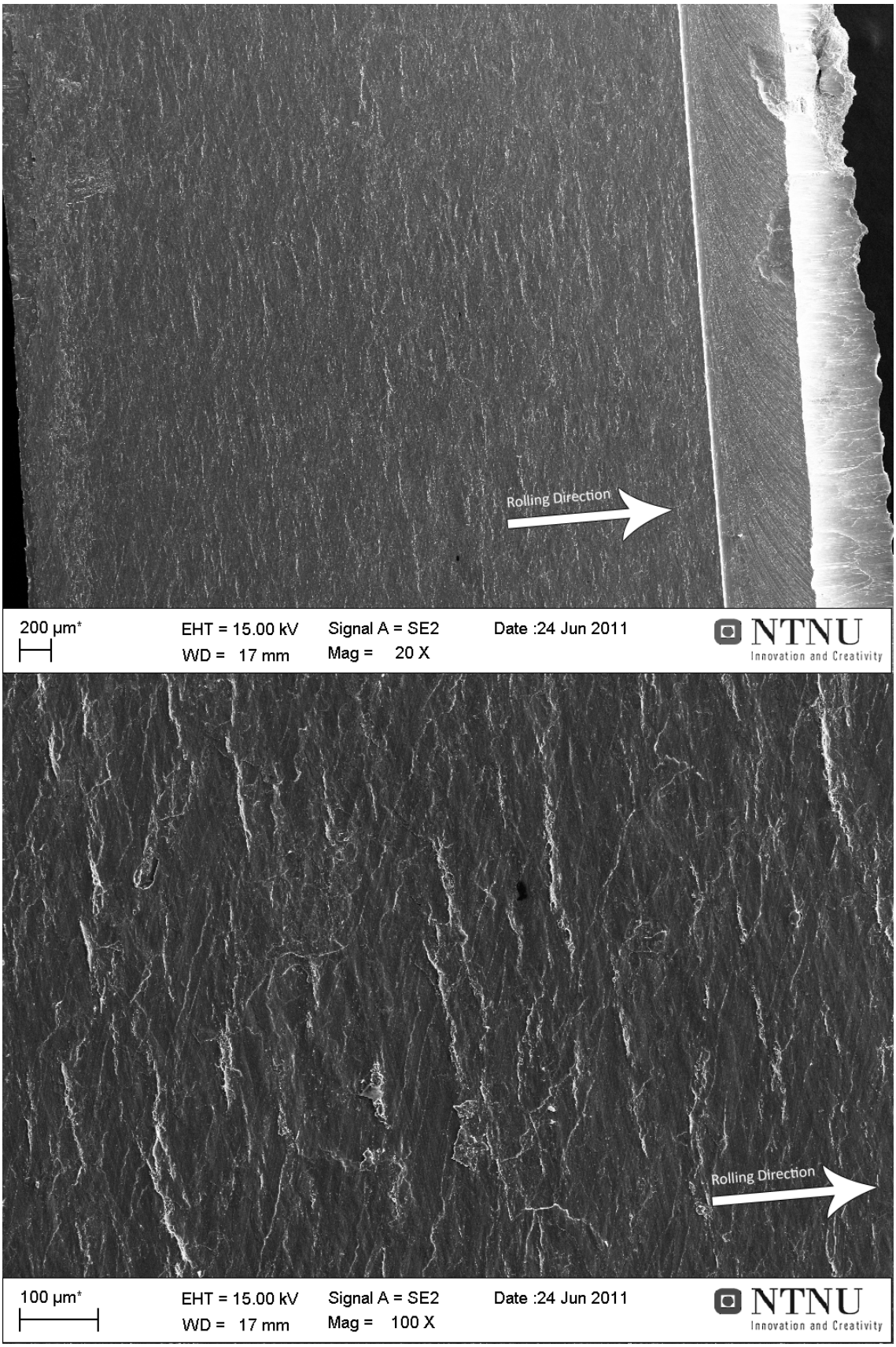

Figure 47: The fracture surface of sample A2NA02 seen from above. Al 1200 Non-annealed, 33% reduction. Showing the bond-lines stretching normal to the rolling direction at 20x and 100x magnification.

4.5 Surface Roughness

A random sample was chosen to determine the surface roughness of plate strips prior to roll bonding. As the time from the strips were brushed to they are roll bonded is crucial to maintain short, roughness testing of each sheet is not practical possible. The chosen sample is scratch brushed under the same circumstances as all other scratch brushing performed in these experiments.

The result from the roughness test on the scratch brushed sample was as follows:

Ra 2.5x5: 2.43 µm

4.6 The Effect of Rolling Speed

The most interesting result, seen in Table 9, of the effect of the rolling speed on the bonding strength was found between the sample sets 21BT/AT and 22BT/AT, which were rolled at the speeds 1.5 and 5 representatively. As the speed scale is exponential increasing makes this a pronounced speed difference. Both sample 22BT and 22AT failed to be peel-tested due to the high bond strength and thin sheets. However by comparison one could tell these samples contained a far better bond then the slower rolled samples. The samples rolled at higher speeds gained a much higher temperature during roll bonding due to adiabatic heating. The temperature in the material during or after cold roll bonding was not measured by any instrument, but the heat differences were noticed by the operator.

However the results found in another section of this same study shows the general accepted idea that higher bonding speed gives weaker bonding, as seen in Figure 33. These observations are discussed further in section 5.7.

Table 9: Results from rolling speed test. [10]

	Initial Properties								End Properties	
	Layer 1		Layer 2						Peel-Test	
#	Alloy	vMises	Alloy	vMises	Brush	Brush Speed	Def. %	Speed	Load	Bonding
13BT	Al (1200)	3,03	Al (1200)	3,03	SB 2	3800 rpm	61,6 %	**3**	6,2 N	weak KB
13AT	Al (1200)	3,03	Al (1200)	3,03	SB 2	3800 rpm	59,3 %	**3**	-	weak KB
14BT	Al (1200)	3,03	Al (1200)	3,03	SB 2	3800 rpm	59,3 %	**2**	-	weak KB
14AT	Al (1200)	3,03	Al (1200)	3,03	SB 2	3800 rpm	59,3 %	**2**	-	weak KB
21BT	Al (1200)	3,03	Al (1200)	3,03	SB 2	3800 rpm	58,1 %	**1,5**	16,5 N	KB
21AT	Al (1200)	3,03	Al (1200)	3,03	SB 2	3800 rpm	58,1 %	**1,5**	33,5 N	KB
22BT	Al (1200)	3,03	Al (1200)	3,03	SB 2	3800 rpm	58,1 %	**5**	-	too strong
22AT	Al (1200)	3,03	Al (1200)	3,03	SB 2	3800 rpm	58,1 %	**5**	-	too strong

4.7 Bond Interface

The interfaces of three samples were investigated in a scanning electron microscope (SEM). All the samples were first molded in an epoxy to ease the initial grinding; first on Si-carbide paper (grit 80 to 2400), followed by polishing down to 1µm. The in the end, two of the samples was finished off with electro polishing, as described in section 3.1.2. Just before the samples was mounted on a sample holder for observation in the SEM, the sample was broken out of its mold and cleaned for two minutes in a bath of acetone by ultrasonic vibrations.

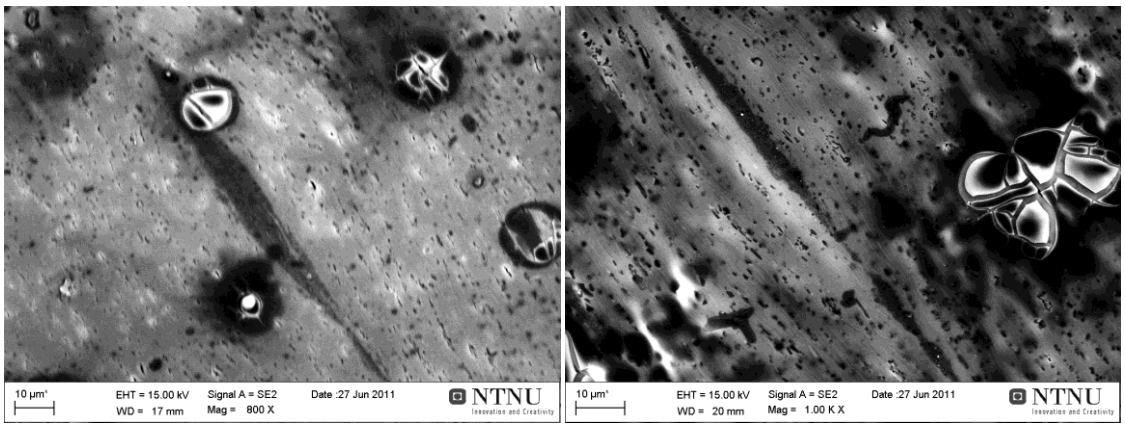

Figure 48: Sample A2NA02 observing the bond interface from the side. From the left a 800x and 1000x magnification image of the interface of roll bonded aluminum. The electro polishing for this sample was not fully satisfactory, but the interface is yet clearly visible.

The electro polishing was not fully satisfactory, but still the samples were passed on to the SEM for investigation. Despite the preparation was far from perfect, it was sufficient to make out what was expected. Figure 48 show a magnified SEM image of what is the fractured oxide layer between the two roll bonded sheets. More images of this interface are found in appendix F.

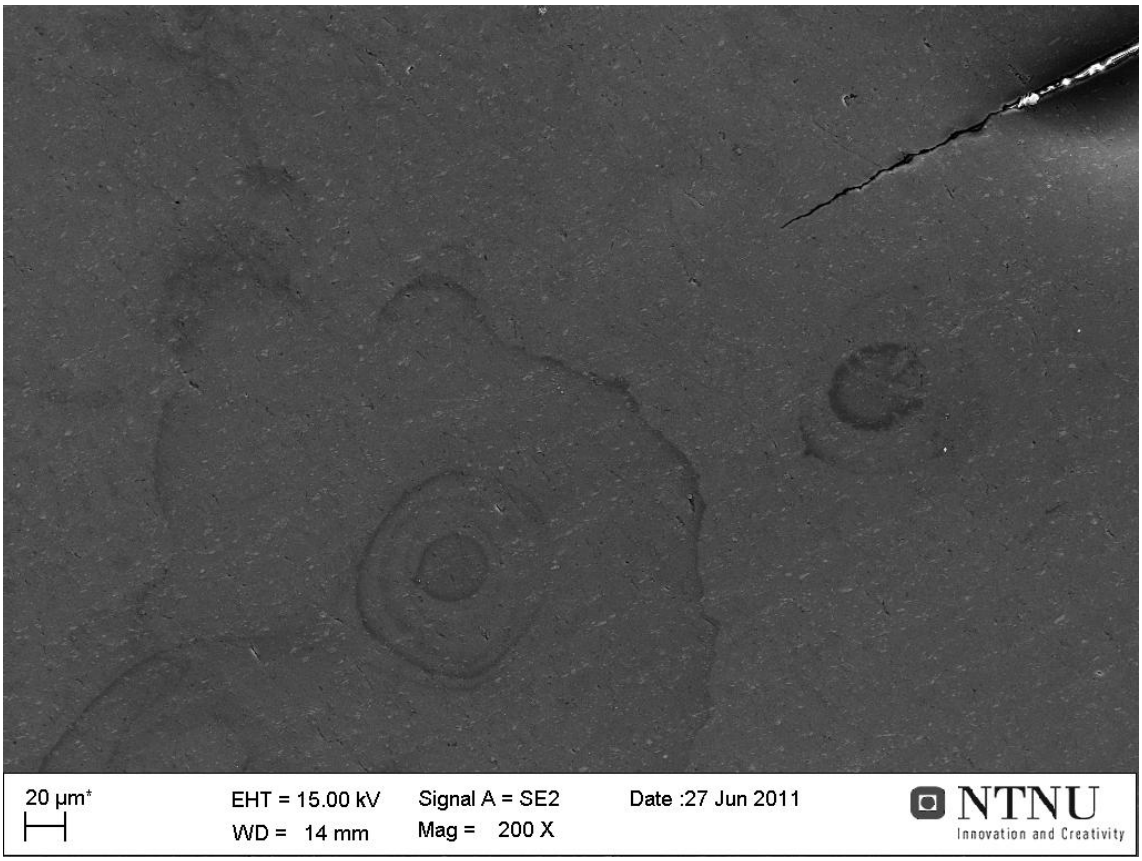

Figure 49: This figure shows a SEM image of a sample that was stopped mid process in roll bonding. The interface seen from the side.

Figure 49 shows an image at 200x magnifications of a sample that was stopped mid process during roll bonding. The sample was cut out, slit in the rolling direction and prepared in the same manner as the other interface-investigated samples, except for the electro polishing. In the top right of Figure 49 the transition between bonded and not-bonded is visible at the end of the crack.

On the second disc shaped sample no interface was found and the surface was not photographed.

5 Discussion

In this chapter the results found is discussed.

5.1 Material Selection

The material selection was composed of a 1200 and a 3103 aluminum alloy, which were work hardened and annealed to different strains.

From Figure 35 a slightly increased strength can be observed in 1200NA from the 1200A, and the same can be seen for the 3103NA compared to the 3103A. When comparing the 1200NA to the 3103NA, no notable difference in bond strength can be found. The same applies for the comparing of 1200A and 3103A.

Even though the strain hardening has an effect on the bond strength, it is very small. The property differences between the 1200 and 3103 alloy seems to be too small to give any fluctuations in the bond strength. In comparison the strain rate at which the samples were tested, has a much higher influence on the measured strength, this is discussed further in section 5.3.4.

5.2 Surface Preparation

When dealing with roll bonding the most important feature for success is a proper surface preparation. If nothing is done to the surface of an aluminum sheet, it will be greasy, have a very thick hard oxide layer and the topography of the surface will not be ideal for a good bonding. All these factors will prevent all the bonding mechanisms and a bond might be practically impossible. This section is discussing the effect of these parameters in more detail.

5.2.1 Degreasing

In a former study on roll bonding by Lauvdal [10], degreasing with ethanol was tested. The high critical deformation threshold (CDT) observed in that study raised concerns. One of the reasons for this was believed to be the use of ethanol instead of acetone for degreasing. Ethanol being less viscous and a poorer solvent then acetone could support this assumption. In this study acetone was utilized and a comparison to the prior study was attempted.

The Al 1200 non-annealed samples from each experiment were chosen as they are of the same material composition and have experienced approximately the same work hardening. Although the peel test does not give any good comparison of the bond strength, it does give a good indication on at which reduction bonding begins. At the peel test carried out with degreasing with ethanol the lowest measured bonding was at 49.0% reduction and a peel-test strength of 27.7N, as found in Table 6. Based on the

trend line in Figure 33 it is reasonable to assume that bonding in this case did not start much lower then at 45% reduction. When comparing this to the lowest tested TBST sample at 29.6% reduction, which were tested to a TBS of 6.63MPa (at 0.2 mm/min) and withstanding 13.02MPa in the SBS test. The SBS test of this sample ended with a fracture in the material itself while the bond held; hence the real SBS is not shown. If a similar estimation was to be made here, based on the trend line found in Figure 39, it would indicate the bonding started around 25% reduction.

Before drawing any conclusion there should be mentioned that the degreasing agent is one of two factors which could cause this dramatic difference. The peel-tested samples were exposed for oxygen in the environment for up to 5 minutes before being roll bonded. This is more than three times longer than The TBST and SBST samples, and allows for formation of a thicker oxide layer. The ideal thickness of an oxide layer on aluminum for roll bonding is not known by the author, but is discussed in section 5.2.4.

In section 5.2.4 a comparison to 5 other experimental studies have been carried out with regard on the thickness of the oxide layer. At two of these studies the exposure time for oxide growth was similar to the one discussed here, 5 minutes, except the elevated heat. These two studies report bonding at hence 24% and 47% reduction, where one strongly supports the effect of acetone vs. ethanol, while the other shows the same result with acetone. The comparison is inconclusive.

The reduction at were bonding starts going from 45% to 25% reduction is a huge improvement, and from what have been discussed above two out of three comparing studies support that acetone is a far better degreasing agent the ethanol, as far as at which reduction bonding begins.

5.2.2 Scratch Brushing

In a study by Zhang et. al. [17] it was found that semibright- and chemical Ni plating gave bonding at a lower reduction then scratch brushing. The publication concludes that Ni plating is the optimum preparations method for al-al cold roll bonding. This conclusion might be true in some or most cases. However, the thoughts of the author are that the term “better” or “optimum” is dependent on the desired properties for the use in mind. In Figure 50, the scratch brushing curve has a steep climb in strength and passes Ni plating in shear strength already at around 42% reduction. In the case of ACRB, a reduction of 50% may be desirable as one can maintain the total thickness of the plate throughout the process. This can have practical industrial advantages such as the roll gap can be kept constant, saving adjusting time, simpler and cheaper mills, or/and fewer rolls. For such situations the higher strength from scratch brushing might be desirable.

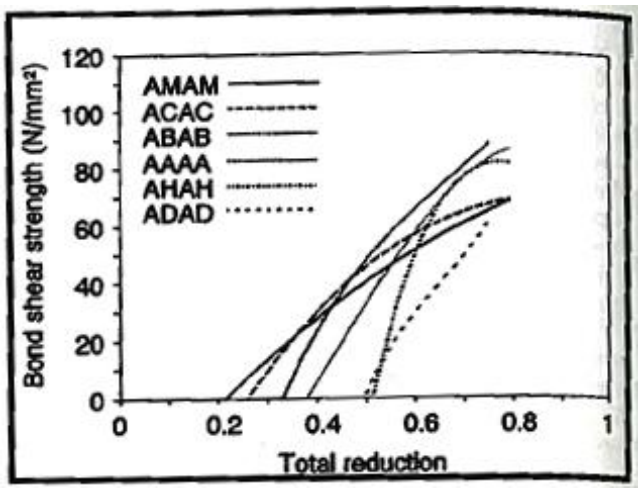

Figure 50: Graph showing the shear strength of a cold roll bonded aluminum strips for increasing reduction. AMAM is for semibright matt Ni plating (starts at 0.21), ACAC is for chemical Ni plating (starts at 0.26) and ABAB is for scratch-brushing (starts at 0.33). The remaining is of less interest for this report. [17]

In a study made 5 years earlier, also by Zhang et. al. [11] the results is basically reversed. The scratch brushed samples now shows bonding almost as low as 20% reduction, much like what was found in this current study with scratch brushing. The chemical NI plating passes now the scratch brushed samples in bond strength somewhere above 40% reduction, as seen in Figure 51. The reason for this contradictory result was not found.

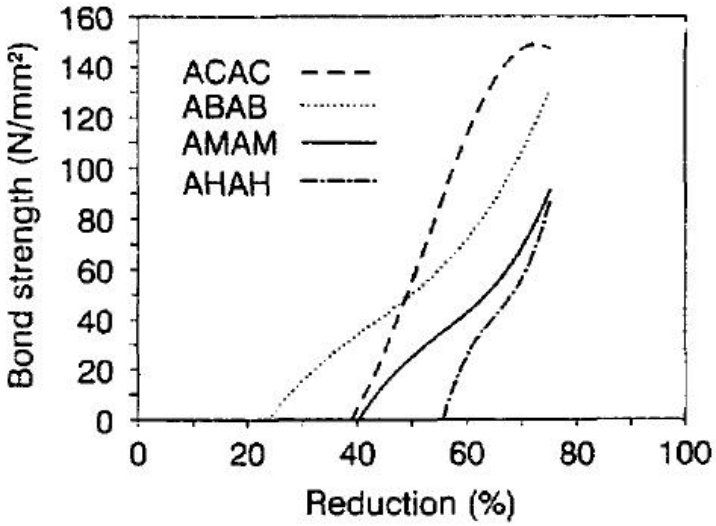

Figure 51: Graph showing the bond strength of a cold roll bonded aluminum strips for increasing reduction. ACAC is for chemical Ni plating (starts at 0.39), ABAB is for scratch brushing (starts at 0.23) and AMAM is for electrochemical matt nickel plating (starts at 0.40). The last curve is of less interest for this report. [11]

5.2.3 Brush Speed and Force

One parameter in question when searching to achieve strong bonds at cold roll bonding, is the local hardening of the surface while scratch brushing the plate or sheet surface. In addition to remove the oxide layer, brushing with a steel brush also deforms and hardens the surface. This straining of the surface makes it harder and less

ductile, and under deformation it will fracture more easily and have a desirable effect on the bonding strength.

In this current study both brushing force and brushing speed was kept at a constant, to allow more time to be focused on the other parameters involved. The effect of these parameters is discussing the results found in a study by Lauvdal [10].

The results from those experiments showed no clear indication that variation in brushing speed or the force had any impact on the bonding strength, beyond a minimum amount. This minimum amount required is not easily quantified or explained, but found rather quickly when performing the task. It should leave a distinct dim finish with a clear shift in reflected light on the surface. When the scratch brushing was increased slightly more a new pattern could be observed if looking closely. This pattern could resemble the skin of an orange, only crumpled. Although the surface was not observed in a light microscope or SEM, this pattern could well be equivalent to the one in Figure 27.

No attempt was performed in discovering a possible limit where even non-scratch brushed sheets of aluminum would bond. However, later in that study a non-scratch brushed area was used to prevent bonding in a small area on the peel-test sample. These samples were rolled up to over 80% reductions without any observations of bonding in this non-scratch brushed area. These results were deemed sufficient to decide a down-prioritizing of these parameters in this current study.

5.2.4 Effect of Oxide Layer

In this experiment the exposure time allowing oxide growth was kept to 90s and SEM analysis of the interface showed the oxide layer to be 5µm thick. To refresh the key preparation factors; acetone was used for degreasing, the samples were scratch brushed and no heating of drying period was performed. Across all the samples bonding was reported as low as at 22.3% thickness reduction, although a very weak bond. When these results was compared to a prior study where the degreasing was carried out with ethanol, found in section 5.2.1, there were indications that the degreasing agent could be the main cause for the huge improvement. This section is looking closer into whether or not the oxide layer thickness has any effect on when bonding starts.

The effect of the oxide layer was compared to five other studies where all included degreasing in acetone and scratch brushing. Two of the studies dried the sample in a furnace for 5 minutes while the other three held the exposure time for oxide growth low and at room temperature.

An experiment carried out by M.Z. Quadir et. al. [6] dried the sheets in an air circulating furnace at 300°C for 5 minutes in addition to the common preparation mentioned above. The peel test carried out proved bonding started at around 47%

reduction. When drying an aluminum sheet in an air circulating furnace at high temperature, the oxide growth is accelerated. It can safely be said that there was a very thick oxide layer on the surface of these sheet prior to roll bonding. From the given data it is natural to assume the thick layer of oxide might have prevented bonding at low reductions. The samples were also roll bonded at 300°C.

In another experiment by W. Zhang et. al. [11] cold roll bonding was carried out after the sheets had gone through the common preparations mentioned and dried in a furnace at 150°C for 5 minutes. Although these where dried at a lower temperature the time allows a considerably amount of oxide to form. The odd part with this test is that bonding is reported as low as at 24% reduction. The bond strength was tested by a type of tensile testing method unfamiliar to the author. This result could indicate that the thickness of the oxide layer has less or no influence on at which reduction bonding begins.

N. Bay et. al. [21] present yet another study where the aluminum sheets where cleaned in acetone, but this time cross shear roll bonded immediately after scratch brushing. It should be mentioned that cross shear roll bonding (CSRB) is a method where upper and lower roll is rotating at different speed, or have different diameter so that the velocity on the roll surfaces is different from each other. This method is commonly used bonding two metals with different hardness. It has also showed improved bond strength by the use of this method.

The short exposure time should leave a rather thin oxide layer, and with bonding proven at 30% and probably considerably lower when considering the bond strength. This result will again be in favor of the theory of thinner oxide layer giving bonding earlier. Of course the use of CSRB is something to take into consideration; in addition to the fact that the samples were annealed post roll bonding, which has a proven positive effect on the bond strength [23].

In a paper by R. Jamaati and M.R. Toroghinejad [22] preparations were carried out with degreasing with acetone, scratch brushing, then cold roll bonded after 120s. A peel test revealed bonding as low as 30% reduction.

One year later R. Jamaati and M.R. Toroghinejad [23] published a similar study where the preparations were the same, and found bonding at around 33%, just slightly higher.

The last two results show bonding at a decent level of reduction. Had it not been for the fact that bonding where found at around 23% reduction, in [11] where the oxide is assumed to be much thicker than in the latter examples, the conclusion would have been easier to draw. Acknowledging parameters outside the ones that have been taken in account which could be of influence to the presented results, a trend will judge the conclusion here.

All three of the experiments with assumed thin oxide layer, four, if the one in this current study is added, show bonding at a relatively low reduction, from 30% and below. On the other scale, the two experiments are divided. One of them is showing that bonding do not occur until a very high reduction, 47%, and another showing bonding alongside the best "thin oxide layer" experiments, at 24% reduction. One could keep in mind the results of the peel test carried out by the author in a prior study [10], where bonding where found at above 45% with 5 min exposure time before cold roll bonding. This study used ethanol to degrease the samples however.

The trend however, the deviation in results, indicates that bonding is likely to occur at a lower reduction when the oxide layer is kept thinner.

5.3 Tensile Bond Strength Test (TBST)

The idea of this test was to be able to measure the tensile bond strength directly, and in a way that the results easily can be compared cross studies. With little to no restrictions to the material properties or geometry or such parameters that is most likely to vary frequently from one test to the next. In addition the measured value will be directly comparable to the yield strength of the material.

Another advantage with this method is that it required very little material to perform the test. All that is needed is a 15 mm (or less) circular disc from the bonded area.

5.3.1 The Machining of the Disc Samples

Since the machining of the coins were done by a workshop, and for most of the time without the authors supervision, the understanding of what forces these sample was exposed to, is not fully documented. The process was supervised on the machining of some of the coins and at that stage it seemed ok. A compression force, which could not be measured, was applied by a screw-clamp tightened by the operator to hold the samples in place in the lathe during the machining. This compression force was one of the concerns in this process. If the compression was high enough it could affect the bond strength, which by obvious reason is very bad for any test sample.

When the first batch of samples were returned from machining this concern became reality, as each and all samples were severely deformed and had deep circular scratches in the surface. The explanation from the workshop was that the material was too soft and the samples had been welded together during the machining. To separate the disc the operator had to use clamping tools and twist the disc to part them. Since the operator had stacked a large amount of samples in the lathe at the same time, to save time, the compression force needed to hold all the samples in place also increased. This high compression force combined with the adiabatic heating from the knife cutting, and low yield strength of the soft aluminum was a recipe for disaster. Needless to say, these samples were trashed.

As mentioned in section 3.2.2.2 a solution was found for this problem; greater care was taken by machining the softest samples one by one and adding a brass plate on each side of each sample to prevent friction welding between the soft aluminum as the knife cut through. Even with this method there were occasionally found samples which were visibly affected. The most common flaw was a small crack opening in the bond interface, visible the naked eye. There is a possibility that the opening was left behind by a poorly bonded area of the roll bonded sheet. All the material sent for machining were carefully chosen from areas of the sheet that should be within the proper bonded region. However, the cause for these cracks cannot be determined.

One theory and concern to how the cracks mentioned above might have occurred, is from the knife cutting the samples. This is a knife that is fixed in a holder that can be moved in 3 axes. The vertical z-axis is fixed at constant height prior to the machining, while the knife is moved in the y-axis to cut the specific diameter of the disc and the x-axis is moving the knife sideways cutting through the material. When this knife is cutting through the samples sideways, it is possible that metal shavings or the blade itself is jammed in between the bonded layers for a short period of time, ripping a small crack in the interface. This may or may not be visible, but could serve as a crack initiation during testing, and what is intended as a 100% tensile test, might now include peel-effects directly influencing the measured strength. No high resolution investigation as performed on the sample s interface prior to the tests, and could in hindsight be an interesting factor to investigate in a further study.

Another concern related to the knives path though the material is the friction heating, which is already mentioned in another relation. If the cutting is done too quick, and poorly cooled, in such soft material, there is a chance of welding the two layers together along the outer rim of disc. This would affect tested strength value in a positive direction, showing a larger strength. For this reason the last part, reducing the disc diameter down to 15.00mm was performed with a constant feed of cooling fluid. From observation in the SEM; no sign of weld zones in the outer edge of the sample was identified, and the concern laid to rest.

The third concern is the cooling fluid used. A possibility of cooling fluid enter between the bonded layers is clearly there. With poorly bonded plates the risk of contamination is even greater. The concern for the knife to create initiation cracks is only contributing to this concern. However, effect on the bond, should cooling fluid “diffuse” in between the layers, is not fully know. Usually these cooling fluids are a water based solution with synthetic oils diluted to 3-10%. Any such effect is also expected to be discovered at a SEM investigation.

5.3.2 The Grooves

Cutting grooves in the side of the sample to reduce the bonded area while maintaining the full glued area, as illustrated in Figure 25, should in theory be a simple way of raising the limit of the test method. When put into practice it was not that easy.

Figure 52: This figure is showing a picture of a sample which split in the metallic bonding during testing. Prior to testing this sample had a groove machined in its side.

Irrespective of how careful the machining was carried out, the results of the tensile test had clear indications that the bond of the sample had been damaged, as seen in Figure 35. This is most likely due to an initiation of a small crack that allowed for peeling of the surface under testing.

The current method for machining the groove in the disc samples prove to have a high risk of affecting the bond in such a way that the following tensile testing would not reveal the true strength. In fact none of the tested samples gave a strength value that would satisfy the assumed bonding strength. Two samples even failed when fixating the samples in the tensile testing machine.

Even though this modification turned out to be a failure in this study, the theory is simple and only a more reliable way for performing the operation is needed. This is mentioned in chapter for further work.

5.3.3 A General Overview

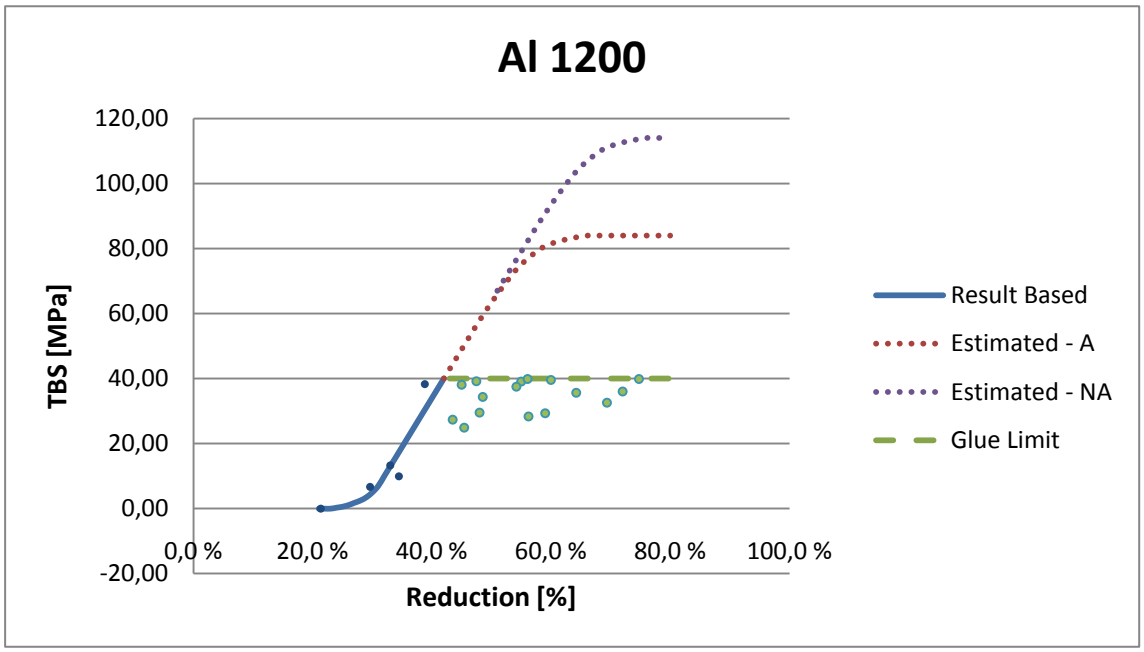

Figure 53: Al 1200. Estimated curve for TBS as a function of reduction.

These two figures (Figure 53 and Figure 54) is meant to give a general impression of how the bond strength of the two alloys, annealed and non-annealed, is affected by the reduction. In addition the current limitations with the tensile test are indicated by the "Glue Limit", at which above, bonding strength cannot be measured. The green and blue blots are measured values for which the curves "Glue Limit" and "Result Based" are based upon.

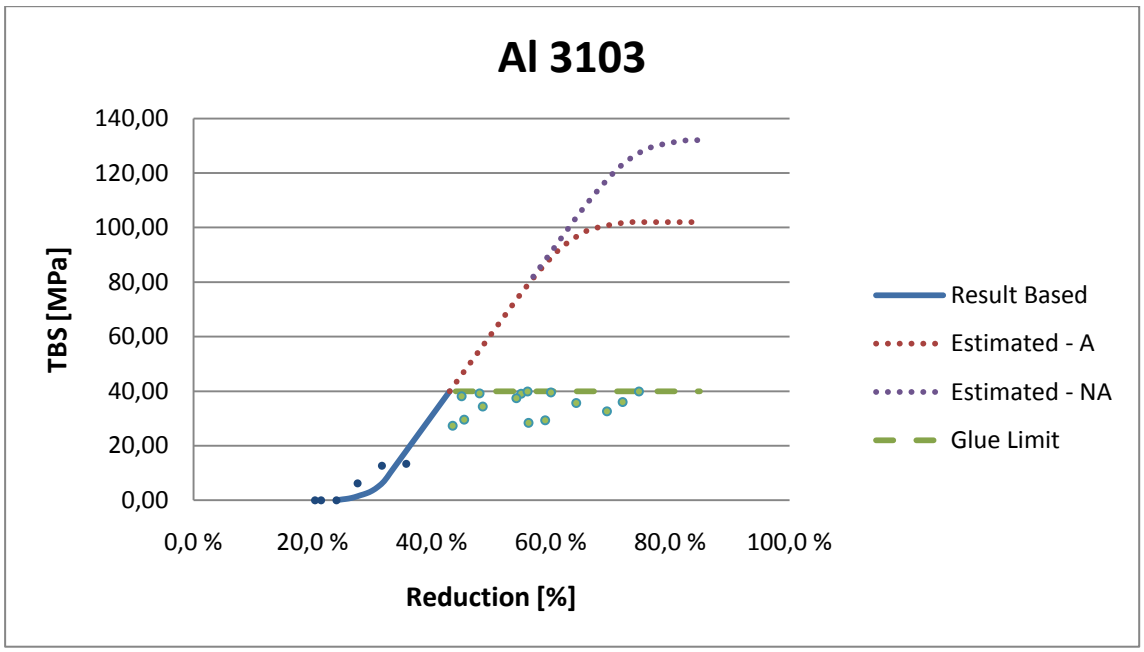

Figure 54: Al 3103. Estimated curve for TBS as a function of reduction..

Figure 53 and Figure 54 show the expectancy on how the bond strength is assumed to increase with increasing reduction. Each graph is built on four equations and plots. The "Result Based" line, as the name indicates, is a curve based on the test results in this thesis. The "Glue Limit" is the limit for which the specific glue used is the weaker of the two bonds. Some methods have been tried out to increase this limit; this is discussed in section 5.3.5. The two other dashed lines is an estimation on how the strength will continue to increase, depending on the work hardening and alloy. These estimations are based on a publication from W. Zhang et. al.[11] where the shape of the graph is found to follow a 3rd grade polynomial equation. Further is the strength increase from work hardening the determining factor for the maximum strength limit at high reduction.

The information used to make these estimations was found on AluMatter[13]. For the annealed (marked with an A)samples which only have been exposed for work hardening during the roll bonding pass after annealing was compared to the Hx4 – half hardened condition classification. The non-annealed (marked with NA) samples were compared to the Hx9 – extra hard condition. In Table 10 below the extracted data is presented. The upper limit of these curves is based on the minimum ultimate tensile stress. As the bond strength between the two layers is dependent on the fraction of actual bonded area, the RMN value found in the table will be much higher than the expected bonding strength. The estimation that about 70% of the area is actually bonded is more likely an overestimation, but a more plausible value. In addition there is a small positive strength increase effect, by the extra work hardening that occurs when base material is extruded between fracturing hard surface layers like oxide. This effect is however neglected in comparison to the generous estimation already given. In support of this neglected increase is the very thin oxide layer observed in these experiments, as seen in Figure 48.The value used in producing the graphs is found under RMN(70%) in Table 10.

Table 10: This table shows the assumed minimum UTS and min yield stress for two degrees of strain hardening. The information is taken from AluMatter.info. [13]

1200	RP02N	RMN	RMN(70%)
Hx4 (A)	100 MPa	120 MPa	84 MPa
Hx9 (NA)	140 MPa	160 MPa	112 MPa

3103	RP02N	RMN	RMN(70%)
Hx4 (A)	110 MPa	140 MPa	98 MPa
Hx9 (NA)	165 MPa	185 MPa	130 MPa

RMN: Minimum Ultimate Tesile Stress
RP02N Minimum Yeild Stress at 0.2%
RMN(70%): 70% of RMN

The margins of error for the estimated lines are considerable large. After all these are estimations and should be treated as such.

The “Glue Limit”, with a value set at 40MPa, is not an absolute limit, as the performance of the glue is largely dependent on the preparations of all connecting surfaces in adhesion process. This is described in section 3.4.1.1. However, the upper limit at a stain rate of 0.2 mm/min seemed to approach 40MPa, and never above. Only in two cases did the strength pass 40MPa (44.37MPa and 48.02MPa), but at a strain rate of 10 mm/min. This effect is discussed further in the following section. With a few exceptions of samples failing to around the 20MPa region, most of the samples where the glue was the weakest link, the strength was rather stable within 34 to 40MPa, once the preparation procedure was stabilized.

5.3.4 Strain Rate

An idea on whether or not the glue that was utilized might have hardening effect when exposed for a high sudden energy burst. Like some vicious fluids can render low resistance to an object moving slowly through it, and virtually act like a solid object, for a short period of time, if struck with a high kinetic energy. Cornstarch mixed with water is an example on such a fluid, along with many salt solutions and molten polymers. It forms a fluid with a viscosity like syrup or a thin paste. These are non-Newtonian fluids and change their viscosity depending on the shear stress-rate it is exposed to [14]. The idea was triggered by these fluids, that the glue, being composed by lots of polymers, could have a similar effect when going through tensile testing at higher strain rate. If this was the case, and the aluminum alloy was less influenced by this effect than the glue, this could be a method for increasing the operational range of this new TBS testing method.

The results did however clearly show a similar increase in both the strength of the glue bond and the bonded sheets, canceling out the gain with increasing strain rate. In fact some results even indicates that the aluminum bond is gaining more of the strengthening effect by increased strain rate than the epoxy glue, as seen in Sample A2NA03-T1 and T2 found in Table B 2. Where T1, strained at 0.2 mm/min, yielded in the metallic bond at 38.29MPa, and T2, strained at 10 mm/min, yielded in the glue bond at 44.37MPa. These two samples can also be seen plotted in Figure 39.

In conclusion; in the reduction range of 30-40% a strain rate at 10 mm/min compared to 0.2 mm/min, showed in average a bond strength that was 10MPa higher. Whether the increase is parallel or increasing as a percentage of the bond strength is not possible to determine with this data-set.

5.3.5 Glue Limitations

Even as the glue failed to test the strong bonded samples, there is little reason to complain about its strength. At its strongest, the glue withstood a tensile force up to

39.89MPa (at 0.2 mm/min strain rate) and 48.02MPa (at 10 mm/min strain rate) which over the area of a disc with a diameter of 15mm equals hence 718 kg and 865 kg. That's above ¾ the weight of an average small car, hanging from something the size of your papilla, or a small coin.

As introduced in section 4.2.2; information found on the datasheet for the glue [18], presented steel as a better material for attaining high adhesive strength, much higher than aluminum. The sample always would be in aluminum, and therefore the bond between it and the glue would be the weakest link no matter how strong the bond from the glue to the rod would be. This fact would never change. However, the reason for attempting this was because the TBS method had currently reached a limit and this method had potential to even out fluctuations with this limit.

When testing a TBST sample the outcome can technically end in fracture in one of five different transitions. The first and most desired outcome, being the metal-to-metal bond in the sample. While the other four is divided equally on each side of the sample. Two bonds in between the rod and the glue and the other two between the glue and the sample. This can be visualized in Figure 31 when imagining that the two open spaces between the rods and the sample is filled with glue. Having four surfaces to clean, scratch and apply glue to, includes a reasonable risk for failure. As it always will be the weakest bond that yields, being able to remove two of the four bond transitions form the equation, will in theory greatly reduce the chances for failure below the assumed strength limit for the glue at 40MPa. The use of steel rods did however not give any overwhelming results and was disregarded in favor of consistency and reduced cutting time due to the much higher harder material.

5.3.6 TBST vs. SBST

The compared bond strength shown in Figure 42 is showing bond strength of the TBS test both stronger and weaker then with the SBST method. The low amount of data makes it hard to draw any hard conclusion. However, the only sensible thing to conclude with, besides deeming the comparison inconclusive, is that the TBS test seemed to be very unstable.

In one scenario one could say that the TBST method measures a higher strength than by the SBST method, but due to various problems with the TBS test, some samples have their bond damaged more than others, during machining etc.

Another scenario could be that the TBST and SBST method should show the same strength, but due to the already mentioned reason, the TBST samples is now affected by both a positive and negative increase in bond strength. The negative being the same reason as previous, but the positive increase due to perhaps small weld zones in the outer rim of the disc.

The conclusion will be that the tensile bond strength test (TBST) method still suffers from startup hiccups, mainly with the machining of the disc, and even more when adding the grooves. This method has shown that it is possible to do 100% tensile bond strength test of bonds, using industrial type glue to distribute the load evenly over the grip surface.

5.3.7 Applicability of the TBST Method

The TBST method as much revealed in the conclusion of section 5.3.6, still has factors to sort out. However the test is currently fully applicable for tensile testing of samples up to a strength of 40MPA, with a very low requirement of test material

This maximum strength limit of 40MPa is mainly due to two factors. The first being that this is the limit of the current glue in use, and to the knowledge of the author there is few other adhesives in the world that is stronger. One type of epoxy adhesive under the name LOCTITE 9514 has reported tensile bond strength even higher than the LOCTITE 9466, currently used. This glue however required curing at a temperature over 120°C or above for reaching this high strength. An attempt was made to get a sample of this glue, but was never attained in time.

The other factor is the difficulty of changing the ratio between the area of metallic bonding to the glued area. If one could keep a large area for gluing while having the strength evenly transferred to a much smaller roll bonded area, the lack in glue strength could perhaps be overcome. The method of making grooves in the side of the disc samples was an attempt on achieving this. This failed due to very thin discs and improper cutting tools and methods.

5.4 Shear Bond Strength Test (SBST)

The SBS test, which was mentioned as the “state of the art” testing method of today, was carried out on samples taken from the same roll bonding sheets as some of the samples that was tested with the TBS test. This was done with a hope of observing a relationship between the two testing methods, as was discussed in section 5.3.6.

In a study [17] where the SBS test method was the main means for testing equation (12) found in section 2.4.2 was used in calculation of the gap overlap. In contradiction to that equation, in this current experiments the calculations for the overlapping area was only based on the yield strength of the material, as kept below an area that would not lead to necking and failure in the material itself. On the other hand some of the samples were poorly bonded and an area, as high as possible, was desired to avoid fracture or damage on the bond during machining or clamping of the sample into the tensile machine.

5.4.1 Angular Deflection

The plots in Figure 44 indicate that the angle deflection increase with increasing bond strength, which is as expected. This variation in angle during testing of SBS will obviously have an influence on the tested value. The pulling force is gradually moving from pulling in a shear direction towards pulling in a partly tensile direction.

To reduce or perhaps avoid the angular deflection, the overlap length l can be reduced. This will reduce the maximum load required to part the bonds and the shear forces due to misalignment is reduced as well. The risk with reducing the overlap length is that the sample is much more fragile, which can result in accidental fracture during machining or when any other force is applied.

Figure 44 is showing a correlation to the bond strength. The angle is increasing with increased bond strength in the samples where the overlap length is kept constant.

At this overlap length any notably angle deflection seems to occur over 20MPa. The yield strength of the individual sample could be interesting to compare to see if there was a threshold for where this effect started. It could be a direct correlation between where the angle deflection starts and a specific fraction of the materials yield strength at a given overlap length. This is mentioned in section 7.

5.5 Fracture Surface Investigation

In the following sections the observations made during the SEM analysis is discussed.

5.5.1 Bond Types

The main bond type found during the SEM investigation is ductile bonds, as seen in the close-ups in Figure 55 and Figure 56. Figure 56 shows the bonding that occurs when the oxide layer cracks during deformation and virgin base material is extruded through the crack. These are characterized by the mountain range looking effects in the surface. The reason for this long shape and direction is explained in section 5.5.2.

In Figure 55 a cluster of small dimples is observed. Such dimples are strongly indicating a propper bonding. The dimples are formed as the virgin metal has bonded around particles, and when the two layers was pulled apart these particle has created voids at the sport they was encapsulated.

The size of the particles in these alloys is particularly small, and in the case in Figure 55 they are on the scale of 200-400nm.

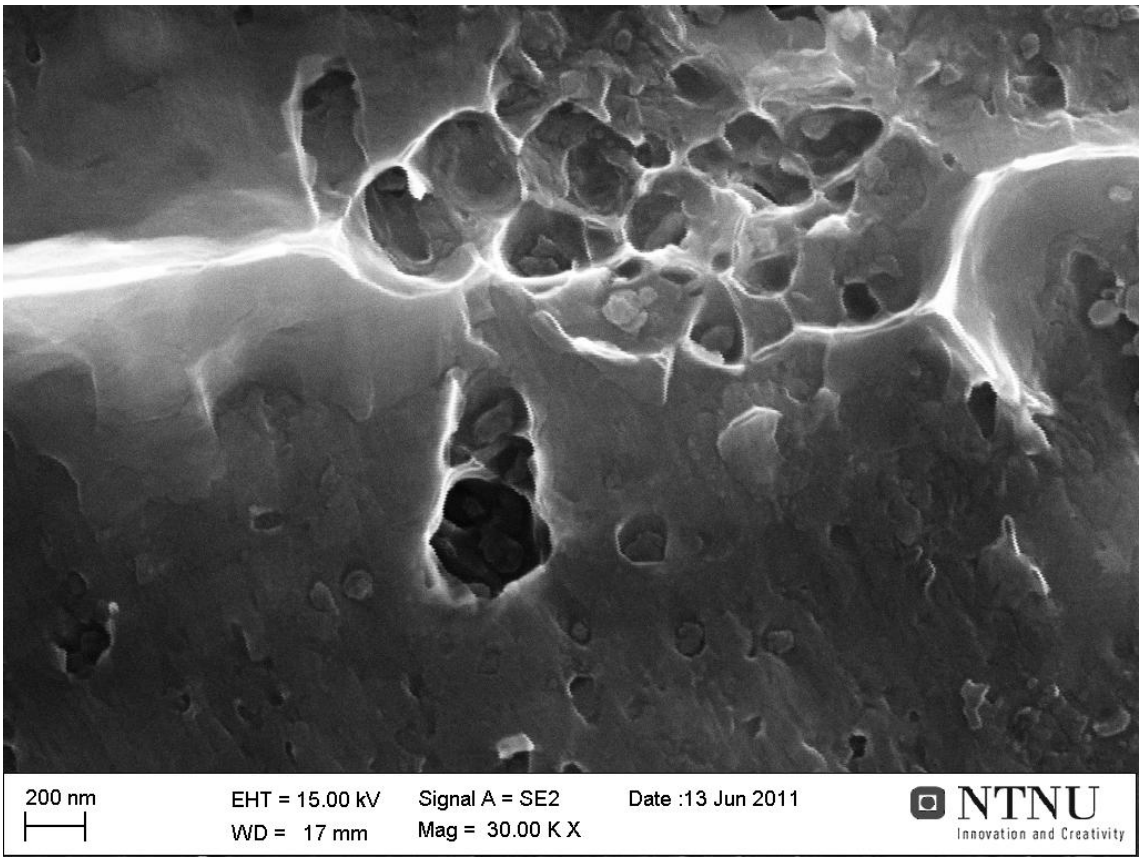

Figure 55: A close-up image the fracture surface of sample B2A05-T1 A showing a proper bonded area, indicated by the dimples. Seen from above.

5.5.2 Crack Direction

The characteristic ductile fracture lines found at higher reduction is a strong indication of how the bonding occurs. This feature support the assumption that bonding occurs in between the cracked up oxide layer. As the material mainly expands only in the rolling direction during roll bonding the oxide layer and hardened surface cracks up and exposes the virgin material in cracks stretching normal to the rolling directions. With higher pressure also allowing metallic interaction and bonding. This tendency is frequently found in the circular tensile test samples, but due to the shape of the sample it was not, without further investigations, possible to determine the direction in relationship to the rolling direction. This was first confirmed when observing the fracture surface one of the SBST samples, where the rolling direction can be recognized from the surface appearance. Figure 47 shows these bond lines going normal to the rolling direction. This effect is also seen in the surface oxide fracture investigation done by H.R. Lee et. Al [20], as seen in Figure 59 for the case of much thicker oxide layers.

5.5.3 Bonded Area

The well bonded area of the fracture surface is easily found, but is a tedious job to measure exactly. The most exact method would be to measure the area of each “stretch lip” as they were named by A. Lilleby [5]. Since the observed lip is just the tip of a ductile fracture point, the actual bonded area is larger. The original area can be

traced back by following the stretch lines down the slope of the lip. In Figure 56 the real bonded area of such a stretch lip is marked. Dividing the found bonded area on the total area will give the fraction of bonded area. Measuring the bond area of each stretch lip over a sufficiently large area is very time consuming, unless a computer with analytical software were made for this purpose.

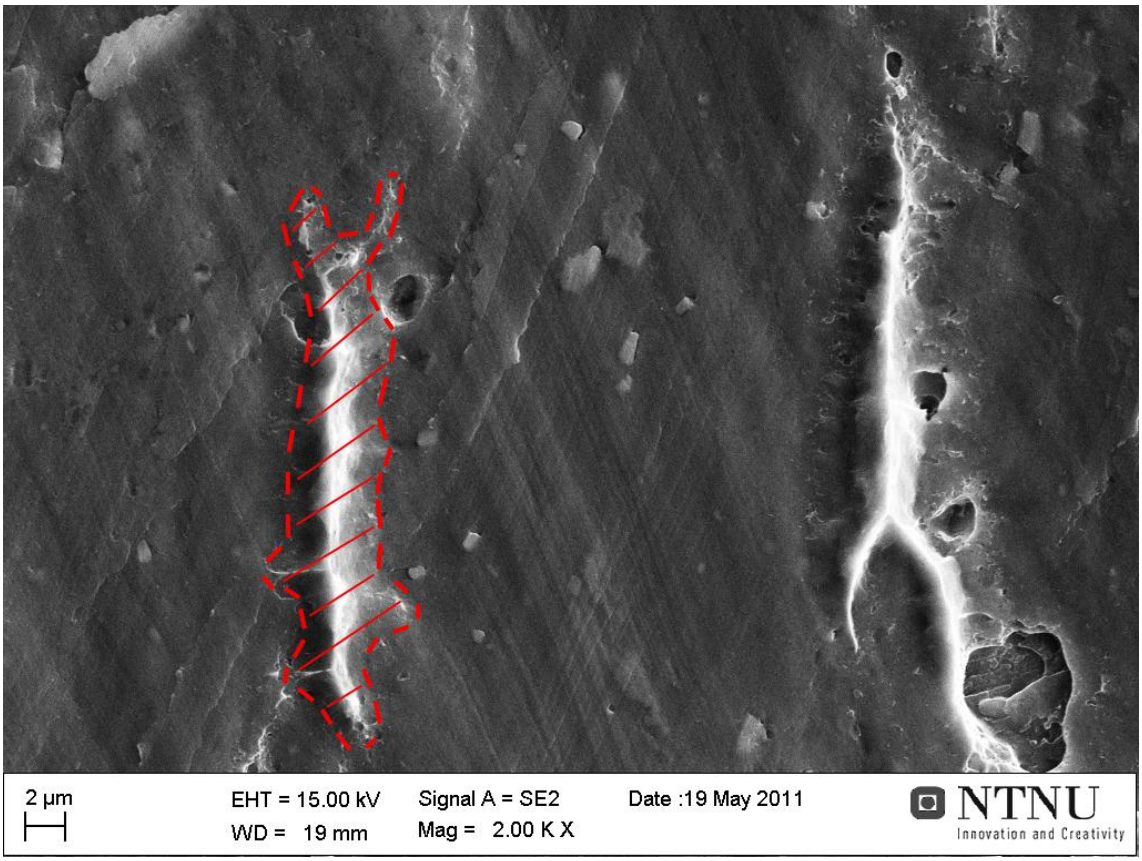

Figure 56: Bonded area around a "stretch lip". Showing the fracture surface of sample A2Na03-T1 A, seen from above.

A simplified method can be used when making a few assumptions. As the sheets are rolled in only one direction the surface expansion is unidirectional and should be evenly distributed over the sheet. If line X is drawn, a certain distance anywhere on the fracture surface in the rolling direction can be represented, as marked by the two examples X_1 and X_2 in Figure 57. By measuring the sum of the width of every stretch lip that the line crosses and dividing it by the total length X, the fraction of bonded area can be found. Since the bonds should be evenly distributed a measurement for line X_1 and X_2 in Figure 57 should give similar results. Of course an average of several lines should be used if determining the bonded area.

$$Fraction\ Bonded\ Area = \frac{\sum \Delta X}{X} \qquad (13)$$

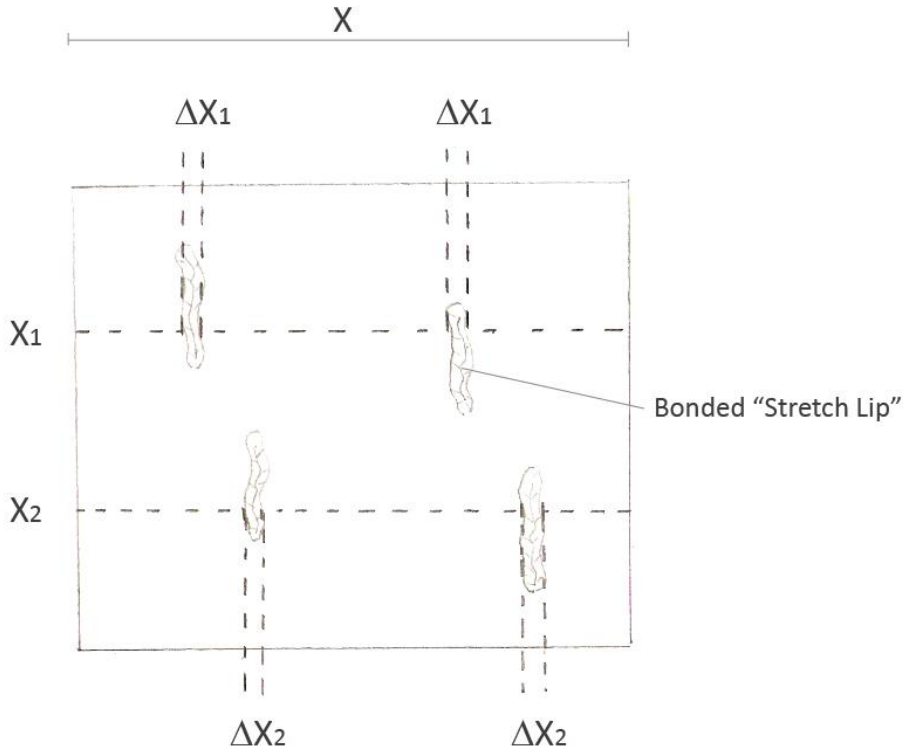

Figure 57: A sketch showing a simplified method for measuring the fraction of bonded surface area.

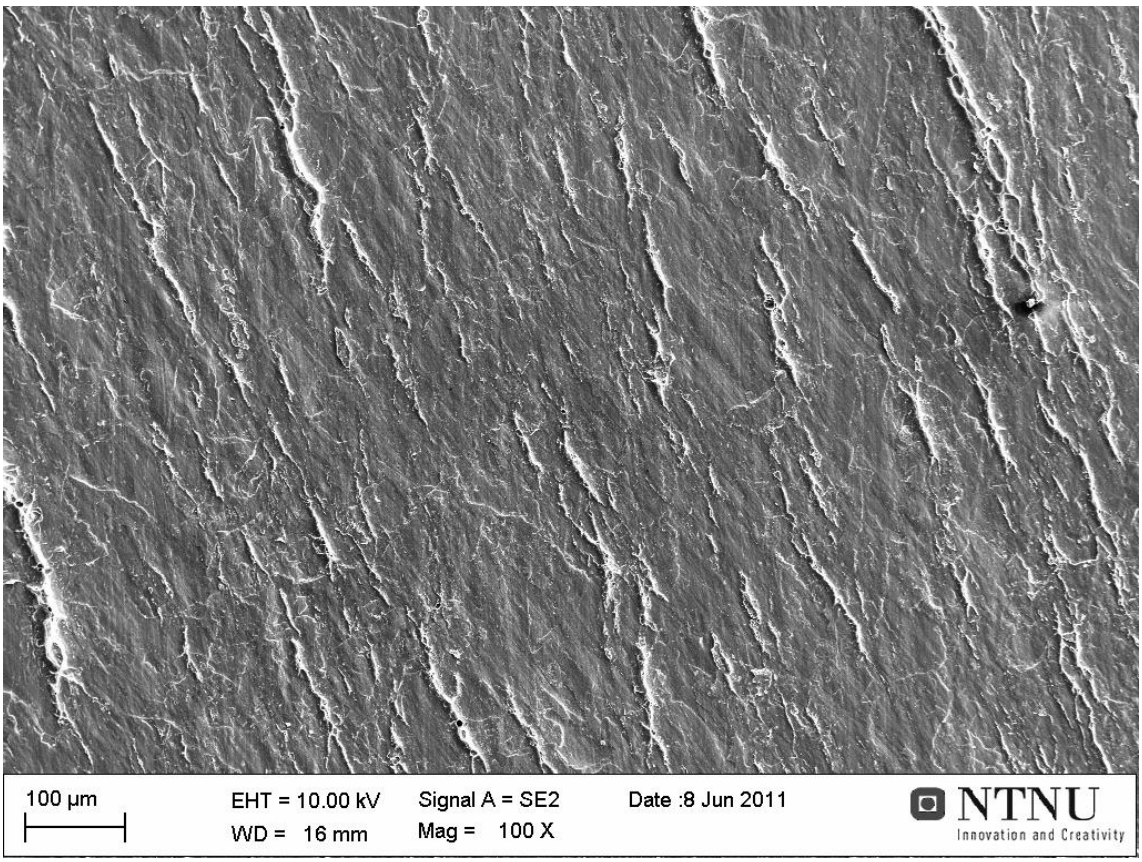

Figure 58: The fracture surface of sample A2NA04-T1 seen from above, showing directional stretch lips.

This method could be performed on a surface as seen in Figure 58. The sample in this figure was roll bonded at a reduction of 48.5% and even measuring the fraction of bonded area this image does not seems to be bonded anywhere close to 48.5% of the surface area. In comparison the sample Figure 59, which is was rolled bonded at 30% reduction seems to show a larger bonded area. When the bonded area does not follow the expansion of the surface, hence the reduction, it seems like the oxide is expanding. In section 5.8 a theory of thinning of oxide is discussed.

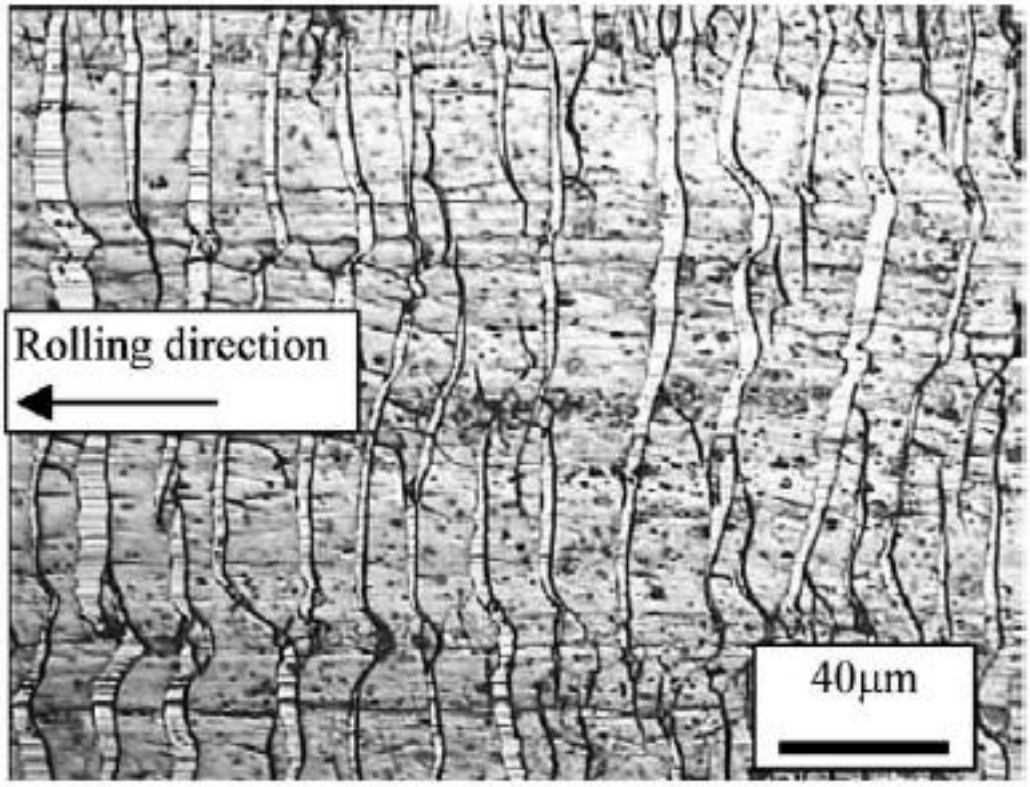

Figure 59: A SEM picture showing crack lines in an oxide covered surface, seen from above. [20]

5.6 The Effect of Rolling Speed

A study by Yan, H. et. al [24] suggest that a slower rolling speed will prolong contact time while the material is compressed between the rolls and hence give time to better bonding, as shown in Figure 60. These experiments were however performed with pre-heating of the samples up to 280°C.

Results found in a pre-study by Lauvdal [10] showed in one case the opposite of this, a strength increase. These data does not disclaim the previous stated suggestion. However, for cold roll bonding there must be another contributing factor. When the speed is increased there is an amount of adiabatic heating produced from deforming the material, that have less time to escape as the temperature builds up. The ways for the heat to escape is through the air, which have a very low thermal conductivity. In addition it can escape through the steel rolls and into the structure of the mill. Initially

some heat can also be transported to the not yet deformed part of the sample due to aluminums high thermal conductivity.

When the roll bonding is performed at room temperature this heat contribution might be the factor increasing the bonding strength by lowering the critical deformation threshold. This factor might be of larger influence than the increase in rolling speed. In cold roll bonding the effect of temperature increase seem to have a much higher impact on the rolling strength than the effect of the contact time between the rolls. At least it could be the case for a certain specter of the speed scale.

An IR-thermometer was used in an attempt to read the surface temperature of the sheets as they exited the mill, but with no result. This current IR-thermometer cannot properly read infrared radiation of an aluminum surfaces.

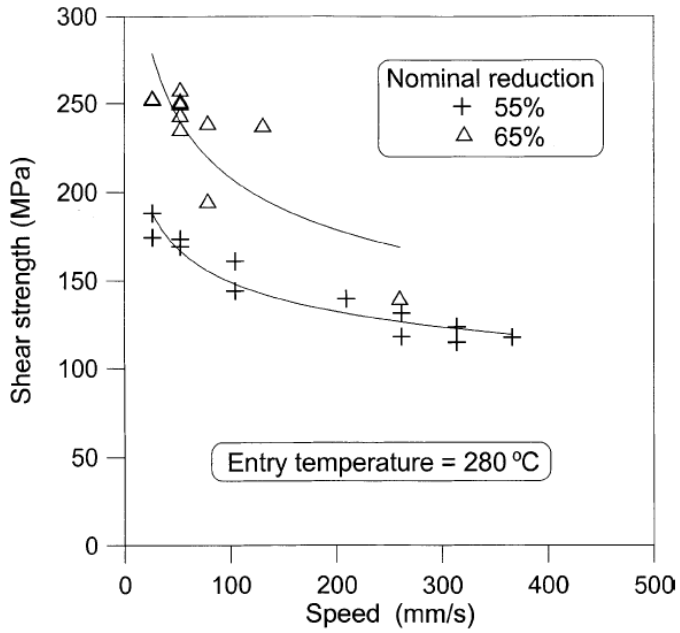

Figure 60: Graph showing the shear strength as a function of the rolling speed and reduction. [20]

Two results were found on the speed effect, and both are presented in section 4.6. Without repeating the results in detail, the results gained from the test between a very low rolling speed of 1.5 (about 5mm/s) and high speed at 5 (about 150mm/s) showed that the samples rolled at speed 5 was far better bonded.

On the other hand, where speed was not intended tested, a trend was still visible when plotted, as seen in Figure 33. The speed here was 3 (26.62 mm/s) and 5 (about 150 mm/s).

The conclusion to be drawn from this is that there is a chance that adiabatic heating from higher rolling speed can have a desired effect on the bond strength when performing cold roll bonding. This could be an interesting factor to study in a further study.

5.7 Below Critical Deformation Threshold (CDT)

The *critical deformation threshold* is defined as the point where the bond is sufficiently strong. Not a very exact description. This section will present the discoveries regarding the low reduction region where bonding begins, an area also known under the name kissing bond.

The reduction is obviously the parameter with the greatest impact on the bond strength after sufficient surface brushing is gained. With increasing strain of the material a larger reduction was acquired to gain bonding. This is because more energy is needed to make the two base materials squeeze between the cracks in the oxide layers and come in contact with the base material when an increased amount of defects is present.

5.7.1 Al 1200NA

The lowest reduction attempted with the Al 1200NA alloy was 29.6%. At this reduction two TBS tests were performed, one at a strain rate of 0.2 mm/min and another at 10 mm/min. The strength measured in these two tests was hence 6.63MPa and 19.49MPa. Also a SBS test was performed on this sample, but this failed in the material rendering the results less valuable. The SBS test peaked at 13.02MPa indicating a minimum strength value on the bond.

Of the three samples tested at this reduction, the sample tested at the strain rate 0.2 mm/min is chosen when predicting the initiation of kissing bonds. At 29.6% reduction in thickness during bonding and the measured TBS of 6.63MPa, this is considered a bond in the high end or above the kissing bond stage. As no lower reduction was tested for this material, the point where bonding starts can only be estimated. From the assumed slope of the other plots for the Al 1200NA samples and comparing to the similar plotline in the Al 1200A graph an assumption is made that bonding could start at about 25% reduction. To repeat, no data was recorded below 29.6% reduction.

5.7.2 Al 1200A

The samples in the annealed batch of the Al 1200 section have the best result for determining the minimum reduction at which bonding begins. Two samples, one with a reduction of 21.4% and another at 22.3% showed to be on opposite sides of this border. One of these split straight after it came out of the mill and was never bonded. The slightly higher deformed one was bonded well enough to survive until it attempted machined into a tensile sample. It then split due to the external forces applied. This alone indicates that a lower limit for bonding has been found, unless small variables in uncontrollable parameters caused this. In addition, samples from the same sheet were sent to machining for the SBS test. This sample on the other hand survived the machining and was successfully tested to a SBS of 4.40MPa. The lower limit for adhesion between the two plates is therefore well defined for roll bonding in this material with the present parameters, and close to 22% reduction.

Due to the margins of error in several of the parameters included in the preparations prior to roll bonding, this limit will assumable be somewhat floating limit in regards of reproducing the results. As the small differences in exposure time to air and oxide growth, degree of scratching and such may play a large role to this limit of roll bonding. Also mechanisms other then the fracture of hard low ductile surface elements and metallic bonding, may play a role in the first kissing bonds phase of bonding.

5.7.3 Al 3103NA

At 20.4% reduction no bonding whatsoever was observed. At a reduction at 27.6% a TBS of 6.17MPa at 0.2 mm/min strain rate was measured. With similar assumptions and estimations bonding could here seem to first occur at around 25% reduction. Yet again, it is important to stress that no real data was recorded below 27.6% reduction.

5.7.4 Al 3103A

In the Al 3103A samples no bonding where found at a reduction of 24.0%. At 28.1% bonding was observed, but the sample fractured while clamping the sample to the tensile machine and the bond strength was categorized as a kissing bond. The following higher deformed samples, at 28.1%, 34.2% and 39.8%, were declared ruined by machining as they both fractured when mounted in the tensile machine.

5.8 Bond Interface

In Figure 61 the interface is clearly visible, and in the center one can see the dark oxide layer stretched out. Something else that is of interest concerning this is the clearly visible lines indicating the deformation. Almost like furrows in wood one can see the lines being bent around harder particles and oxide, and one can see how the oxide layer has cracked and made an opening so that the virgin material could extrude through and make contact in a metallic binding.

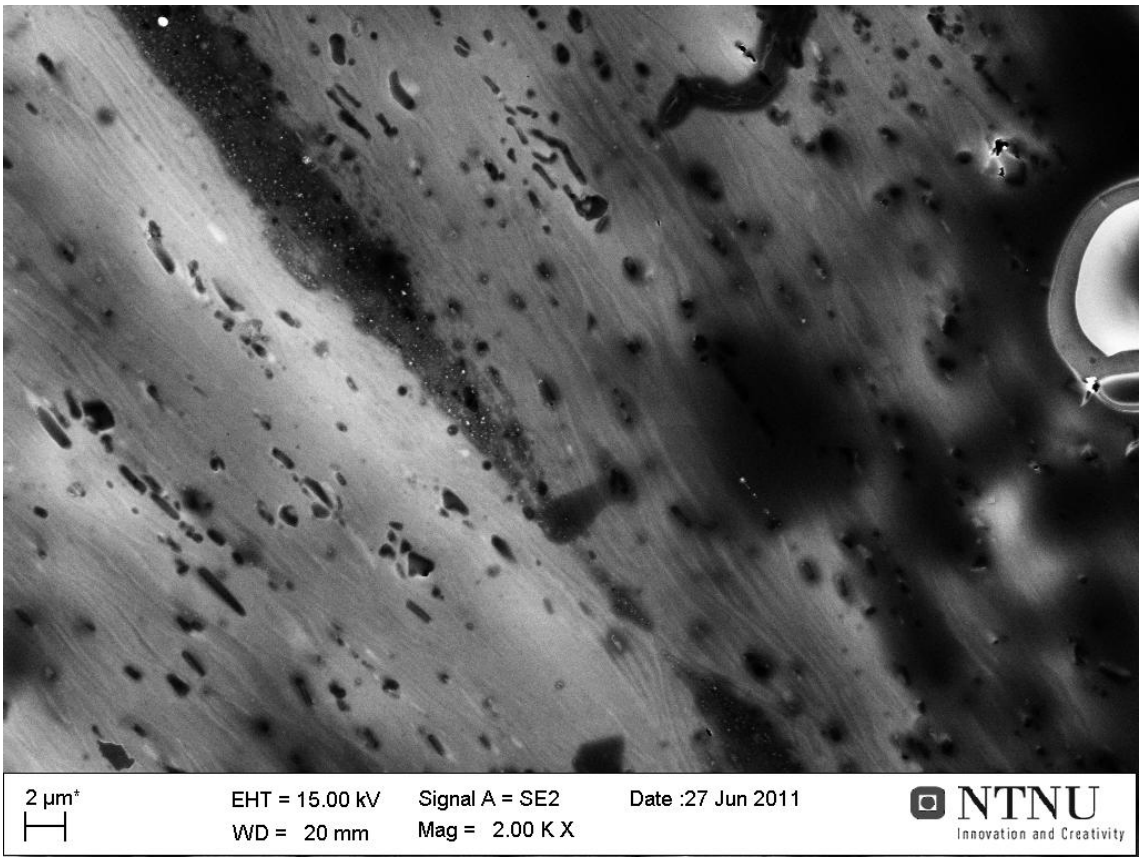

Figure 61: The interface of sample A2NA02 seen from the side. At 2000x magnification one can clearly see the deformation lines. The dark part stretching in the middle is the oxide layer, and in between metallic bonding can be observed.

The fact that we can see such a distinct opening in the oxide layer could indicate that the sample was cut along the rolling direction, or close to parallel. The author believes at this point that it may be possible to determine the rolling direction by looking for the weak lines left by the roller in the surface of the sample. This, however, the project had not enough time to confirm. By looking at the surface of sample A2NA02 seen in Figure 61, it was unofficially concluded that the cut was within a few degrees angle of the rolling direction.

In the image of the sample that was stopped mid process, in Figure 49, it was not possible to make out any interface line. This sample did not undergo any electro polishing and is likely to explain why the interface is not apparent. However, the interface was visible under low magnification in light microscope during the polishing process in some of these samples, before it disappeared in the polishing stage.

In the same surface observations as the sample in Figure 61 the rolling direction for the second disc sample was found to make a close to 45 degrees angle with the line of the cut. No interface was found during the SEM imaging of this sample either.

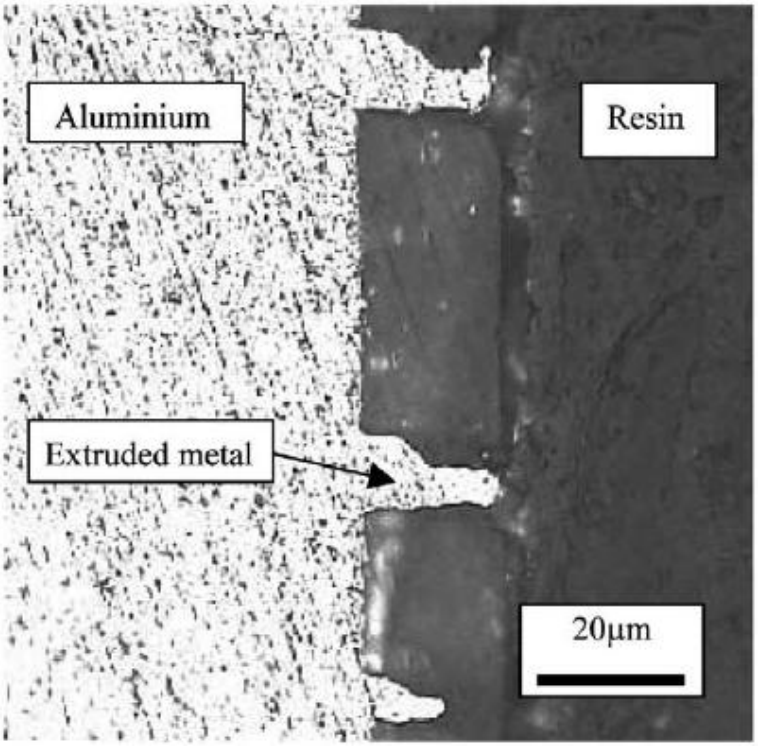

Figure 62: Oxide layer seen from the side. Extruded aluminum trough cracks in thick oxide layer. [20]

The shape of the oxide layer in Figure 61 is very unlike any other found in most interface pictures this author have seen. Compared to the shape of the oxide layer in Figure 62, which has sharp edges, this new seems like it has been deformed and flattened.

There is a significant difference in the thickness of the oxide in these two figures. While the oxide thickness in Figure 61 is about 4-5µm thick, the oxide in Figure 62 is 4 times thicker in its 20µm. Four theories on how this oxide might have been formed are aerated in the following pages.

5.8.1 Theory I: Thinning of Oxide

One theory trying to explain the effect is thinning of oxide. Figure 63 from a) through c) tries to illustrate this theory. The oxide is evenly distributed as the two layers are brought together, just before any deformation has taken place, as seen in a). As the material is deformed, the oxide layer starts to crack, as seen in Figure 62. The deformation proceeds and gaps between the oxides grow and allows for more bonding. At the same time, the oxide starts to deform on some level and creates the shape seen I c). This theory is considered little plausible, as the aluminum oxide is a extremely hard substance.

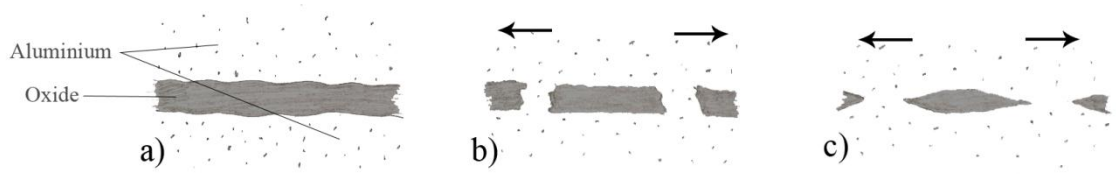

Figure 63: A sketch of bond interface seen from the side, illustrating the progression in theory I.

5.8.2 Theory II: Uneven Oxide Layer Thickness

When the oxide forms on a roughly scratch brushed surface, the thickness over the surface is unevenly distributed, as illustrated in Figure 64 a). When the sample is deformed and stretched in the rolling direction, it is natural that the oxide layer breaks off in the thinnest and weakest regions, seen in b). As the deformation continues, the oxide is moved further apart. The thinning in the end of each oxide is simply because the oxide shattered in the thinnest region.

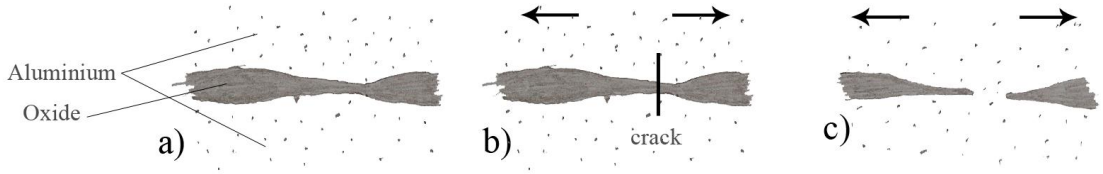

Figure 64: : A sketch of bond interface seen from the side, illustrating the progression in theory II.

5.8.3 Theory III: Crack Direction

Another theory, with no base in known oxide behavior is the following: The oxide layer cracks in an angle, in a straight line through, or perhaps changing direction, cutting out a v-shape. This is illustrated in Figure 65 c) or the v-shaped in b). Due to the thin oxide layer the crack-tips seems bigger. Under further deformation the v-opening might be closed together under the pressure, resulting in a slim pointy end. With the straight line cut, only some slight bending towards the center is needed to align the pointy end to something similar of what is observed in Figure 61.

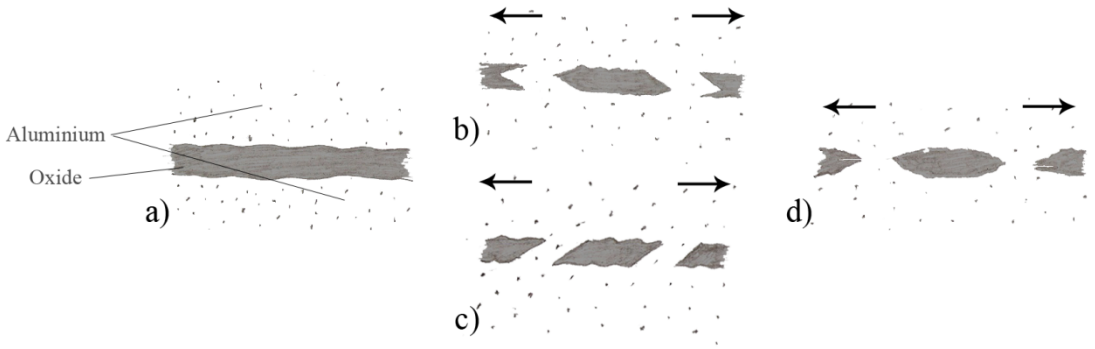

Figure 65: : A sketch of bond interface seen from the side, illustrating the progression in theory III.

5.8.4 Theory IV: "Pulverized" Oxide

Theory four is somewhat similar to theory one in the way that it can help explain a thinning of the oxide. And as the fracture surface investigation could indicate, the bonded area is not following the increase in reduction when comparing the amount of

bond lines to the reduction. The drawings in Figure 66 will help guide this explanation. Part a) in the figure shows the two aluminum surfaces prior to scratch brushing, an evenly distributed oxide layer. When the surface is scratched some oxide is ripped off and thrown away from the sample. However some oxide might just be grinded to smaller particles and thrown back down at the surface, most likely distributed in a manner influenced of the scratch brushed surface. These are grooves going normal to the rolling direction. New oxide is instantly formed on the exposed surface, creating the thinnest part of the layer seen in b). If oxide is thrown back in a pattern, this will lead to an uneven distribution of oxide when roll bonded, as illustrated in c). The oxide layer is now partly composed by perhaps even more brittle oxide, as much of it is compressed oxide particles. The uneven distribution explains the varying thickness.

Upon further deformation the oxide is compressed and stretched, and as in theory II it also here dislocates at the weakest points, which is in the thinnest regions. In addition, as this oxide is much more brittle, perhaps somewhat like sandstone, it is crushed under the high external load; the whole mass might stretch like stepping on a pile of sand. Or the shear forces in the transition zone between the oxide and the metal breaks off and drags loose oxide fragments down the slope and out to the tips.

This theory could seem a bit more plausible than the others, and when looking closely at the oxide in Figure 61 it does look like alienated particles are dislocated around the tip.

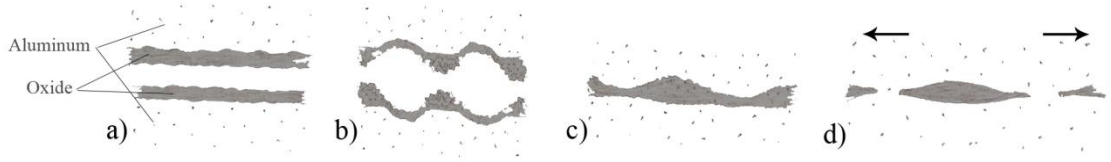

Figure 66: : A sketch of bond interface seen from the side, illustrating the progression in theory IV.

6 Conclusion

The basic conclusions that can be drawn from these discussions are as following:

The Material Effect

The two aluminum alloys used in this experiment, the 1200 and 3103, did not turn out to have any notable variations on the bond strength. This is according to their close similarity in strength.

Acetone vs. ethanol

Acetone can with reasonably probability be said to be a better degreasing agent than ethanol may, due to which reduction bonding starts. The actual influence on the bonding strength at higher deformation is not confirmed.

The Effect of the Oxide Layer Thickness

The comparisons experiments where the oxide layer was believed to be the main variable, the results were somewhat uncertain. However the general trend did support the assumption that bonding does start at a lower reduction when the oxide layer is thinner.

Effect of rolling speed

Results indicate that the adiabatic heating from increased rolling speed may have a significant influence on the bond strength when operating with cold roll bonding.

Effect of the General Preparation

In all general preparation method allowed bonding to start at the following reductions at the given alloy and prior annealing:

Table 11: Table showing at the lowest reduction bonding was acquired.

Material	Reduction
Al 1200 Non-Annealed	29.6%
Al 1200 Annealed	22.3%*
Al 3103 Non-Annealed	27.6%
Al 3103 Annealed	28.1%

*This is the only value where the limit is accurate within less than +/- 1% margin.

The Tensile Bond Strength Test (TBST)

The strain rate at which the samples are tested is an important factor to take into account when comparing measured bond strengths. At the reduction range 30-40% a strain rate at 10 mm/min compared to 0.2 mm/min showed in average a bond strength that was 10MPa higher. Whether the increase is linear or percentage based is undetermined.

The current testing range for the TBS test is from around 4MPa to 40MPa. The lower limit is based on the machining part of the preparations, where there is a considerable risk that poorly bonded samples are parted due to the forces involved. This limit can be lowered dramatically by altering the preparation approach, and should shear the same potential limit as the SBS test.

The upper limit is confined on two fronts; the current glue has a bond strength of 40MPa and finding a stronger glue would directly improve this limit. The other option is to increase the area ratio between the glued surface area over the roll bonded surface area. Machining a groove over the interface of the disc is one approach to achieve this.

The experimental machining of grooves to increase glue/bond area ratio turned out to damage the bond in the process. New and improved methods of machining are needed to achieve positive results using this method.

The TBST method, with its current limitations can serve as a complimentary test method to the already established ones at the low to medium range of bond strength, which in these experiments correlates to <40% reduction. As the test required a minimum of sample material to be performed, it is very suitable for experiments with limited sample size or testing products in a production line.

Angular Deflection in the Shear Bond Strength Test (SBST)

An angular deflection while performing the SBS testing was observed, and it showed to increase with the bond strength (and reduction). The angular deflection was found to start over bond strength of 20MPa.

TBST vs. SBST

Comparing the TBST method to the SBST method indicated that the TBST method is currently unstable. The TBST method is most likely to report higher or equal bond strength compared to a SBS test on the same sample material. To determine this however, the inaccuracy of the TBS test is too big.

Fracture Surface

During the fracture surface investigation in the SEM, clear proof of ductile bonding was found at higher reductions. The ductile bonds, by the given name “stretch lips”, run in intervals normal to the rolling direction.

The fraction of area bonded over non-bonded did not seem to follow the percentage of reduction, which indicate a thinning of the oxide layer. This could also be supported by the shape of the oxide observed in the interface. Four theories were presented on how this shape might have occurred. None were confirmed.

7 Suggestion to Future Work

Scratch Brushing

In a further study, there would be an interest looking into this parameter with regard on the brushing direction and how the surface roughness and directions of the grooves" may impact the bond.

Rolling speed & Adiabatic Heating

The observation that a slower rolling speed have had a positive effect on the bonding strength and that the same positive effect is found on cold roll bonding only at higher speeds, could be of interest to look closer into. Further an investigation on how small temperature increases would affect the bonding strength at cold roll bonding.

Simulated Accumulated Cold Roll Bonding

How is the bonds affected by ACRB? A simple test by starting with a thick enough sample and cold roll bonding it to for instance 50% reduction. Then, without stacking or preparing the sample surface, CRB the sample to 25% of the original thickness. The next to 12.5% and so on. Between each step, a sample is extracted for closer investigations. Additionally can half the samples from each pass can be annealed before continuing to the next step. This way gathering information on the annealing influence in the process. Is annealing needed to reach high levels of ACRB to remove accumulating stresses that can lead to brittle fracture? How often an to what degree is annealing needed?

Fraction Bonded Surface Area vs. Reduction and Bond Strength

Bond strength should in theory follow the same % scale as the fraction boned area multiplied with the yield strength. Investigating a quantitatively analysis of the fraction bonded surface area on these samples, or samples with the same thinning effect of oxide layer.

TBST Samples

An investigation of the bond interface on the surface of a test sample prior to TBS testing could reveal if and how the machining procedure damages the samples. If the scattering result in TBST data is not due to this is it perhaps just due to poorly bonded areas?

Further new experimental studies can be carried out on the "groove" method for improving the test range of the TBST. The first initiative would be to roll bond thicker plates, to ease the practical circumstances around the machining. Thicker plates would allow for experimentation of different shapes of groove-cuts. What is better for evenly distribute the tensile load; v-shapes, circular shapes, squared shapes…? If the surface area of the bond can be reduced to an half, while the glued surface remains

unchanged, the range of the TBST method would instantly be increased from 40MPa to 80MPa.

Some glues report bond strengths higher than the one currently used. Most of these glues require however curing at elevated temperatures. En example of one of these glues have been mentioned; the LOCTITE 9514.

SBST

The angular deflection found during the SBS testing could be investigated further, to determine at which limits it does occur, and calculating a better estimate of the true strength when it does occur.

8 Bibliography

[1] **Dieter, George E.** *Mechanical Metallurgy*. London: McGraw-Hill, 1988

[2] **Rolling & Drawing**, Copyright © Brynmorgen Press 2001, http://www.ganoksin.com/borisat/nenam/metal-rolling-n-drawing.htm

[3] http://www.atomefabrik.com/pages_tetsuo/finish.htm

[4] **Bay, N**. *Mechanisms Producing Metallic Bonds in Cold Welding*, 1983

[5] **Lilleby, Anders** *Experimental and Finite Element Studies of Cold Pressure Welding of Commercial Purety Aluminium by Divergent Extrusion*. Trondheim : s.n., 2009

[6] **Quadir, M.Z.** *Influence of processing parameters on the bond toughness of roll-bonded aluminium strip*, 2008

[7] **Li, Long** *Progress in cold roll bonding of metals*, 2008

[8] http://www.ndt-ed.org/EducationResources/CommunityCollege/Materials/Mechanical/Tensile.htm

[9] **Askeland, D.R. & Phulé, P.P.** *The Science and Engineering of Materials.Chap. 8-6* US: ©Thomson Canada Limit, 2006.

[10] **Lauvdal, S.** *Roll Bonding Properties at Room Temperature.* NTNU Trondheim, 2010

[11] **Zhang, W. and Bay, N.** *Influence of Hydrostatic Pressure in Cold-Pressure Welding.* Inst. Of Manuf. Eng., Techn. Univ. Denmark, 1992.

[12] http://www.aluminium.matter.org.uk/aluselect/06_composition_browse.asp

[13] http://www.aluminium.matter.org.uk/aluselect/09_mech_browse.asp?

[14] http://en.wikipedia.org/wiki/Non-Newtonian_fluid

[15] **Nes, E.** *Modelling of work hardening and stress saturation in fcc metals*, Progress in Materials Science, Vol. 41, pp 129-193, 1998

[16] **Humphreys, F.J. and Hatherly, M.** *Recrystallization and Related Annealing Phenommena* 2nd Ed., Chap. 6, 2004

[17] **Zhang, W. and Bay, N.** *Cold Welding – Experimental Investigation of the Surface Preparation Methods*, 1997

[18] **LOCTITE Hysol® 9466™** *Technical Data Sheet*. Henkel Technologies, 2006

[19] **Grong, Ø** *Metallurgical modeling of welding* 2nd Ed., Institute of Materials, London, 1997

[20] **H.R. Le, M.P.F. Sutcliffe, P.Z. Wang, G.T. Burstein** *Surface oxide fraction in cold aluminum rolling*, Acta Mater.52, 2004

[21] **Bay, N.** *Cross shear roll bonding* J. Mater., 1994

[22] **Jamaati, R.** *Investigation of the parameters of the cold roll bonding (CRB) process*, 2009

[23] **Jamaati, R.** *Effect of friction, annealing conditions and hardness on the bond strength of Al/Al strips produced by cold roll bonding*, 2010

[24] **Yan, H.** *A study of warm and cold roll-bonding of an aluminum alloy*, 2004

[25] **Designation: D1876-8** *Standard Test Method for Pell Resistance of Adhesives (T-Peel Test)*[1], 2011

[26] **Saito, Y., Tsuji, N., Utsunomiva, H., Sakai, T. and Hong, R. G.** *Ultra-fine grained bulk aluminum production by accumulative roll-bonding (ARB) process*. Acta Mater. Vol. 39, pp 1221-1227, 1998

Appendix

A – Rolling Progression to Sheets
B – Table of all Tensile- and Shear-Test Samples
C – Adhesion Log
D – SEM Pictures: Tensile Samples
E – SEM Pictures: Shear Samples

A - Rolling Progression to Sheets

Table A 1: Logged thickness on each pass during cold rolling of material to the desired thickness.

	Batch			
pass	**A1 1200**	**B1 3103**	**A2 1200**	**B2 3103**
0	20,00mm	20,05mm	20,00mm	20,00mm
1	17,00mm	17,20mm	18,30mm	18,40mm
2	15,90mm	16,00mm	16,05mm	16,15mm
3	14,40mm	14,50mm	13,65mm	13,75mm
4	12,80mm	12,90mm	11,50mm	11,60mm
5	11,20mm	11,30mm	9,40mm	9,50mm
6	9,60mm	9,70mm	7,30mm	7,40mm
7	8,00mm	8,10mm	5,65mm	5,75mm
8	6,45mm	6,52mm	4,55mm	4,40mm
9	4,86mm	4,96mm	3,55mm	3,60mm
10	3,80mm	3,88mm	2,50mm	2,60mm
11	2,77mm	2,86mm	1,92mm	2,01mm
12	2,00mm	2,25mm	1,40mm	1,47mm
13	1,90mm	1,98mm	1,10mm	1,10mm
14	1,77mm	1,82mm	1,03mm	0,98mm
15	1,65mm	1,76mm		
16	1,60mm	1,64mm		
17	1,45mm	1,44mm		
18	1,40mm	1,38mm		
19	1,27mm	1,27mm		
20	1,20mm	1,21mm		
21	1,08mm	1,14mm		
22	1,00mm	1,03mm		

B - Tables of all Tensile and Shear Samples

Al(1200) Annealed																								
A1	20,00mm	Strength of Bond				Trashed sample		Tensile Test						Kissing Bond	Shear Test									
A2	20,00mm	Strength of Glue/Material						T1		mm/min	T2		mm/min		l	b	Stress	Load	mm/min					
no	vMises	PT (min)	t0	tRB	CDT	Diameter																		groove
A1A01	0,00	150	2,00	0,82	59,0 %	15,00mm		29,31 MPa	5 177 N	0,1														
A1A02	0,00	140	2,40	0,96	60,0 %	15,00mm		39,59 MPa	6 992 N	0,1														
A1A03	0,00	130	2,80	1,01	63,9 %	13,20mm		45,80 MPa	6 262 N	2,0														
A1A04	0,00	120	3,20	0,98	69,4 %	15,00mm		32,61 MPa	5 759 N	0,1														
A1A05	0,00	120	3,20	1,02	68,1 %	15,00mm																		
A1A06	0,00	110	3,54	0,99	72,0 %	15,00mm		36,02 MPa	6 362 N	0,1														
A1A07	0,00	110	3,80	0,96	74,7 %	13,20mm		39,84 MPa	5 448 N	2,0														
A1A08	0,00	110	3,54	1,01	71,5 %	15,00mm									9,97mm	9,00mm	6,33 MPa	568 N						
A1A09	0,00	110	3,54	1,02	71,2 %	15,00mm																		
A1A10	0,00	110	3,54	1,03	70,9 %	15,00mm									9,99mm	9,00mm	8,49 MPa	763 N						
A1A11	0,00	110	3,54	1,05	70,3 %	15,00mm									9,60mm	9,30mm	8,53 MPa	762 N						
A2A01	0,00	90	2,06	1,62	21,4 %	15,00mm		0,00 MPa	0 N	-	-	-	-		1,00mm	1,00mm	0,00 MPa	0 N	-					
A2A02	0,00	90	2,06	1,60	22,3 %	15,00mm		0,57 MPa	100 N	-					10,00mm	10,04mm	4,40 MPa	442 N	0,2					
A2A03	0,00	90	2,06	1,50	27,2 %	15,00mm		3,40 MPa	600 N	-					10,00mm	10,04mm	8,33 MPa	836 N	0,2					
A2A04	0,00	90	2,06	1,35	34,5 %	15,00mm		9,87 MPa	1 744 N	0,2														
A2A05	0,00	90	2,06	1,22	40,8 %	15,00mm		0,22 MPa	39 N	0,2	12,41 MPa	1 621 N	0,2											

Table B 1: The results both TBST and SBST for AA1200 Annealed sample.

Al(1200) Non-Annealed																										
A1	20,00mm	Strength of Bond				Trashed sample	Tensile Test													Shear Test					
A2	20,00mm	Strength of Glue/Material						T1		mm/min	T2		mm/min	T3		mm/min	l	b	Stress	Load	mm/min
no	vMises	PT (min)	t0	tRB	CDT	Diameter																				
A1NA01	3,46	150	2,00	1,05	**47,5 %**	15,00mm																				
A1NA02	3,25	120	2,40	1,08	**55,0 %**	15,00mm	**39,03 MPa**	6 893 N	0,1																	
A1NA03	3,07	120	2,80	1,07	**61,8 %**	15,00mm																				
A1NA04	2,92	120	3,20	1,02	**68,1 %**	15,00mm																				
A1NA05	2,80	150	3,54	1,01	**71,5 %**	15,00mm																				
A1NA06	2,80	150	3,54	1,55	**56,2 %**	15,00mm	**28,35 MPa**	5 008 N	0,1																	
A1NA07	2,72	120	3,80	1,36	**64,2 %**	15,00mm	**35,64 MPa**	6 295 N	0,1																	
A1NA08	3,46	150	2,00	1,06	**47,0 %**	15,00mm																				
A1NA09	3,25	120	2,40	1,08	**55,0 %**	15,00mm																				
A1NA10	3,07	120	2,80	1,09	**61,1 %**	15,00mm																				
A1NA11	2,92	120	3,20	1,06	**66,9 %**	15,00mm																				
A1NA12	2,80	150	3,54	1,58	**55,4 %**	15,00mm																				
A1NA13	2,72	120	3,80	1,38	**63,7 %**	15,00mm																				
A2NA01	3,43	90	2,06	1,45	**29,6 %**	15,00mm	**6,63 MPa**	1 171 N	0,2	**19,49 MPa**	3 443 N	10,0				10,00mm	10,04mm	**13,02 MPa**	1 307 N	0,2
A2NA02	3,43	90	2,06	1,38	**33,0 %**	15,00mm	**13,28 MPa**	2 346 N	0,2	**21,31 MPa**	3 763 N	10,0				5,00mm	10,01mm	**15,98 MPa**	800 N	0,2
A2NA03	3,43	90	2,06	1,26	**38,8 %**	15,00mm	**38,29 MPa**	6 763 N	0,2	**44,37 MPa**	7 836 N	10,0				2,50mm	10,02mm	**29,54 MPa**	740 N	0,2
A2NA04	3,43	90	2,06	1,06	**48,5 %**	15,00mm	**30,85 MPa**	5 448 N	10,0	**34,33 MPa**	6 064 N	0,2	**29,76 MPa**	5 257 N	0,2	2,50mm	10,00mm	**39,12 MPa**	978 N	0,2
A2NA05	3,43	90	2,06	1,02	**50,5 %**	15,00mm				**16,49 MPa**	2 912 N	10,0				2,50mm	10,00mm	**38,16 MPa**	954 N	0,2

Table B 2: The results both TBST and SBST for AA1200 Non-annealed sample.

Al(3103) Annealed																								
B1	20,00mm	Strength of Bond				Trashed sample		Tensile Test									Shear Test							
B2	20,05mm	Strength of Glue/Material							T1	mm/min	T2	mm/min	T3	mm/min			l	b	Stress	Load	mm/min	Left
no	vMises	PT (min)	t0	tRB	CDT	Diameter																		
B1A01	0,00	120	2,00	1,04	**48,0 %**	15,00mm	**29,50 MPa**	5 210 N	0,2															
B1A02	0,00	120	2,40	1,00	**58,3 %**	15,00mm																		
B1A03	0,00	120	2,78	0,94	**66,2 %**	15,00mm																		
B1A04	0,00	120	3,28	1,00	**69,5 %**	15,00mm																		
B1A05	0,00	120	3,64	1,15	**68,4 %**	15,00mm																		
B1A06	0,00	120	3,96	1,29	**67,4 %**	15,00mm																		
B2A01	0,00	90	1,96	1,54	**21,4 %**	15,00mm	**0,00 MPa**	0 N	-	-	-	-	-	-	-	-	-	-	-	-	-			
B2A02	0,00	90	1,96	1,49	**24,0 %**	15,00mm	**0,00 MPa**	0 N	-	-	-	-	-	-	-	-	-	-	-	-	-			
B2A03	0,00	90	1,96	1,41	**28,1 %**	15,00mm	**2,83 MPa**	500 N	-															
B2A04	0,00	90	1,96	1,29	**34,2 %**	15,00mm	**1,18 MPa**	208 N									10,00mm	2,50mm	**25,64 MPa**	641 N				
B2A05	0,00	90	1,96	1,18	**39,8 %**	15,00mm	**0,00 MPa**	0 N									10,01mm	2,50mm	**23,42 MPa**	586 N		groove		
B2A06	0,00	90	1,96	1,07	**45,4 %**	15,00mm	**24,91 MPa**	4 400 N		**10,88 MPa**	1 261 N	0,2	**19,47 MPa**	2 492 N	0,2		10,03mm	2,50mm	**27,88 MPa**	699 N		groove		

Table B 3: The results both TBST and SBST for AA3103 Annealed sample.

Al(3103) Non-Annealed																								
B1	20,00mm	Strength of Bond		Trashed sample			Tensile Test										Shear Test							
B2	20,05mm	Strength of Glue/Material					T1		mm/min	T2		mm/min	T3		mm/min		l	b	Stress	Load	mm/min			
no	vMises	PT (min)	t0	tRB	CDT	Diameter																		
B1NA01	3,46	120	2,00	1,10	**45,0 %**	15,00mm	**38,11 MPa**	6 732 N	0,2															
B1NA02	3,46	120	2,00	1,13	**43,5 %**	15,00mm	**27,36 MPa**	4 833 N	0,2	**21,09 MPa**	3 725 N	0,2												
B1NA03	3,25	120	2,40	1,10	**54,2 %**	15,00mm	**37,45 MPa**	6 615 N	0,2															
B1NA04	3,25	120	2,40	1,13	**52,9 %**	15,00mm																		
B1NA05	3,08	120	2,78	1,07	**61,5 %**	15,00mm																		
B1NA06	2,89	240	3,28	1,55	**52,7 %**	15,00mm																		
B1NA07	2,77	120	3,64	1,60	**56,0 %**	15,00mm	**39,89 MPa**	7 046 N	0,2															
B1NA08	2,67	120	3,96	2,07	**47,7 %**	15,00mm																		
B2NA01	3,49	90	1,96	1,56	**20,4 %**	15,00mm	**0,00 MPa**	0 N	-	-	-	-	-	-	-		-	-	-	-	-			
B2NA02	3,49	90	1,96	1,42	**27,6 %**	15,00mm	**6,17 MPa**	1 090 N	0,2	**0,05 MPa**	8 N	10,0												
B2NA03	3,49	90	1,96	1,34	**31,6 %**	15,00mm	**12,70 MPa**	2 244 N	0,2	**23,17 MPa**	4 093 N	10,0					2,50mm	10,00mm	**21,92 MPa**	548 N	0,2			
B2NA04	3,49	90	1,96	1,26	**35,7 %**	15,00mm	**13,33 MPa**	2 355 N	0,2	**21,89 MPa**	3 866 N	10,0												
B2NA05	3,49	90	1,96	1,14	**41,8 %**	15,00mm	**20,99 MPa**	3 708 N	0,2	**48,02 MPa**	8 482 N	10,0	**34,34 MPa**	6 066 N	0,2		2,50mm	10,00mm	**29,00 MPa**	725 N	0,2			
B2NA06	3,49	90	1,96	1,03	**47,4 %**	15,00mm	**39,15 MPa**	6 914 N	0,2								5,00mm	9,99mm	**22,06 MPa**	1 102 N	0,2			

Table B 4: The results both TBST and SBST for AA3103 Non-annealed sample.

C - Adhesion Log

			Bonding Strength					Surface Preparation	
Sample	Glue	CT	Diameter	Load	Strain-rate	T-Strength	Yielded	Grit	Method*
test	Bostik Epoxy Rapid	days	20,0 mm	6 286 N	0,1 mm/min	**20,02 MPa**	Glue	-	Aceton
test	Bostik Epoxy Rapid	days	15,0 mm	-	0,1 mm/min		Glue	-	Aceton
test	Hysol 9466 A&B	22 h	15,0 mm	5 494 N	0,1 mm/min	**31,11 MPa**	Glue	320	1
test	Hysol 9466 A&B	22 h	15,0 mm	5 246 N	0,1 mm/min	**29,70 MPa**	Bond	320	1
A1NA06-T1	Hysol 9466 A&B	91 h	15,0 mm	5 008 N	0,1 mm/min	**28,35 MPa**	Glue	120	2
A1NA07-T1	Hysol 9466 A&B	113 h	15,0 mm	6 295 N	0,1 mm/min	**35,64 MPa**	Glue	120	2
none	Hysol 9466 A&B	113 h	15,0 mm	5 696 N	0,1 mm/min	**32,25 MPa**	Glue	120	2
none	Hysol 9466 A&B	93 h	15,0 mm	6 991 N	0,1 mm/min	**39,58 MPa**	Glue	120	2
A1NA02-T1	Hysol 9466 A&B	93 h	15,0 mm	6 893 N	0,1 mm/min	**39,03 MPa**	Glue	120	2
A1A01-T1	Hysol 9466 A&B	138 h	15,0 mm	5 177 N	0,1 mm/min	**29,31 MPa**	Glue	120	2
A1A02-T1	Hysol 9466 A&B	138 h	15,0 mm	6 992 N	0,1 mm/min	**39,59 MPa**	Glue	120	2
A1A04-T1	Hysol 9466 A&B	138 h	15,0 mm	5 759 N	0,1 mm/min	**32,61 MPa**	Glue	120	2
A1A06-T1	Hysol 9466 A&B	138 h	15,0 mm	6 362 N	0,1 mm/min	**36,02 MPa**	Glue	120	2
B1NA01-T1	Hysol 9466 A&B	115 h	15,0 mm	6 732 N	0,2 mm/min	**38,11 MPa**	Glue	120	3
B1NA02-T1	Hysol 9466 A&B	115 h	15,0 mm	4 833 N	0,2 mm/min	**27,36 MPa**	Glue	120	3
B1NA03-T1	Hysol 9466 A&B	115 h	15,0 mm	6 615 N	0,2 mm/min	**37,45 MPa**	Glue	120	3
B1NA07-T1	Hysol 9466 A&B	115 h	15,0 mm	7 046 N	0,2 mm/min	**39,89 MPa**	Glue	120	3
A2NA01-T1	Hysol 9466 A&B	143 h	15,0 mm	1 171 N	0,2 mm/min	**6,63 MPa**	Bond	120	3
A2NA02-T1	Hysol 9466 A&B	143 h	15,0 mm	2 346 N	0,2 mm/min	**13,28 MPa**	Bond	120	3
A2NA03-T1	Hysol 9466 A&B	143 h	15,0 mm	6 763 N	0,2 mm/min	**38,29 MPa**	Bond	120	3
A2NA04-T1	Hysol 9466 A&B	143 h	15,0 mm	5 793 N	10,0 mm/min	**32,80 MPa**	Bond	120	3
A1A07-T1	Hysol 9466 A&B	143 h	13,2 mm	5 448 N	2,0 mm/min	**39,83 MPa**	Glue*	120	4
A1A03-T1	Hysol 9466 A&B	143 h	13,2 mm	6 262 N	2,0 mm/min	**45,78 MPa**	Glue*	120	4
B2NA03-T1	Hysol 9466 A&B	142 h	15,0 mm	2 244 N	0,2 mm/min	**12,70 MPa**	Bond	120	3
B2NA04-T1	Hysol 9466 A&B	142 h	15,0 mm	2 355 N	0,2 mm/min	**13,33 MPa**	Bond	120	3
B2NA05-T1	Hysol 9466 A&B	142 h	15,0 mm	3 708 N	0,2 mm/min	**20,99 MPa**	Glue	120	3
B2NA06-T1	Hysol 9466 A&B	142 h	15,0 mm	6 914 N	0,2 mm/min	**39,15 MPa**	Glue	120	3
A2A04-T1	Hysol 9466 A&B	76 h	15,0 mm	1 744 N	0,2 mm/min	**9,87 MPa**	Bond	120	3
A2A03-T1	Hysol 9466 A&B	76 h	15,0 mm	100 N	0,2 mm/min	**0,57 MPa**	Bond	120	3
B2NA02-T1	Hysol 9466 A&B	76 h	15,0 mm	1 090 N	0,2 mm/min	**6,17 MPa**	Bond	120	3
B2NA05-T2	Hysol 9466 A&B	76 h	15,0 mm	8 482 N	10,0 mm/min	**48,02 MPa**	Glue	120	3
A2NA01-T2	Hysol 9466 A&B	51 h	15,0 mm	3 443 N	10,0 mm/min	**19,49 MPa**	Bond	120	3
A2NA02-T2	Hysol 9466 A&B	51 h	15,0 mm	3 763 N	10,0 mm/min	**21,31 MPa**	Bond	120	3
A2NA03-T2	Hysol 9466 A&B	51 h	15,0 mm	7 836 N	10,0 mm/min	**44,37 MPa**	Glue	120	3
A2NA05-T1	Hysol 9466 A&B	51 h	15,0 mm	2 912 N	10,0 mm/min	**16,49 MPa**	Glue	120	3
B2NA02-T2	Hysol 9466 A&B	68 h	15,0 mm	8 N	10,0 mm/min	**0,05 MPa**	Bond	120	3
B2NA05-T3	Hysol 9466 A&B	68 h	15,0 mm	6 066 N	0,2 mm/min	**34,34 MPa**	Glue	120	3
B2NA03-T2	Hysol 9466 A&B	68 h	15,0 mm	4 093 N	10,0 mm/min	**23,17 MPa**	Bond	120	3
B2NA04-T2	Hysol 9466 A&B	68 h	15,0 mm	3 866 N	10,0 mm/min	**21,89 MPa**	Bond	120	3
B2A06-T1	Hysol 9466 A&B	48 h	15,0 mm	4 400 N	0,2 mm/min	**24,91 MPa**	Glue	80	3
B2A05-T1	Hysol 9466 A&B	48 h	15,0 mm	0 N	0,2 mm/min	**0,00 MPa**	Bond	80	3
B2A04-T1	Hysol 9466 A&B	48 h	15,0 mm	208 N	0,2 mm/min	**1,18 MPa**	Bond	80	3
A2A05-T1	Hysol 9466 A&B	48 h	15,0 mm	39 N	0,2 mm/min	**0,22 MPa**	Bond	80	3
A2A05-T2	Hysol 9466 A&B	97 h	12,9 mm	1 621 N	0,2 mm/min	**12,41 MPa**	Bond	80	3
A2A05-T3	Hysol 9466 A&B	97 h	-	-	0,2 mm/min		-	80	3
A2NA04-T2	Hysol 9466 A&B	97 h	15,0 mm	6 064 N	0,2 mm/min	**34,33 MPa**	Glue	80	3
B2A06-T2	Hysol 9466 A&B	97 h	12,2 mm	1 261 N	0,2 mm/min	**10,88 MPa**	Bond	80	3
A2NA04-T3	Hysol 9466 A&B	72 h	15,0 mm	5 257 N	0,2 mm/min	**29,76 MPa**	Glue	80	3
B2A06-T3	Hysol 9466 A&B	72 h	12,8 mm	2 492 N	0,2 mm/min	**19,47 MPa**	Bond	80	3
B1NA02-T2	Hysol 9466 A&B	72 h	15,0 mm	3 725 N	0,2 mm/min	**21,09 MPa**	Glue	80	3
B1A01-T1	Hysol 9466 A&B	72 h	15,0 mm	5 210 N	0,2 mm/min	**29,50 MPa**	Glue	80	3

Table C 1: Results log in relation to the TBST.

D - SEM Pictures: Tensile Samples

The following figures show a selection of SEM pictures taken at various magnification of the fracture surface of the tensile test samples. In most of the pictures a denomination A and B, following the sample number relates to which of the two fracture sides that is observed. All images is taken from above the sample.

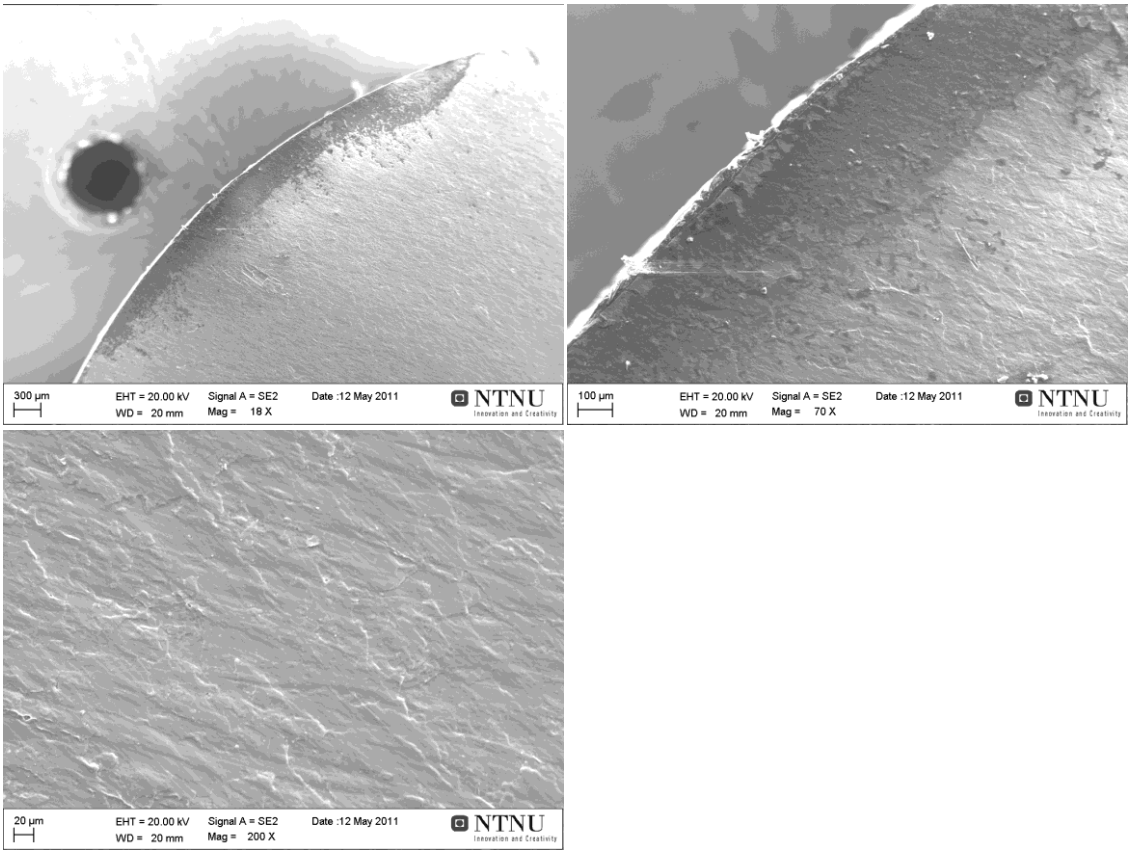

Figure D 1: Sample A2NA01-T1; 6.63MPa at 29.6% reduction.

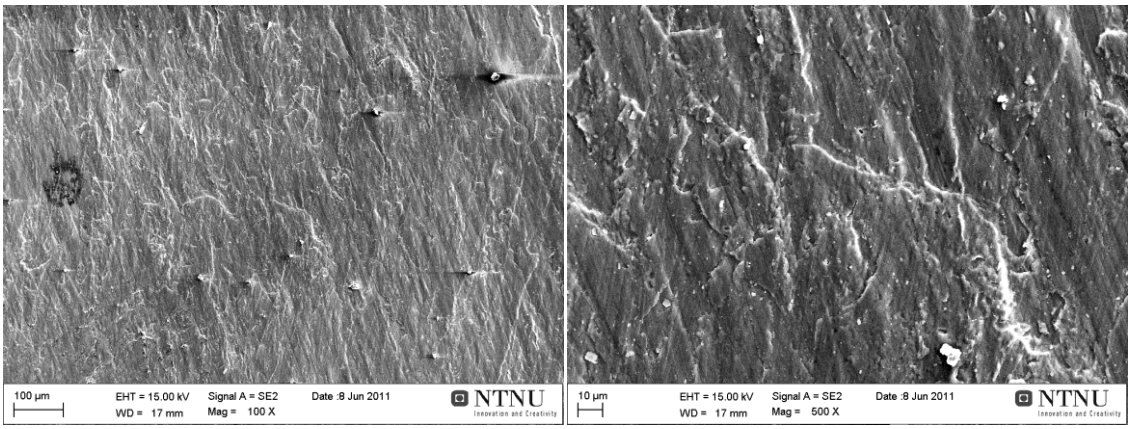

Figure D 2: A2NA01-T2 A; 19.49MPa at 29.6% reduction.

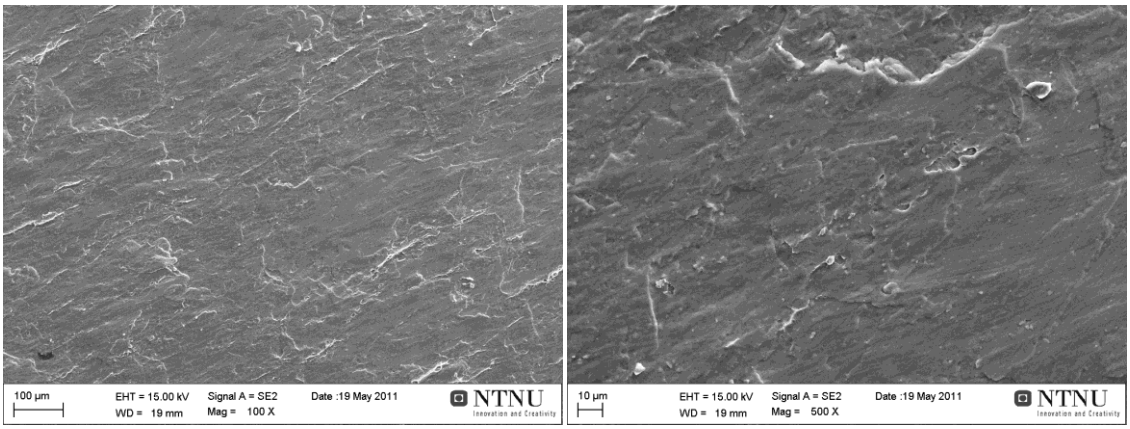

Figure D 3: A2NA02-T1 A; 13.28MPa at 33.0% reduction.

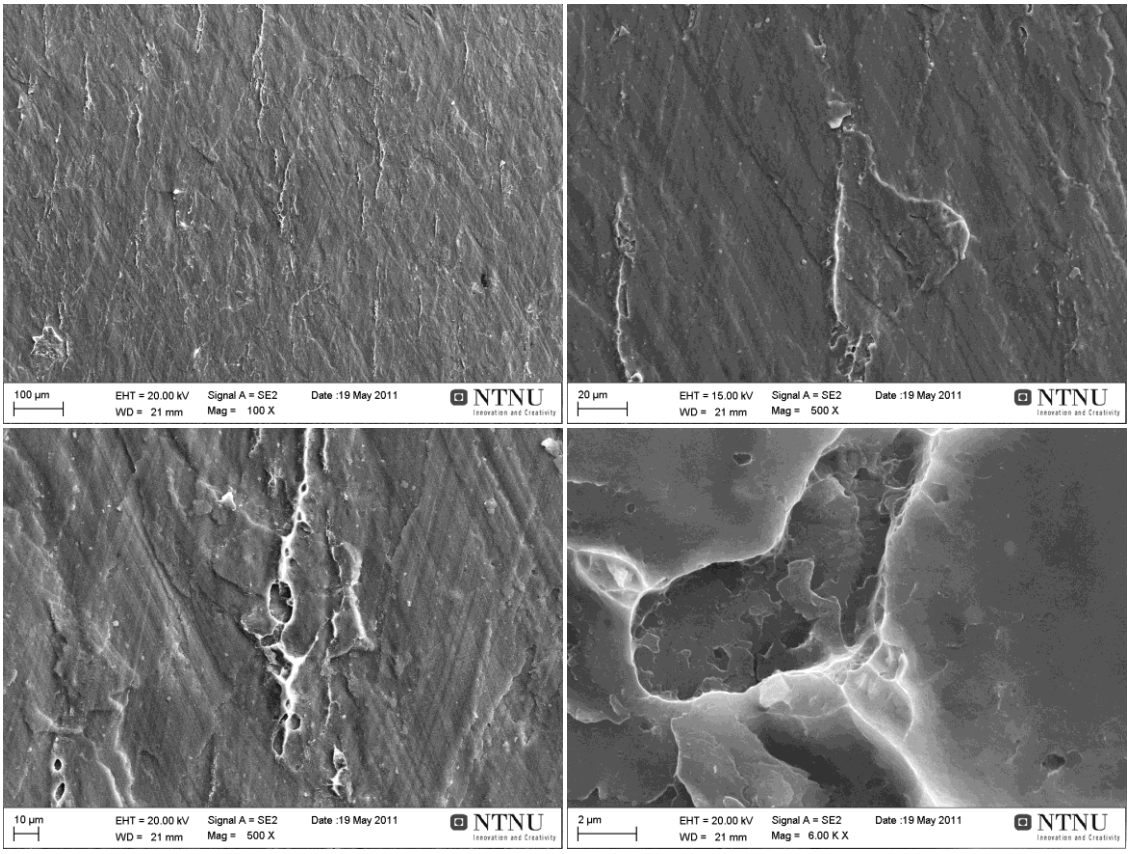

Figure D 4: A2NA02-T1 B; 13.28MPa at 33.0% reduction.

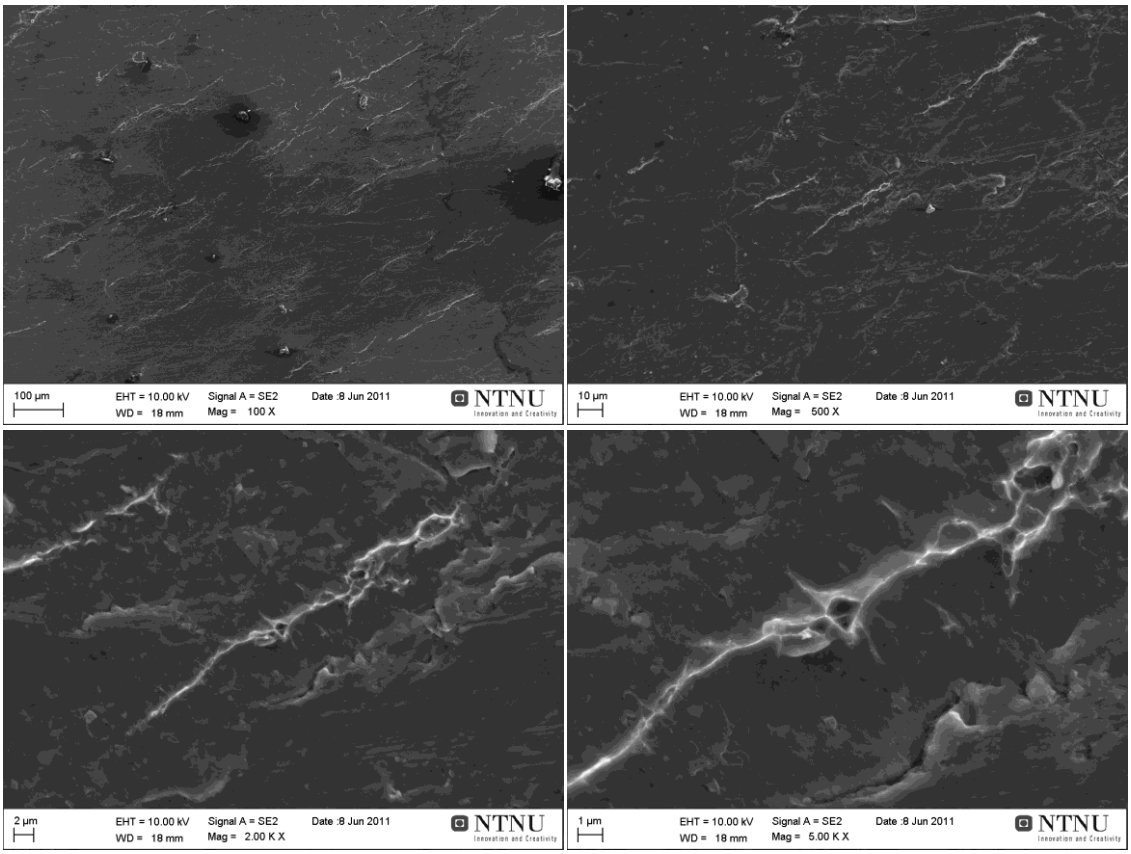

Figure D 5: A2NA02-T2 A; 21.31MPa at 33.0% reduction.

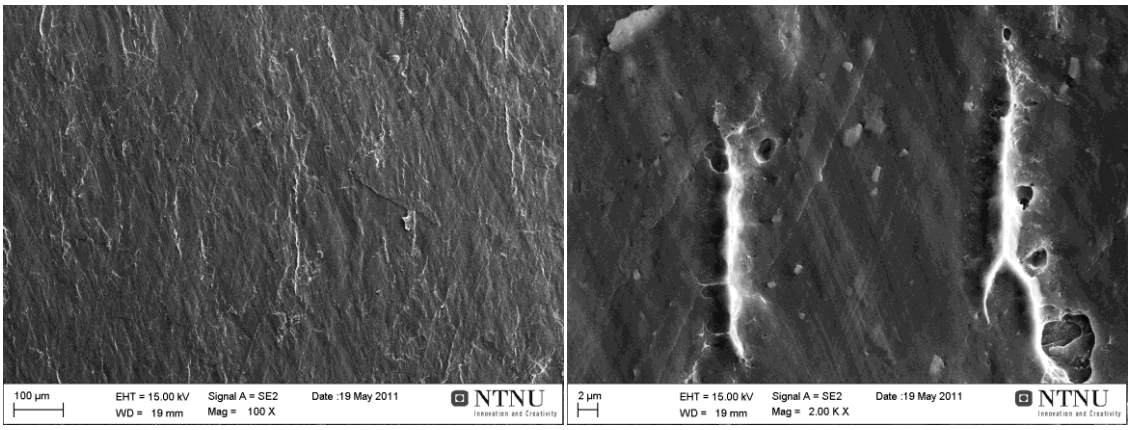

Figure D 6: A2NA03-T1 A; 38.29MPa at 38.8% reduction.

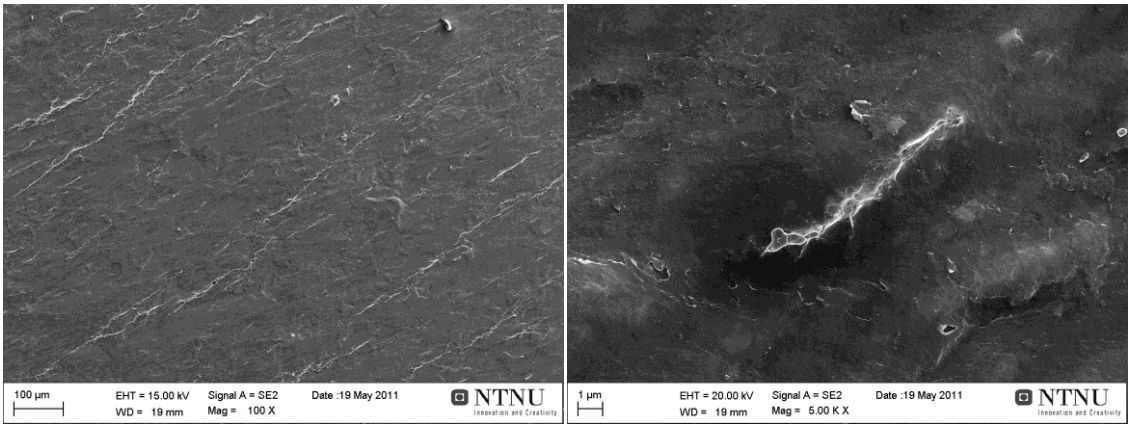

Figure D 7: A2NA03-T1 B; 38.29MPa at 38.8% reduction.

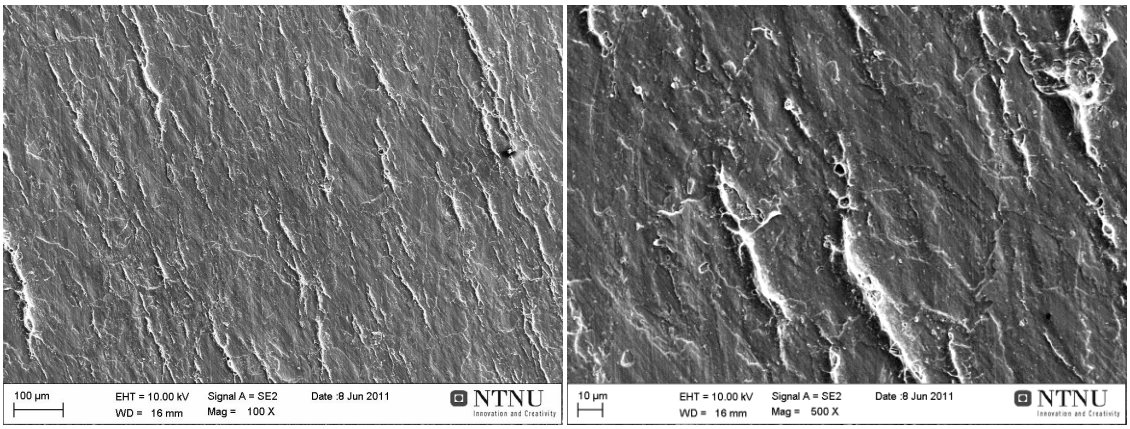

Figure D 8: A2NA04-T1 A; 32.80MPa at 48.5% reduction.

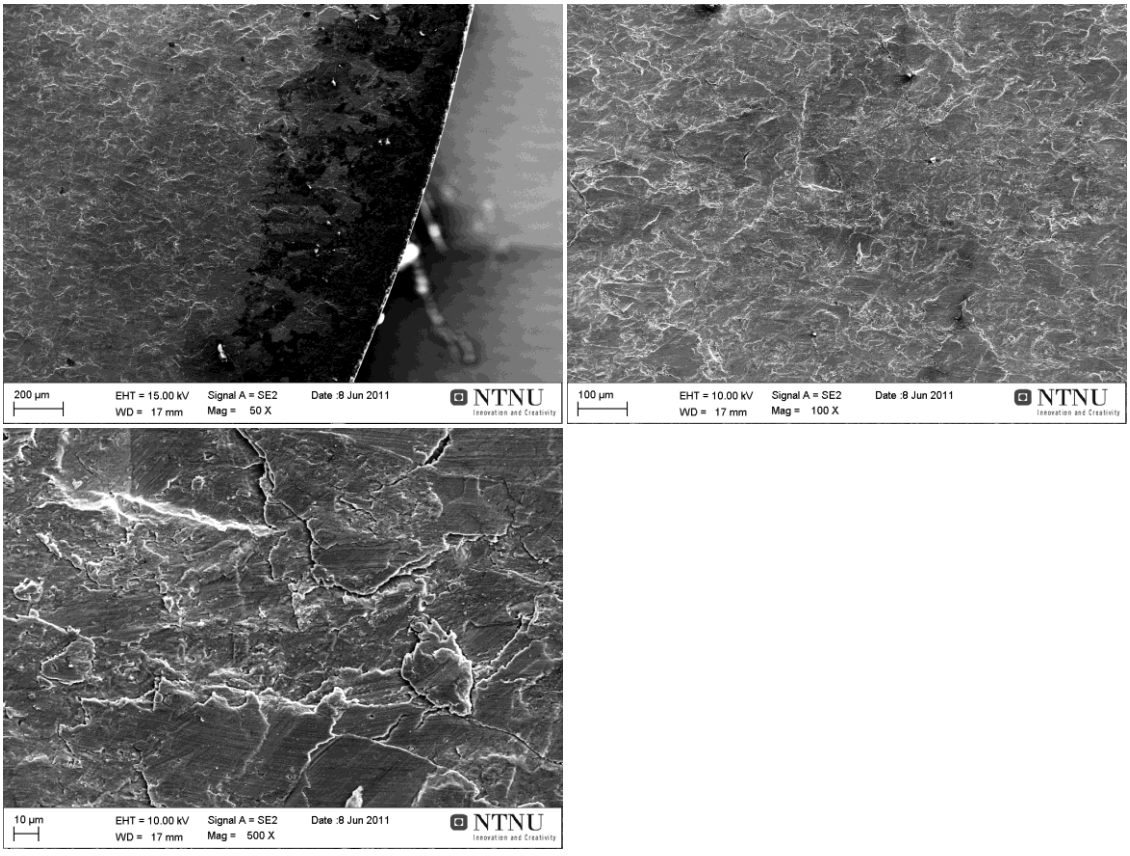

Figure D 9: A2A03-T1 A; ~0.57MPa at 27.2% reduction.

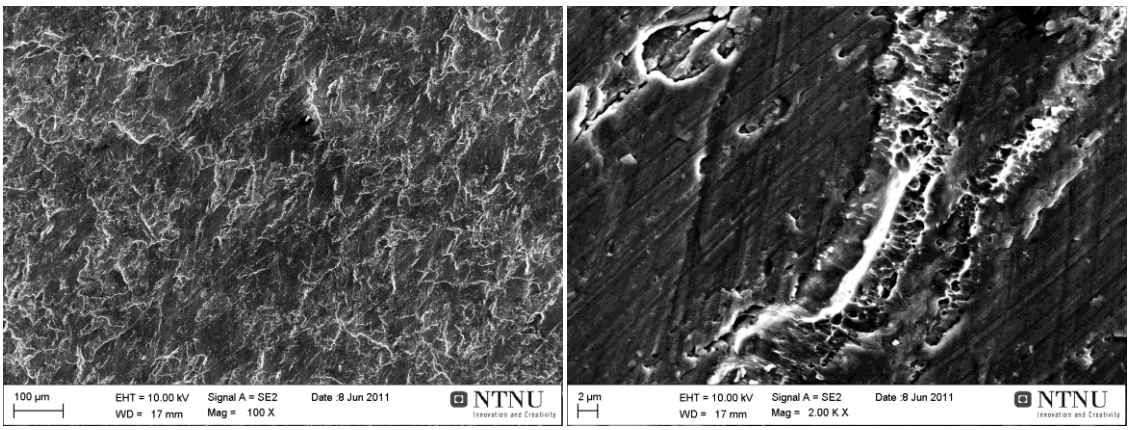

Figure D 10: A2A04-T1 A; 9.87MPa at 34.5% reduction.

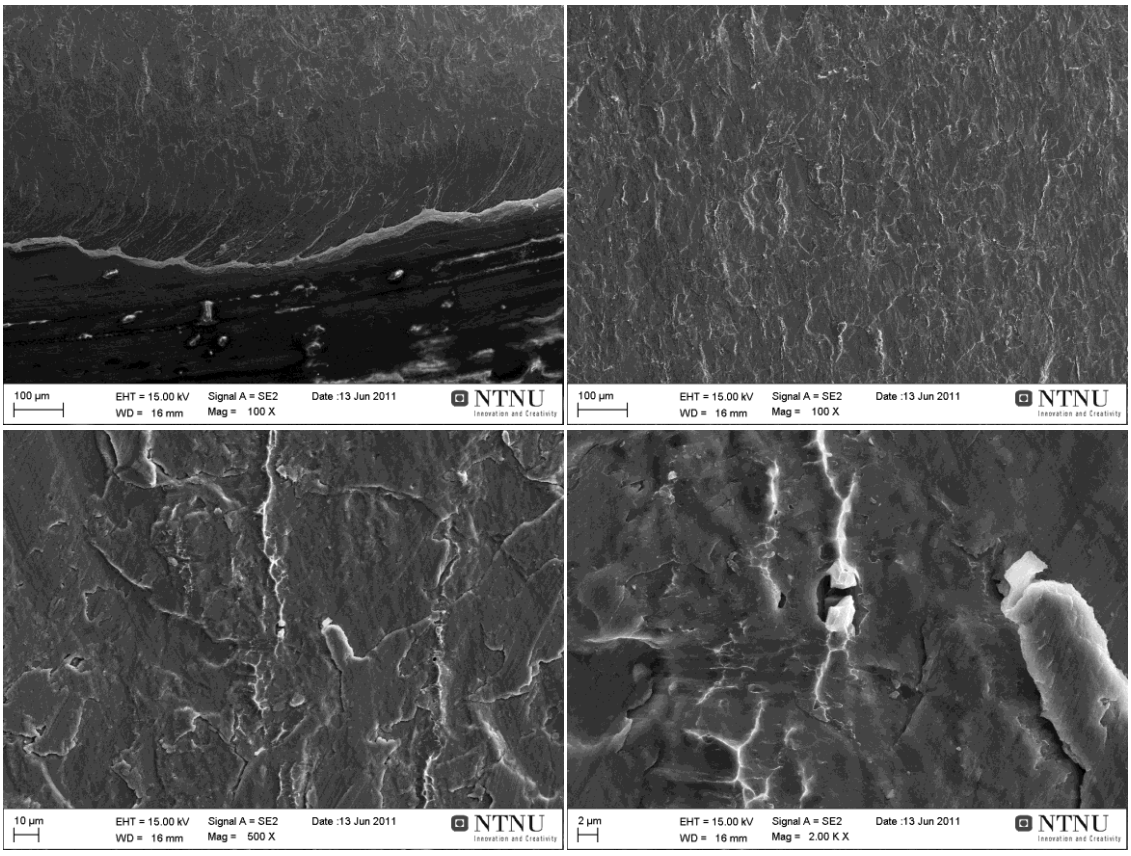

Figure D 11: A2A05-T1 A; ~0.22MPa at 40.8% reduction. Broke when mounted.

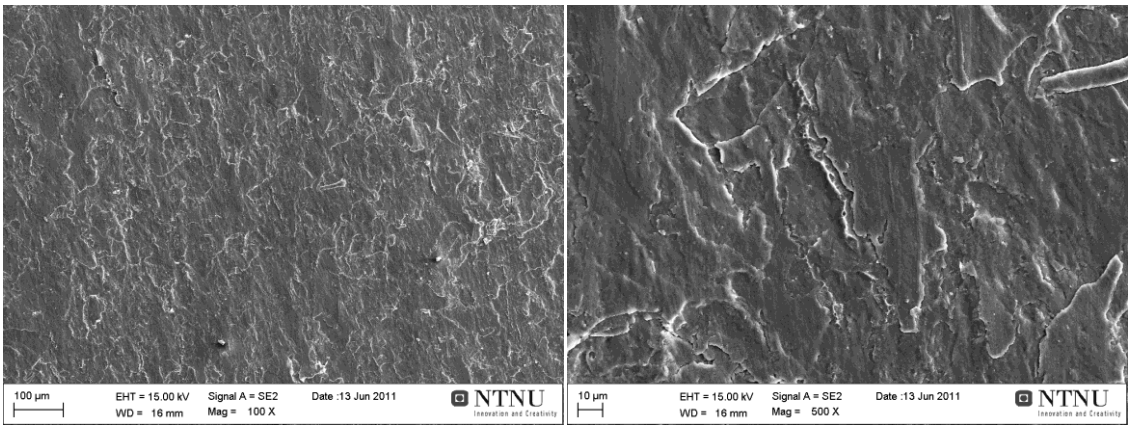

Figure D 12: A2A05-T2 A; 12.41MPa at 40.8% reduction.

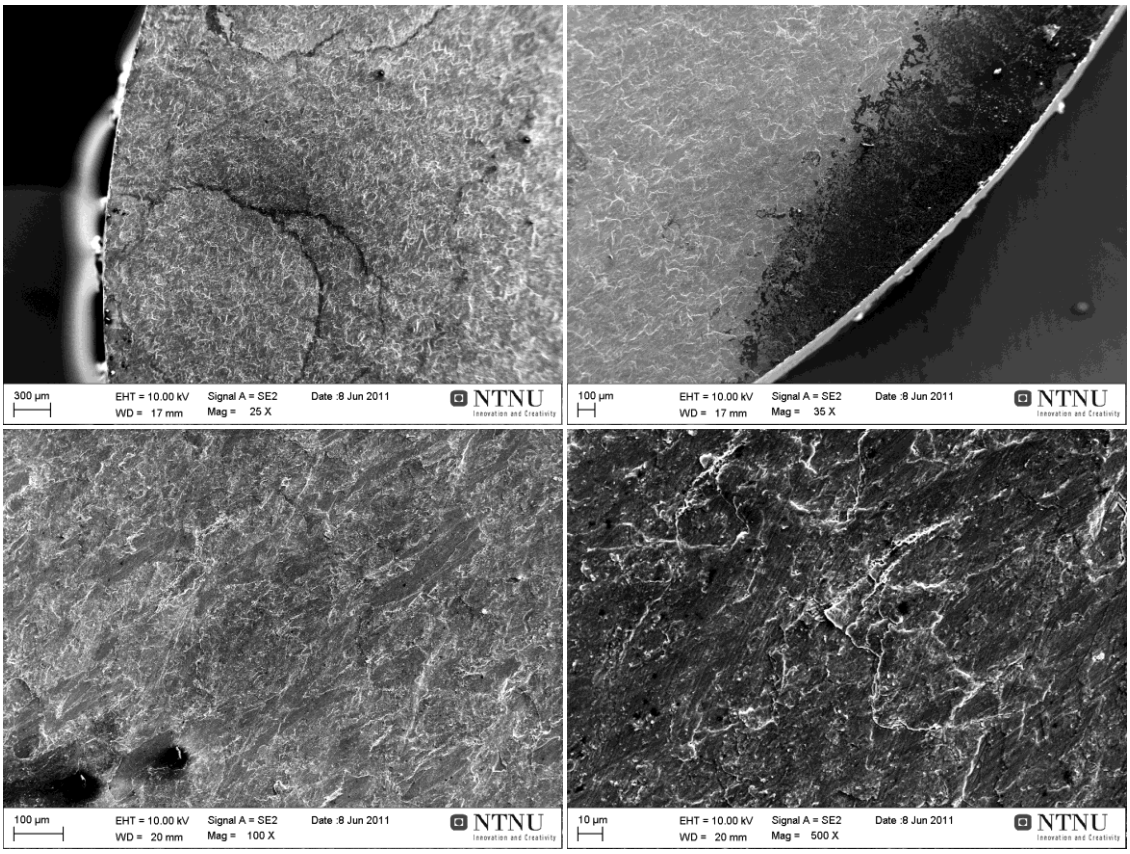

Figure D 13: B2NA02-T1 A; 6.17MPa at 27.6% reduction.

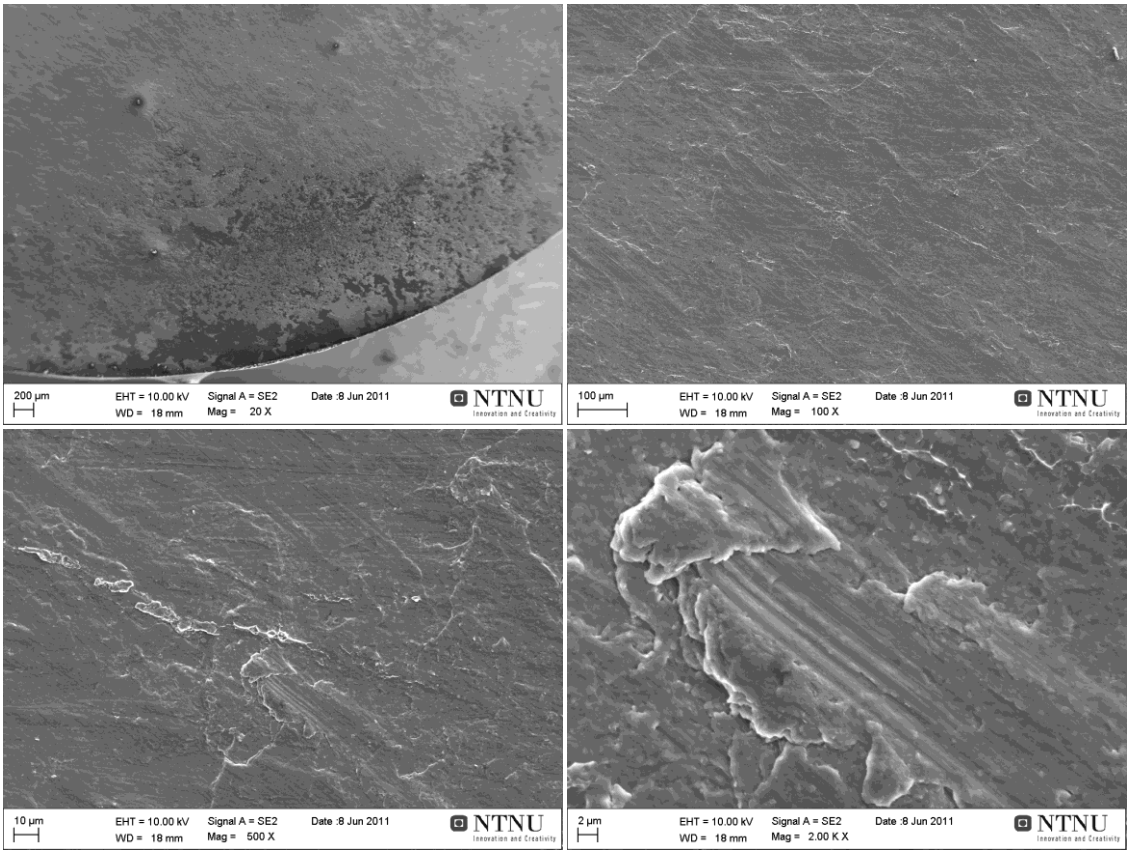

Figure D 14: B2NA02-T2 A; ~0.05MPa at 27.6% reduction. Broke when mounted.

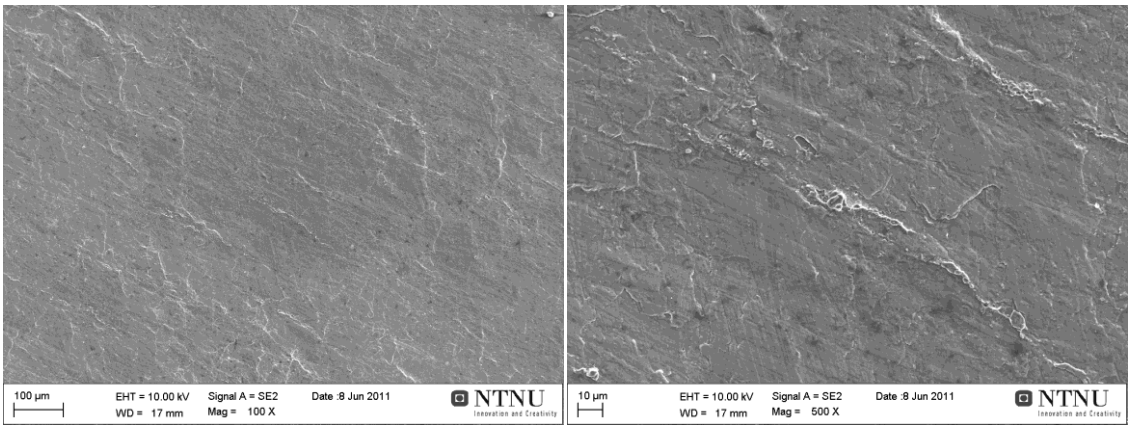

Figure D 15: B2NA03-T1 A; 12.70MPa at 31.6% reduction.

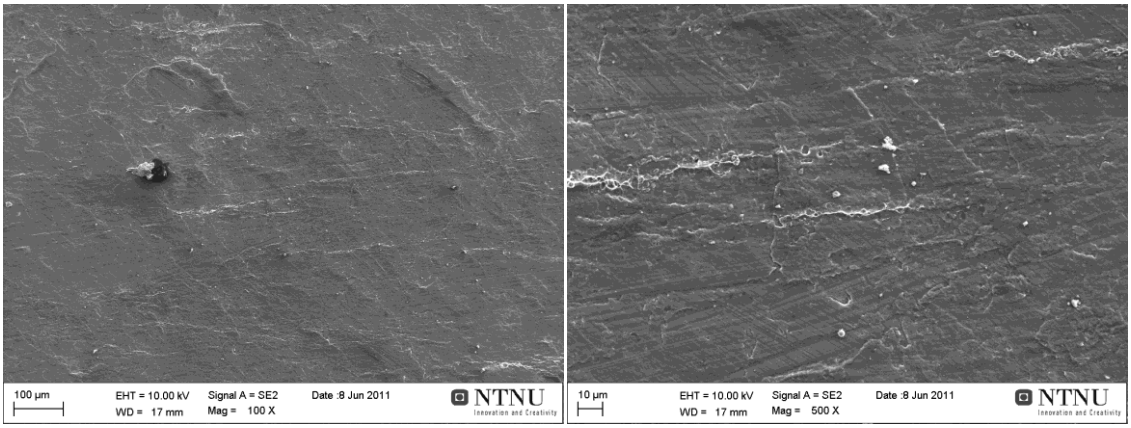

Figure D 16: B2NA03-T2 A; 23.17MPa at 31.6% reduction.

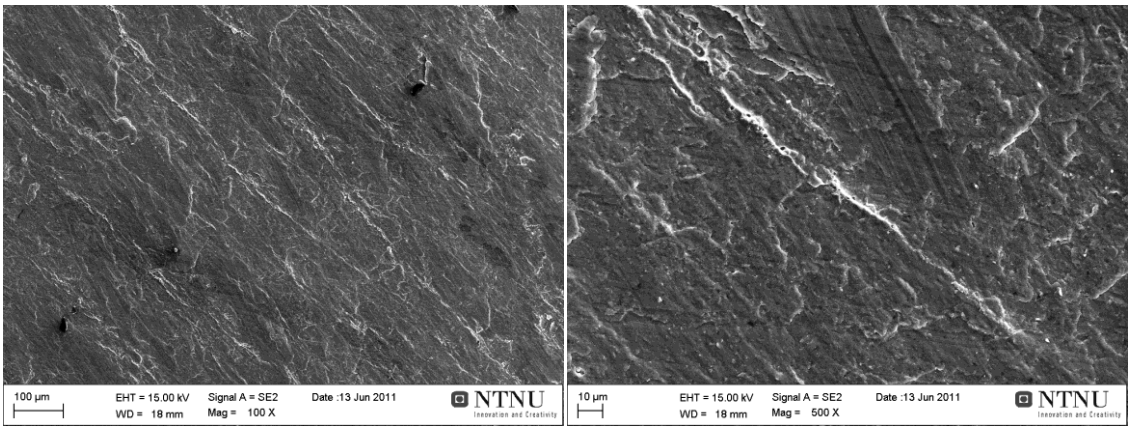

Figure D 17: B2NA04-T2 A; 21.89MPa at 35.7% reduction.

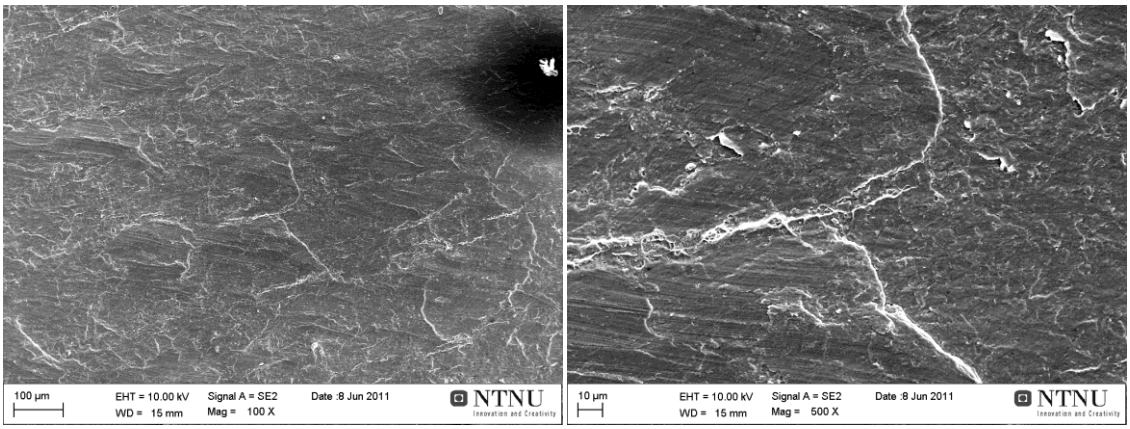

Figure D 18: B2NA04-T1 A; 13.33MPa at 35.7% reduction.

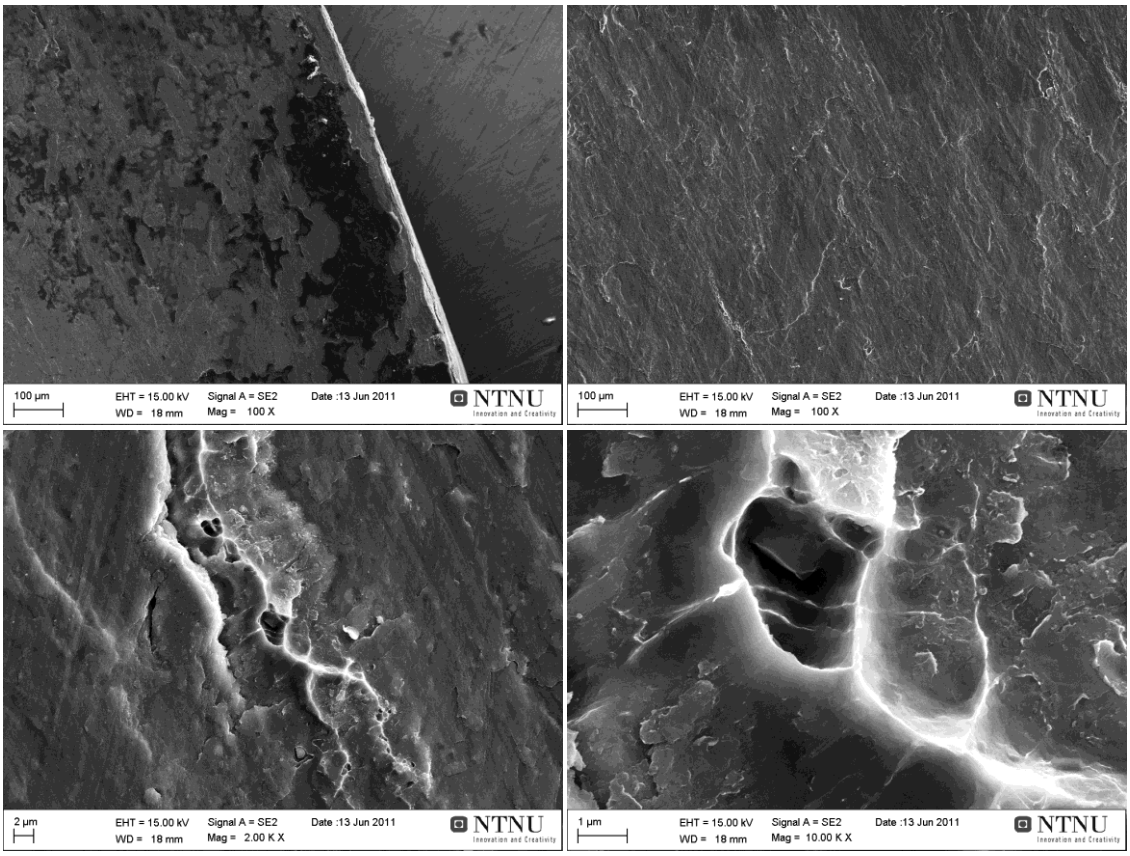

Figure D 19: B2A04-T1 A; ~1.18MPa at 34.2% reduction. Weakened /Damaged.

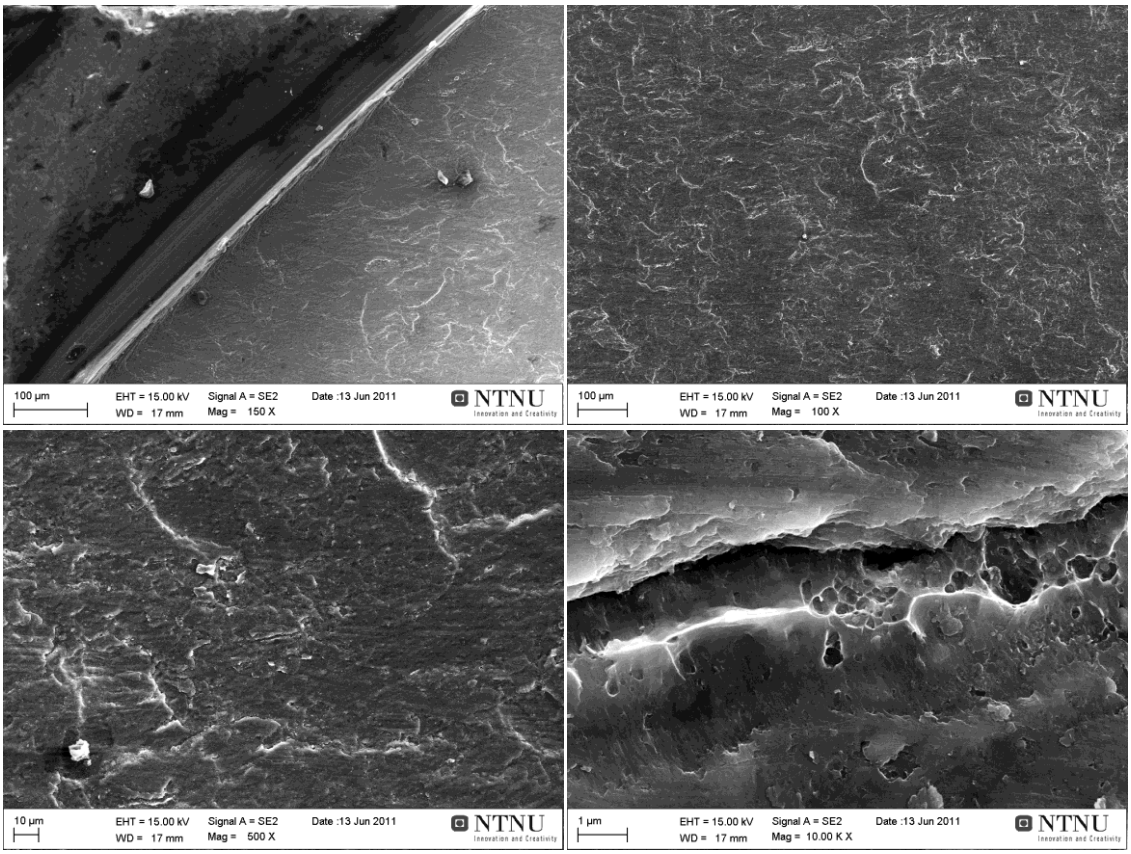

Figure D 20: B2A05-T1 A; ~0MPa at 39.8% reduction. Broke when mounted.

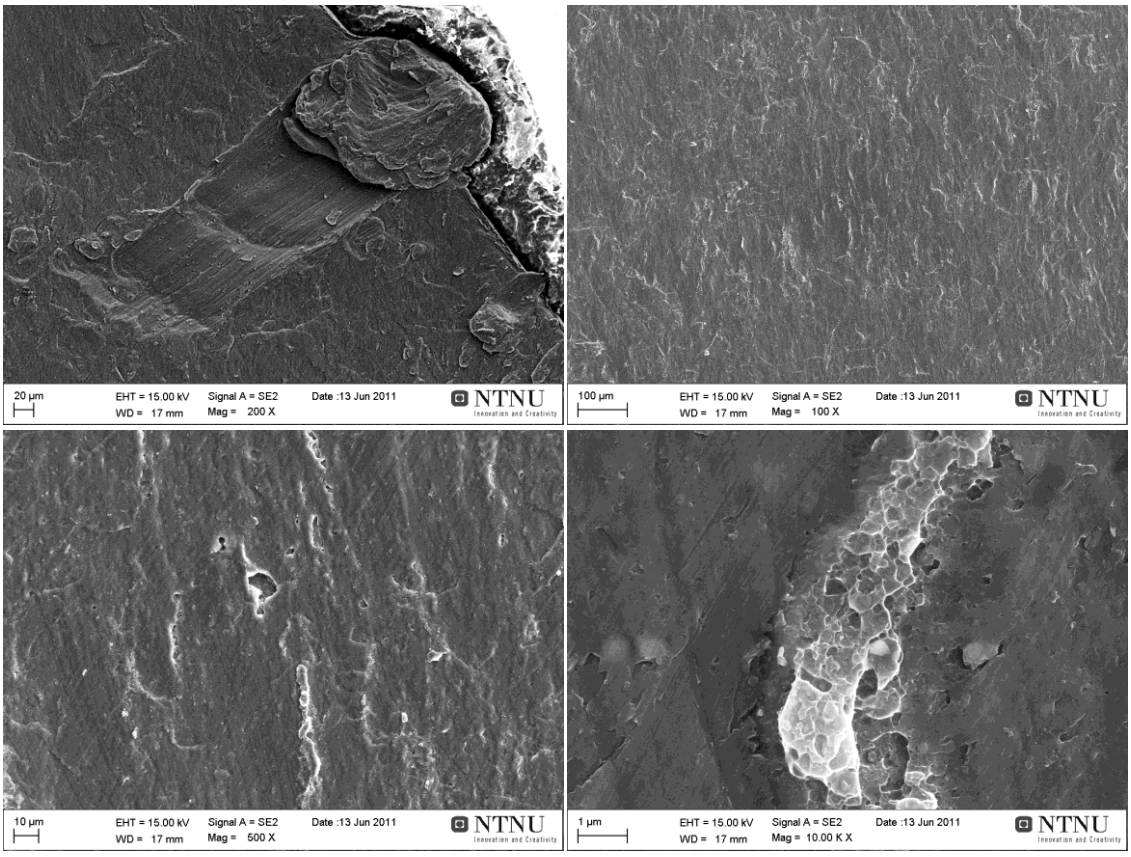

Figure D 21: B2A06-T2 A; 10.88MPa at 45.4% reduction.

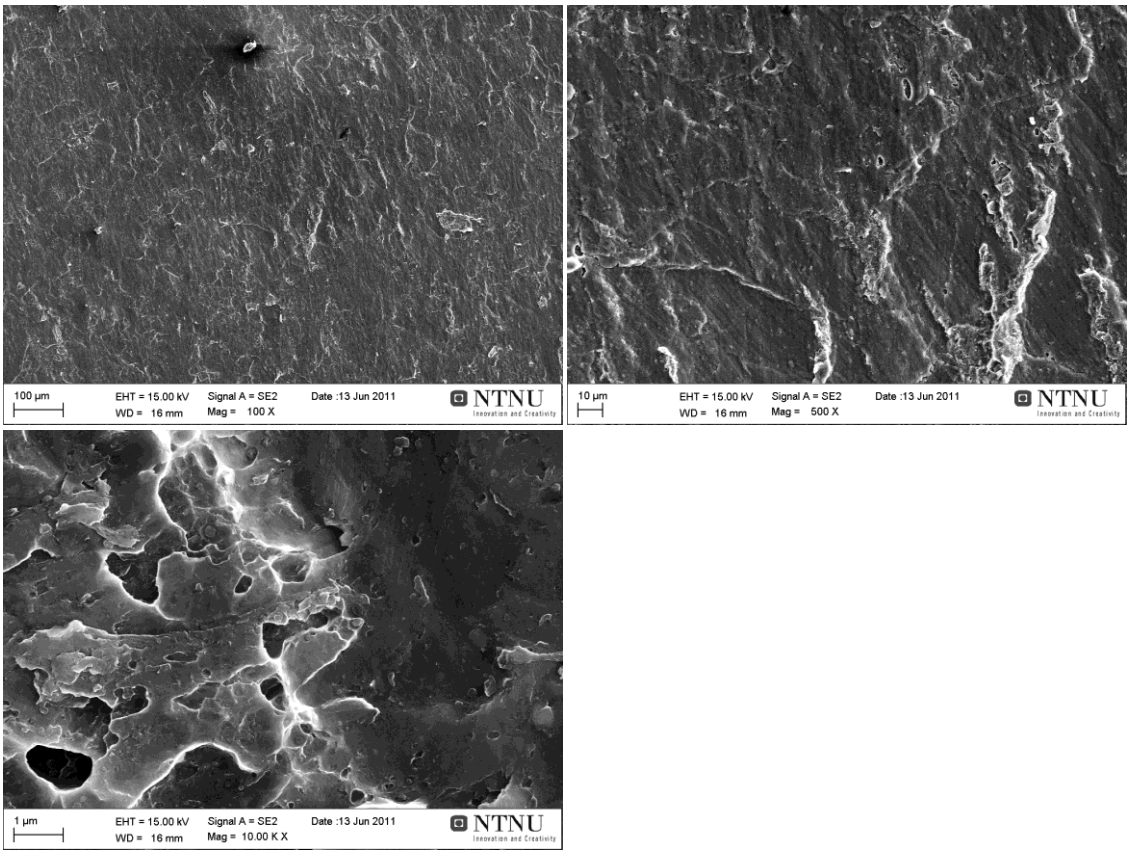

Figure D 22: B2A06-T3 A; 19.47MPa at 45.4% reduction. Forgot to remove glue from groove, hence a too high strength was measured.

E - SEM Pictures: Shear Samples

The following figures show a selection of SEM pictures taken at various magnification of the fracture surface of the Shear test samples. All images are taken from above the sample.

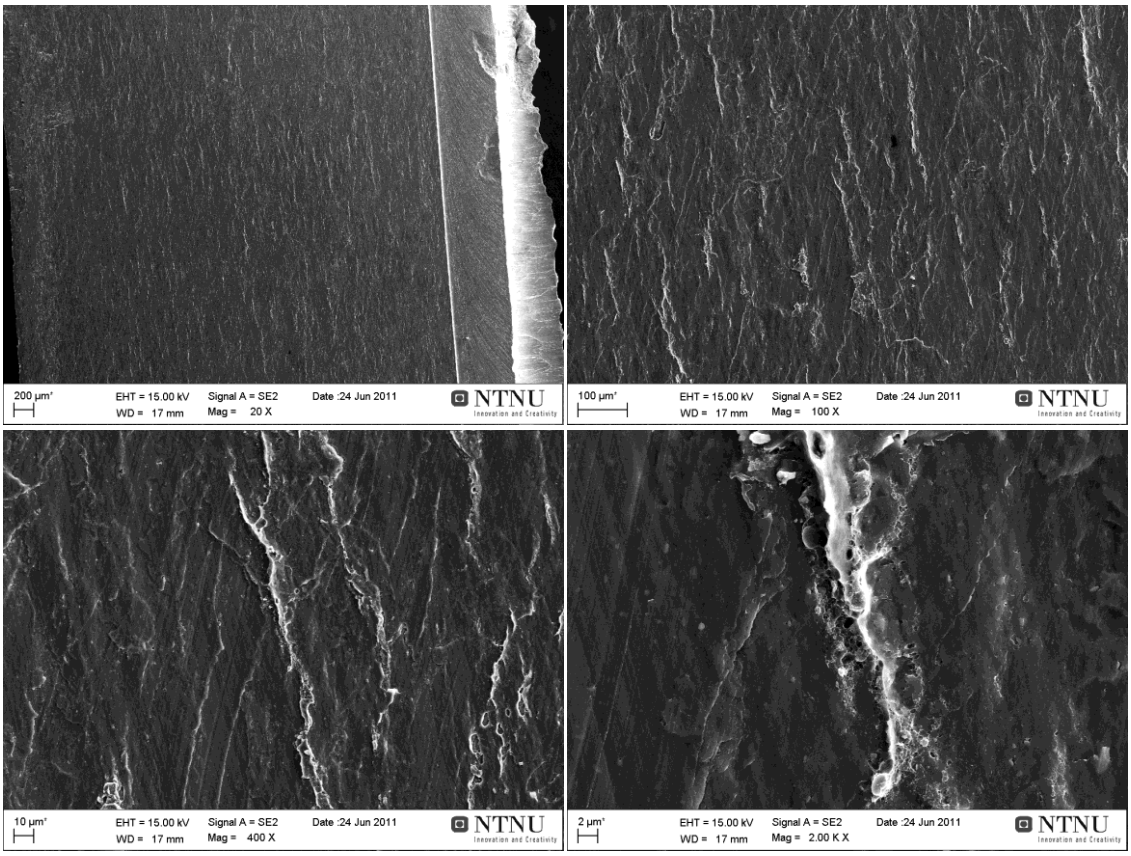

Figure E 1: A2NA02; 15.98MPa at 33.0% reduction.

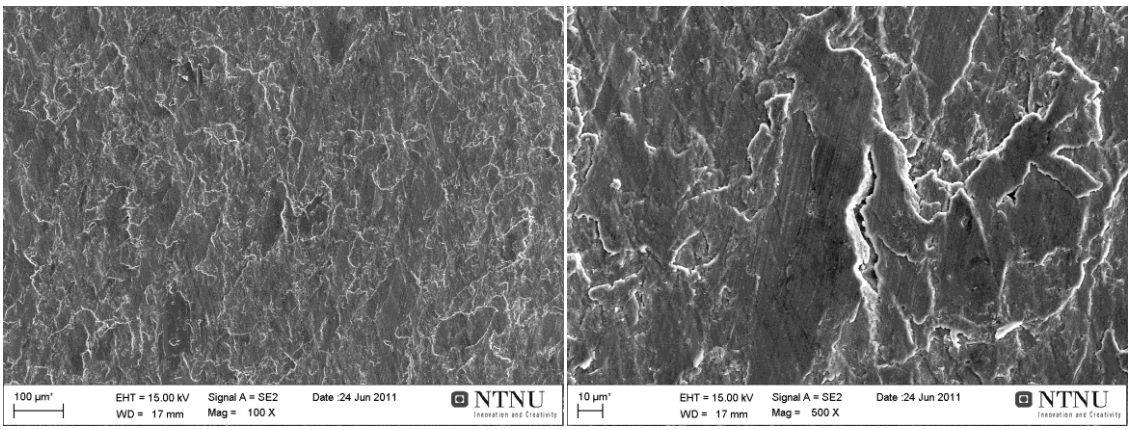

Figure E 2: A2A02; 4.48MPa at 22.3% reduction.

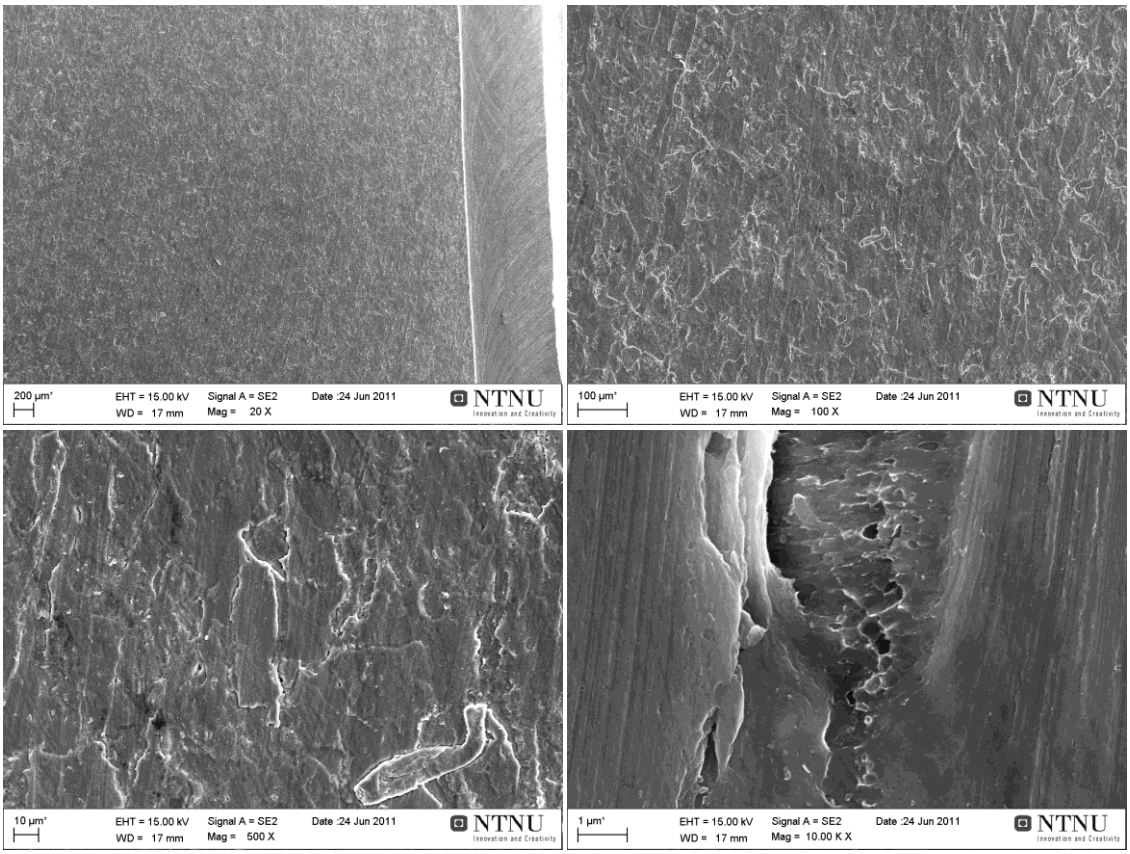

Figure E 3: A2A03; 8.36MPa at 27.2% reduction.

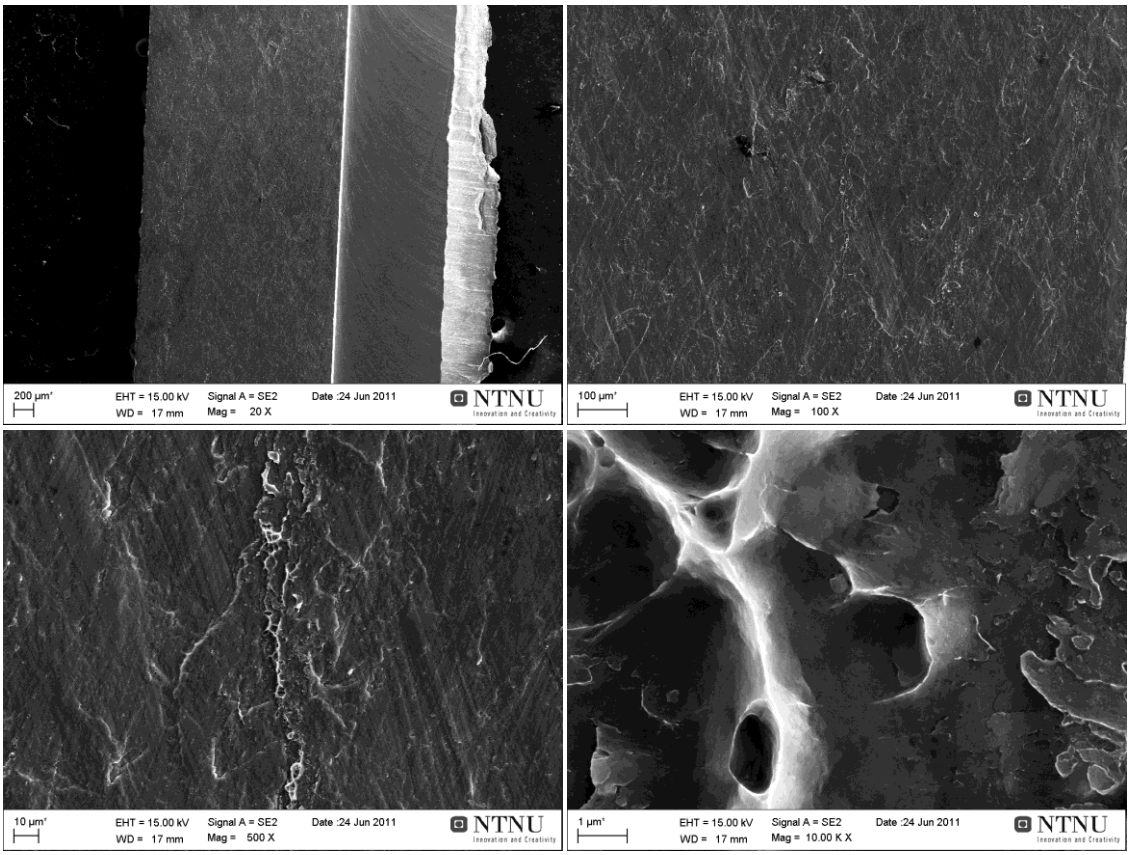

Figure E 4: B2NA03; 21.92MPa at 31.6% reduction.

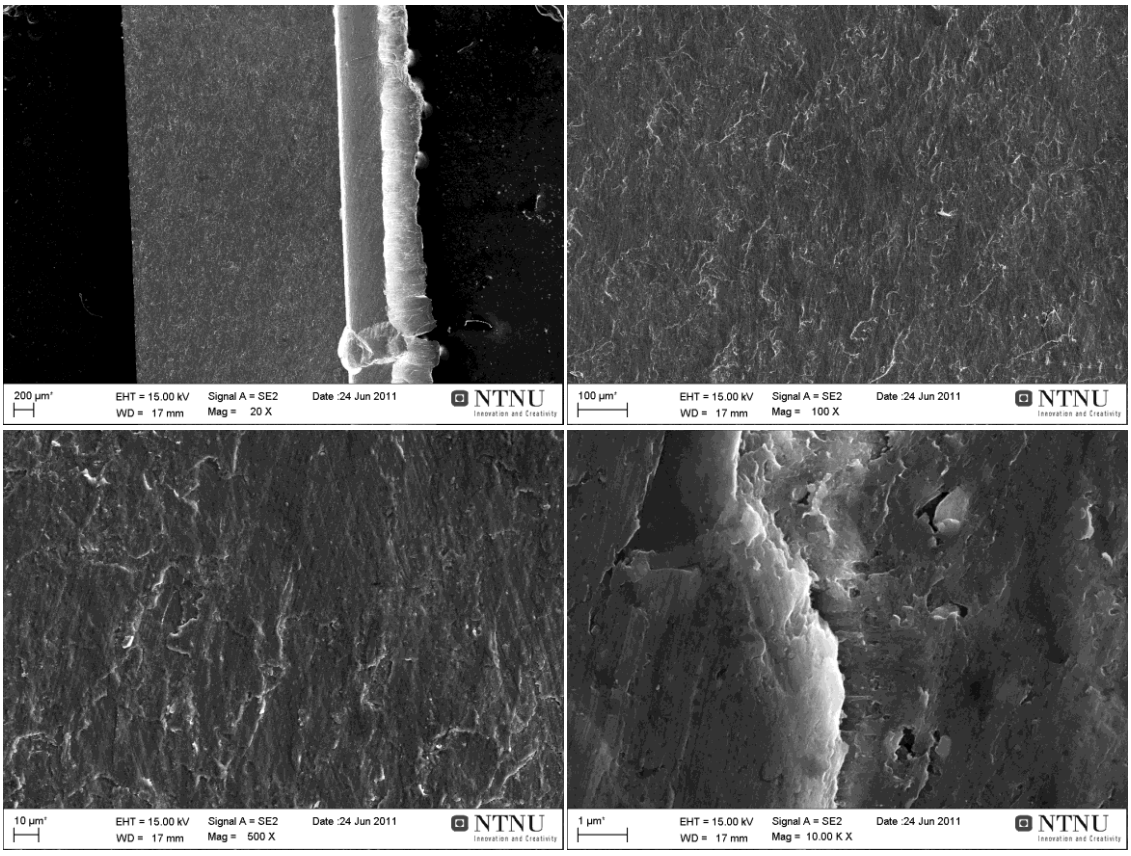

Figure E 5: B2A04; 25.64MPa at 34.2% reduction.

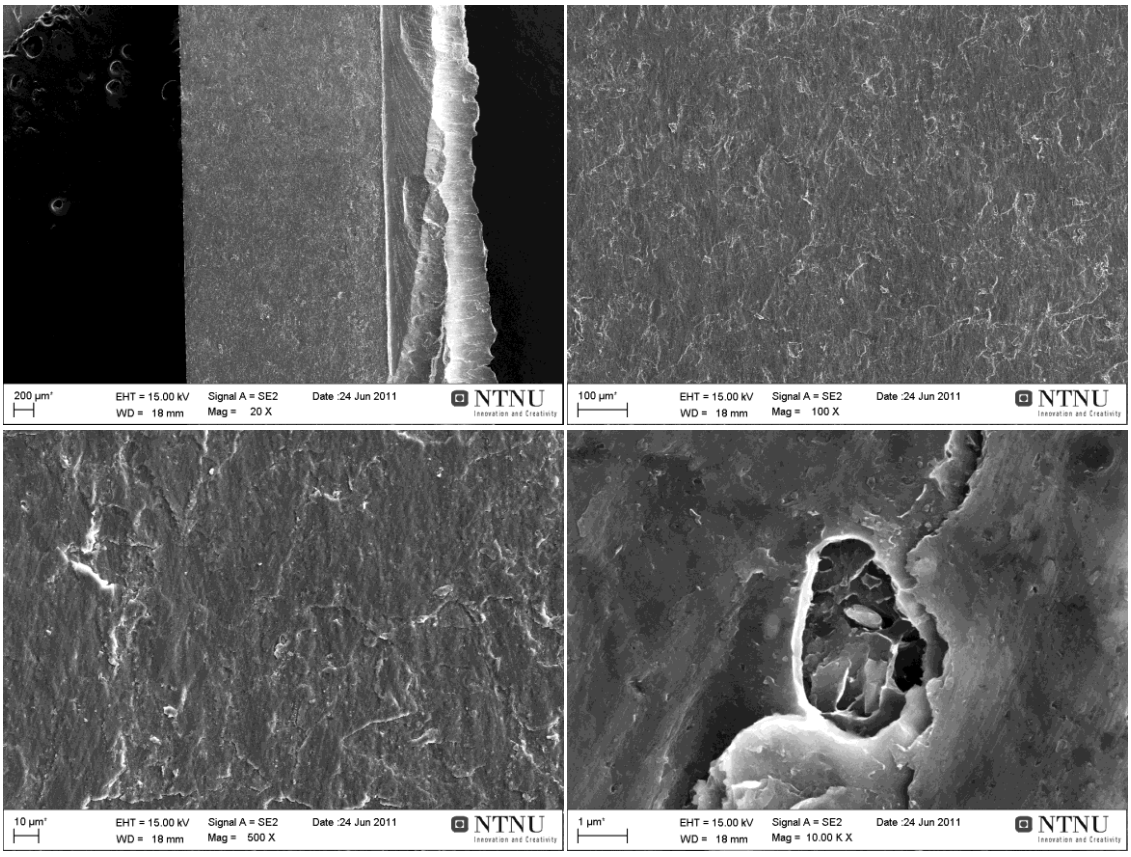

Figure E 6: B2A05; 23.42MPa at 39.8% reduction.

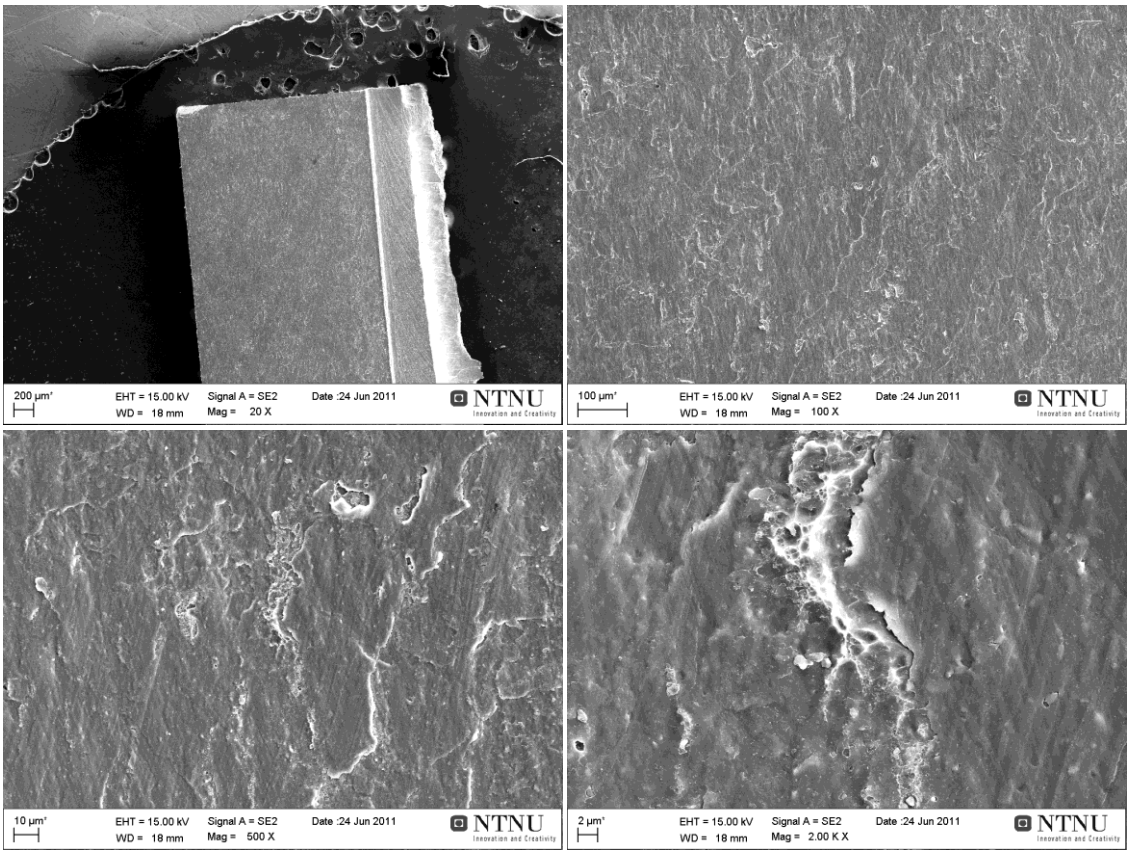

Figure E 7: B2A06; 27.88MPa at 45.4% reduction.

F - SEM Pictures: Bond Interface

The following figures show a selection of SEM pictures taken at various magnification of the bond interface of sample A2NA02. All images are taken from the side of the sample.

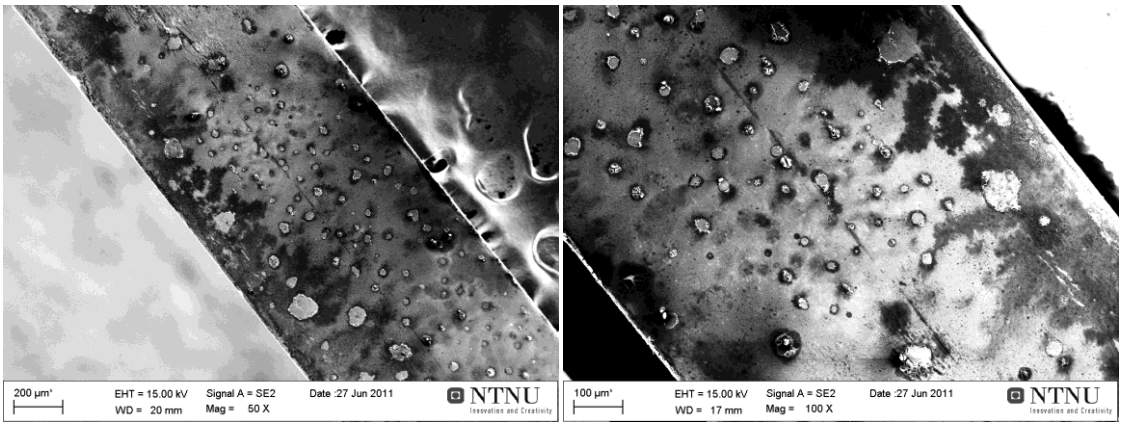

Figure F 1: The interface shown at 50x and 100x magnification.

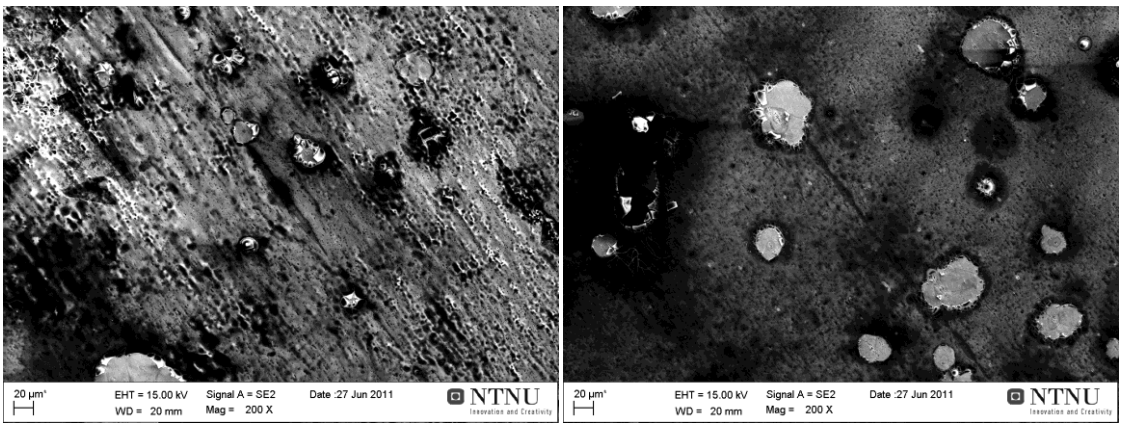

Figure F 2: The interface shown at 200x magnification.

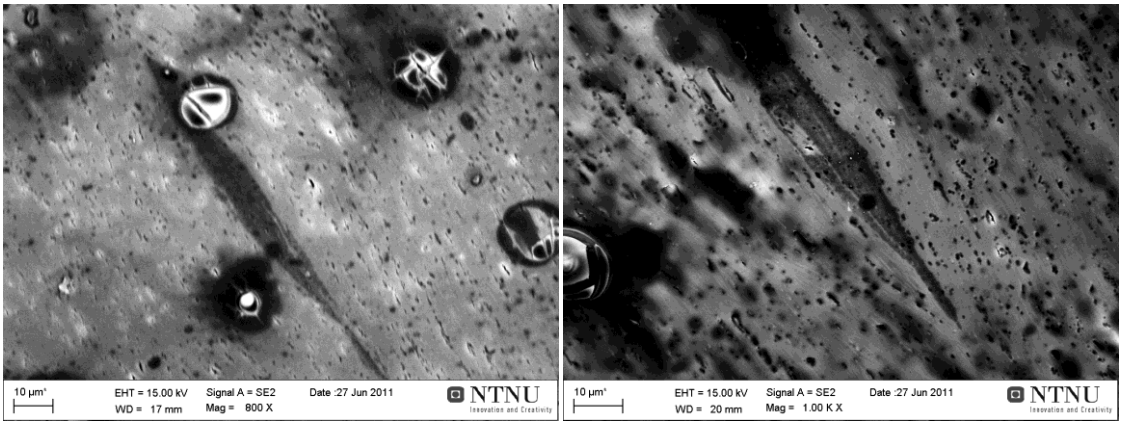

Figure F 3: The interface shown at 800x and 1´000x magnification.